α-Bungarotoxin as a Tool for Exploring Naturally Insensitive Ion Channels

Jing Liu

B.S., China Pharmaceutical University, 1998

A Dissertation Submitted in Partial Fulfillment of the Requirements for the Degree of Doctor of Philosophy in the Division of Biology and Medicine at Brown University

PROVIDENCE, RHODE ISLAND

May 2010

This dissertation by Jing Liu is accepted in its present form by the Division of Biology and Medicine as satisfying the dissertation requirement for the degree of Doctor of Philosophy.

Date _____ _____
Edward Hawrot, Ph.D.

Recommended to the Graduate Council

Date _____ _____
Anita Zimmerman, Ph.D.

Date _____ _____
Julie Kauer, Ph.D.

Date _____ _____
Wayne Bowen, Ph.D.

Date _____ _____
Michele Jacob, Ph.D.

Approved by the Graduate Council

Date _____ _____
Sheila Bonde, Ph.D.
Dean of the Graduate School

ACKNOWLEDGEMENT

I would like to express my deepest gratitude to the following people who have al1 contributed to my persona1 and professional growth:

My tremendous thesis committee, Anita Zimmerman, Julie Kauer, Wayne Bowen and Michele Jacob. I want to thank them for lending me their valuable time and for providing me with excellent advice and suggestions toward the end of my graduation.

Edward Hawrot, my thesis advisor. I am, of course, most indebted to Ed, for allowing me the opportunity to pursue my graduate studies in his laboratory, for his endless patience and tremendous understanding in helping me to achieve my goals. Ed is truly one of the most brilliant scientists that I have ever worked with.

I would also like to express my thanks to the following individuals for helping to make my years as a graduate student a forever memorable experience:

Yi Gu, for her valued friendship, advice and constant encouragement.

Philip Caffery, for his timely encouragement and proofreading with my writings.

Leonard Moise, for his assistance and hands-on teaching with many experiments.

Dean Nancy Thompson, for her help and keeping me focused on my goals.

All present and previous members of the Hawrot lab.

I would also like to thank all my family, for their unconditional love and support. Finally, I want to extend my special thanks to Chris Haines for his love and unbelievable tolerance.

TABLE OF CONTENTS

Chapter II Electrophysiological and pharmacological characterization of a genetically modified nicotinic α3 subunit in superior cervical ganglion neurons from a knock-in mouse expressing an α-bungarotoxin sensitive, heteromeric nicotinic acetylcholine receptor

LIST OF ILLUSTRATIONS

LIST OF ABBREVIATIONS

ACh	acetylcholine
AChBP	acetylcholine binding protein
AMPA	alpha-Amino-3-hydroxy-5-methyl-4-isoxazole-propionate
ANS	autonomic nerve system
BDZ	benzodiazepine
Bgtx	α-bungarotoxin
cDNA	complementary deoxynucleic acid
CNS	central nerve system
C- terminal	carboxy terminal
CTX	α-conotoxin MII
DMPP	1,1-dimethyl-4-phenylpiperazinium
DNA	deoxynucleic acid
EC_{50}	concentration of compound eliciting 50% maximal effect
EGFP	enhanced green fluorescence protein
GABA	gamma-aminobutyric-acid
$GABA_AR$	gamma-aminobutyric-acid
GFP	green fluorescence protein
GluR	glutamate receptor
GPCR	G-protein coupled receptor
HAP	high affinity peptide
IC_{50}	concentration of inhibitor required for 50% inhibition
I_{SA}	somatodendritic A-type K^+ current

I_{TO}	transient outward current, (in cardiac myocytes)
KchIP	potassium channel-interacting protein
kD	kilo Dalton
K_d	dissociation constant
Kin	knock in
Ko	knock out
Kv	voltage-gated potassium channel
LGIC	ligand-gated ion channel
MLA	methyllycaconitine
MW	molecular weight
nAChR	nicotinic acetylcholine receptor
NFM-H	heavy chain of neurofilament
NGF	nerve growth factor
NMR	nuclear magnetic resonance
N- terminal	amino-terminal
PCR	polymerase chain reaction
PNS	peripheral nerve system
RNA	ribonucleic acid
SCG	superior cervical ganglion
TIRF	total internal reflection fluorescence
VAChT	vesicular acetylcholine transporter
VTA	ventral tegmental area
WT	wild type

ABSTRACT

Abstract of "α-Bungarotoxin as a Tool for Exploring Naturally Insensitive Ion Channels", by Jing Liu, Ph.D., Brown University, May 2009.

In this thesis, α-bungarotoxin (Bgtx) was validated as a tool for exploring the function and regulation of three otherwise Bgtx-insensitive ion channels: the first is a transgenic mouse model featuring a genetic modified neuronal nicotinic α3 subunit; the second is voltage-gated potassium Kv4.2 channel; the third is a subtype of γ-aminobutyric acid type A receptors ($GABA_ARs$) containing α1β2 subunits. The findings of this thesis are summarized below.

a) We devised a novel genetic knock-in mouse model with a modified neuronal nicotinic α3 subunit. The α3 subunit bears 5 amino acid substitutions (α3/α1[5]), which confer a functional sensitivity to Bgtx. Using whole-cell patch clamp technique, the initial electrophysiological characterizations show that α3/α1[5]-containing receptors were functionally expressed and readily identifiable in cultured dissociated mouse superior cervical ganglion (SCG) neurons. Moreover, its pharmacological and biophysical properties are also largely unaltered at the macroscopic level.

b) To better understand the trafficking mechanisms that regulate voltage-gated Kv4.2 channel and to facilitate its fluorescence imaging of the channels in neurons, a short Bgtx

binding sequence HAP, was introduced into the extracellular loop of the channel. The results show that Bgtx binds specifically to HAP-tagged Kv4.2 expressed in mammalian cells and primary neuron cultures. The data also show that the introduced Bgtx binding sequence is functionally well-tolerated.

c) Using two-electrode voltage clamp measurements, we show that Bgtx also binds to and blocks a subtype of un-modified $GABA_AR$s expressed in oocytes, containing solely $\alpha 1$ and $\beta 2$ subunits. These results may also introduce a previously unrecognized tool for analysis of $GABA_AR$s.

CHAPTER I

α-BUNGAROTOXIN OVERVIEW

1.0 INTRODUCTION

1.1 Techniques for studying ion-channels

The completion of the Human Genome Project was celebrated in April 2003 and sequencing of the human chromosomes is essentially "finished". The estimated number of human protein-coding genes is about 20,000-25,000 in the human genome. Although only a subset of the genes are expressed in the human brain, the brain is estimated to have about a hundred billion nerve cells, two million miles of axons, and a million billion synapses, making it the most complex structure, natural or artificial, on earth. Yet during the last 80 years or so, our understanding of the brain has advanced greatly due to a stream of techniques being developed to manipulate and analyze the neuronal function with ever increasing power.

Molecular cloning has made it possible to identify the genes and determine the primary structure of proteins. Site-directed mutagenesis and functional studies in heterologous expression systems have begun to elucidate how proteins such as ion channels work at the molecular level. High resolution structures of domains from channels and receptors are being obtained for the first time. Recently, the technology of "gene targeting" has made it possible to create mutations in specific mouse genes or even

in defined brain regions, enabling the dissection of the role of individual proteins in brain function. As consequence, genes that cause neurological diseases have been identified, and the function roles that genes play in normal nervous system have been revealed. All these developments increase the chances for treatment and cure.

1.2 The discovery of Bgtx and muscle-type nAChR

Remarkably, for many of us today, just over 30 years ago, receptors were still considered hypothetical entities! The first receptor cDNAs cloned were four subunits of the nicotinic acetylcholine receptor (nAChR). Nature greatly facilitated the isolation and purification of the nAChR protein (and showed how to isolate other receptors) by providing investigators with two important tools: an animal source highly enriched with the nicotinic acetylcholine receptor and a highly potent snake toxin that binds selectively and essentially irreversibly to the receptor protein. The first was the electric organ of electric fish, a modified muscle that uses the nicotinic receptor expressed at high levels to generate a large current to paralyze its prey. In the *Electrophorus* electric organ, there are 10^9–10^{10} identical acetylcholine-containing synapses; in *Torpedo*, 400 g of fresh electric tissue can yield milligram quantities of receptor protein. These electric organs were, therefore, a highly enriched source and model for the study of nicotinic acetylcholine receptors. The second was venom from Taiwanese many-banded krait (Bungarus multicinctus) containing a component which binds with high affinity and specificity to nicotinic receptors in the electric organ. In the early 1970s, a number of laboratories used affinity columns with these neurotoxins and purified nicotinic receptor from the electric

organ of fish in milligram quantities. The availability of large quantities of nicotinic receptor made it possible to produce specific antibodies and to determine the protein sequence of the nicotinic receptor subunits. The availability of large quantities of purified receptor also enabled the determination of subunit stoichiometry. Moreover, electrophysiological techniques enabled the elucidation of several fundamental biophysical properties of the nAChRs including quanta-release of the neurotransmitter acetylcholine from the presynaptic terminals.

Recognizing the potential value of Bgtx, neuroscientists quickly used the potent and highly selective Bgtx to isolate the acetylcholine receptor substance from the electric organ. There is perhaps no better example to highlight the significant contributions made by venom peptides to science and medicine than α-bungarotoxin, which spawned the field of molecular pharmacology.

1.3 Neuronal Bgtx receptors

Scientists later discovered that Bgtx binding receptors were also present in mammalian brain tissue. Although neuronal Bgtx-binding proteins are similar in many respects to muscle nicotinic acetylcholine receptors, their functional properties have eluded researchers for many years. Nevertheless, Bgtx receptors were the first neuronal nicotinic receptors purified and appeared to be composed of two or more subunits of different molecular weight. Bgtx receptors from various preparations contained α7 subunits but not α3, α5, β2, or β4 subunits (Chen and Patrick 1997). The subunits found

in neuronal Bgtx receptors include α7, α8 and α9 subunits (Gotti, Hanke et al. 1992; Elgoyhen, Johnson et al. 1994; Anderson, Troyanovskaya et al. 1997). Of these three nicotinic subunits, only α7 subunits are found in mammalian nervous tissue. α9 subunits are only present in cochlea and vestibular organs, whereas no mammalian homolog for chick α8 subunits has been observed. Adding to the confusion about the subunit composition of Bgtx rceptors was the observation that heterologous expression of α7 subunits in many different cell lines results in little to no expression of Bgtx-binding sites (Cooper and Millar 1997; Palma, Maggi et al. 1999). However, Bgtx binding proteins have been cloned and expressed in oocytes and homomeric receptors composed of α7 subunits were identified as mammalian neuronal Bgtx receptors. Several biochemical and biophysical studies have also demonstrated that the native Bgtx-binding sites are composed solely of α7 subunits in rat neuronal cells (Chen and Patrick 1997)

Ultimately, the discovery of Bgtx enabled the localization of the nAChR in situ and identification of subtypes of the receptor in various muscle and neural tissues, making the nAChR one of the most thoroughly characterized receptors today.

1.4 Structure of Bgtx

Bgtx belongs to the three-finger α-neurotoxin family. Snake venom-derived α-neurotoxins bind the muscle-type and, in some cases, homo-pentameric neuronal nAChRs with high affinity and are grouped into two sub-families: short chain and long chain neurotoxins. Short chain neurotoxins have 60-62 amino acids. Long chain toxins

have 66-74 amino acids and a fifth disulfide at the tip of the second loop. Solution NMR and x-ray crystallographic studies show that all α-neurotoxins share a tertiary structure known as the three-finger fold, a four-disulfide globular core from which emerge three loops or fingers and a C-terminal tail. The x-ray crystal structure of Bgtx has been reported and refined (Love and Stroud 1986; Basus, Billeter et al. 1988; Kosen, Finer-Moore et al. 1988). The three-dimensional structure of Bgtx is shown in Figure1. Bgtx is 74 amino acids in length, molecular weight of about 8,000, and contains a fifth disulfide bond. Bgtx, apart from the COOH-terminal tail, is a relatively flat molecule with all three main-chain loops roughly in one plane covering an area of about 40 x 30-Å with a depth of about 20 Å (Love and Stroud 1986). The two strands of the middle polypeptide loop together with one strand from the third (COOH-terminal) loop form a triple-stranded, anti-parallel β sheet, which is the major secondary structure in the molecule and is a common feature throughout this family of proteins.

It must be emphasized that snake venoms are not the exclusive source of α-neurotoxins. The venoms of marine cone snails also represent a rich library of neuropharmacologically active peptides called conotoxins that target a wide variety of receptors and ion-channels. In particular, α-conotoxins are short disulfide-rich peptides that are capable of discriminating between the different ligand-binding interfaces of the muscle nAChR as well as some that are selective for various subtypes of neuronal nAChRs.

1.5 Structure of complex of bound Bgtx with peptides

More recently, the high-resolution refined three-dimensional solution structure of unbound Bgtx was also obtained (Moise, Piserchio et al. 2002). More importantly, the structure of a peptide corresponding to critical binding domain of the α1 nAChR subunit in complex with Bgtx was solved using NMR spectroscopy (Zeng, Moise et al. 2001). α18-mer is an 18-amino acid peptide derived from major toxin binding determinant of muscle type nAChR. Studies reveal important information about the interaction between the 18-mer and Bgtx upon complex formation. A further report, from our lab, of the NMR structure of the complex formed between Bgtx and a 19-mer peptide derived from the α7 subunit of the chick nAChR reveals binding-induced stabilization of the flexible tip of finger II in Bgtx (Moise, Piserchio et al. 2002). The study also reveals the aromatic residues in α7 19-mer as critical neurotoxin-binding determinants (Figure 2). The peptide containing the entire extracellular domain of of α1 nAChR subunit in complex with Bgtx was also reported (Dellisanti, Yao et al. 2007). The authors reported the crystal structure of the extracellular domain of the mouse nAChR α1 subunit bound to Bgtx at 1.94 Å resolutions. This structure is the first atomic-resolution view of a nAChR subunit extracellular domain, revealing receptor-specific features such as the signature Cys-loop and the N-linked carbohydrate chain. The toxin binds to the receptor through extensive protein-protein and protein-sugar interactions. Moreover, the structure showed a well-ordered water molecule and two hydrophilic residues deep in the core of the α1 subunit.

In summary, the structure-function study using unbound or bound Bgtx with nAChR-derived sequences greatly facilitates the investigation of toxin-receptor interface

and provides the deep insights into structure-function relationships in the nAChRs.

1.6 Using Bgtx to study normally Bgtx-insensitive receptors and ion channels

1.6.1 Bgtx-insensitive α3 and β4 nAChR subunits

Based on the understanding of the molecular determinants responsible for Bgtx binding to the nicotinic α1 subunit, rat α 3 residues 184-191 were replaced with the corresponding regions from the *Torpedo* α1 subunit (Levandoski, Lin et al. 1999). In this study, a cluster of five α1 residues (Trp-184, Trp-187, Val-188, Tyr-189, and Thr-191) were introduced into the α3 subunit (α3/α1[5]). Following co-expression of the chimeric α3/α1[5] subunit with β4 subunits in *Xenopus* oocytes, α3/α1[5]-containing receptors were blocked by Bgtx with nanomolar affinity. Another α3 chimeric subunit, α3/α7[6], similar to α3/α1[5] but incorporating the corresponding residues from the Bgtx-sensitive α7 subunit, also conferred potent Bgtx sensitivity when co-expressed with the β4 subunit. The findings demonstrate that the residues between positions 184 and 191 of the Bgtx-sensitive subunits α1 and α7 play a critical functional role in the interaction with Bgtx. This work also paved way for the development of the transgenic mouse model discussed in chapter 2.

Similarly, an 11-amino-acid sequence (WVYYTCCPDTP) derived from the tip of Loop C in the *Torpedo* α1 subunit containing residues important for Bgtx binding, conferred Bgtx binding and functional block when placed into β4 subunit, normally Bgtx

insensitive (Sanders and Hawrot 2004). Interestingly, the toxin inhibition was shown to be allosteric, not competitive as with neuromuscular nicotinic receptors. The authors suggested that Bgtx binding to the placed sequence, inserted at a subunit-subunit interface diametrically distinct from the agonist-binding site, interferes with subunit interface movements critical for receptor activation. The results, once again, suggested that strategically engineered pharmatope tagging, as a general strategy, could offer a powerful new tool for the study of membrane proteins.

1.6.2 Non-nicotinic ligand-gated ion channel AMPA and $GABA_A$ receptors

α-Amino-3-hydroxy-5-methyl-4-isoxazole-propionate (AMPA) receptors mediate excitatory synaptic transmission and are dynamically regulated during synaptic plasticity in the CNS. To image and monitor membrane trafficking of AMPA receptors to synapses, Sekine-Aizawa and Y Huganir developed AMPA receptor subunits tagged with a 13-aa Bgtx binding sequence (WRYYESSLEPYPD) (Sekine-Aizawa and Huganir 2004). By using this approach, the total receptor expression, surface expression, internalization, and insertion of receptors into the plasma membrane were visualized and quantified in fixed or live cells including cultured neurons. This 13-aa Bgtx binding sequence "WRYYESSLEPYPD", derived from a phage-display peptide library, was first reported by S Fuchs group (Harel, Kasher et al. 2001). This 13-aa sequence is named HAP standing for "the high affinity peptide" (see 3.1.7 for more details).

Yury Bogdanov and et al., developed tools to visualize $GABA_A$ receptor endo- and exocytosis in addition to their accumulation at synaptic sites by creating modified receptor subunits that are capable of binding Bgtx with high affinity (Bogdanov, Michels et al. 2006). The authors engineered $GABA_A$ β3 subunit with the HAP sequence. By using the $GABA_A$ receptors that are capable of binding Bgtx and commercially available Bgtx derivatives, the imaging study demonstrated that newly inserted extrasynaptic receptors are capable of directly accessing synaptic sites. The study provided direct evidence that synaptic $GABA_A$ receptors are directly recruited from extrasynaptic receptors.

1.6.3 G-protein coupled $GABA_B$ receptor

To examine the dynamic behavior of $GABA_B$ receptors, Li Wilkins and et al., devised a method using Bgtx binding site-tagged $GABA_B$ R1 subunit (Wilkins, Li et al. 2008). In the study, $GABA_B$ R1 subunit was tagged with HAP sequence (WRYYESSLEPYPD). The $GABA_B$ receptor is a heterodimeric G-protein-coupled receptor (GPCR), which requires R1 and R2 subunits to co-assemble to form functional receptors. When co-expressed tagged $GABA_B$ R1 subunit with the R2 subunit, receptor mobility could be tracked using the Bgtx-conjugated rhodamine. In this way, the rates of internalization and membrane insertion for these receptors could be measured with fixed and live cells. The results indicate that $GABA_B$ receptors rapidly turnover in the cell membrane, with the rate of internalization affected by the state of receptor activation.

Importantly, this study demonstrated the Bgtx-based strategy of receptor tagging seems ideally suited to monitor GPCR trafficking.

1.7 The "new" trick and "old" Bgtx

Since the advent of Bgtx as a pharmacological probe to dissect the biology of the nAChRs, a wide array of toxin derivatives including radioactive, fluorescent, and biotinylated conjugates have been developed and are commercially available. In addition, incorporating a high affinity- Bgtx -binding site into numerous ligand-gated ion channels and GPCR has demonstrated its usefulness for allowing the tracking of receptors. Previous reports from our lab and elsewhere demonstrated the specificity of Bgtx binding and verified selective recognition of extracellular Bgtx binding sequence. From the studies described above, it is evident that if carefully engineering the Bgtx binding sequence, one may obtain useful insights into the tagged membrane proteins. This strategy involves genetic fusion of sequence recognized by Bgtx into transmembrane proteins. It is a simple and generally applicable method. In some cases, as our lab demonstrated, Bgtx binding to such sequence even produces functional blockade of receptor action through an allosteric as opposed to a competitive mechanism. This provides one further advantage to a tagged receptor subunit in that Bgtx can now be used not only to label but also functionally inhibit receptor complexes. In my dissertation, I show that we have pushed this approach to an even more ambitious level by creating a knock-in mouse to explore the physiological function of the α3 subunit whose investigation has been hampered by a lack of subtype-specific ligands. From the initial

use of gene cloning to identify families of related proteins, to defined genetic manipulation to create transgenic knock-out or knock-in mouse, molecular biology has gained us remarkable insights into how our brain and body function. In my dissertation, I will illustrate how studies of ion channel can be pursued by exciting new method, plus "old" Bgtx and conventional electrophysiological measurements. In closure, Bgtx, 40 years on, still serves as one of key players in scientific discovery and medicine as an ultra-selective pharmacological probe.

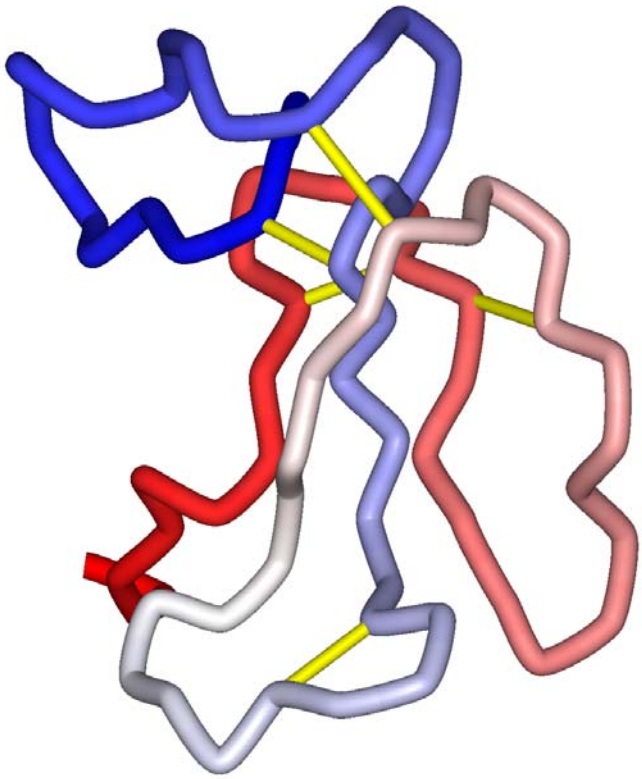

Figure 1. Schematic representation of the three-dimensional structure of α-bungarotoxin, colored from N-terminal end (blue) to C-terminal end (red). Disulfide bonds are shown in gold. single chain protein with a globular core cross-linked by five invariant disulfide bonds. Source: PDB（Protein Data Bank ）,1IDI: The NMR solution structure α-bungarotoxin，Zeng, H., Moise, L., Grant, M.A., Hawrot, E.

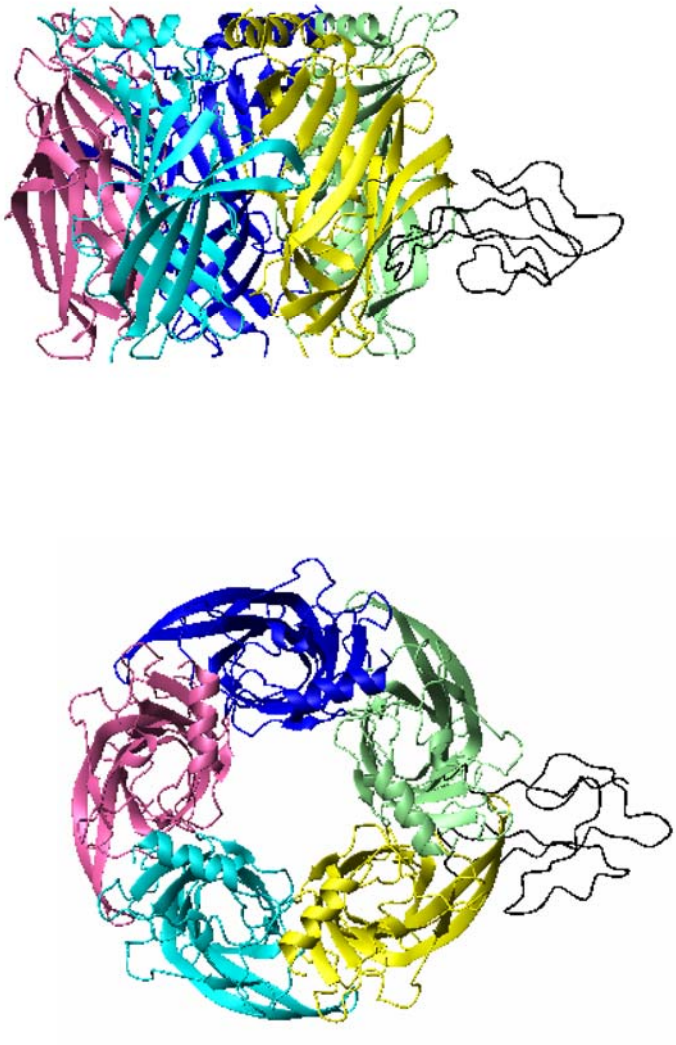

Fgure 2. Homology model of Bgtx bound to the nAChR. View of the predicted Bgtx-nAChR interaction. Bgtx as presented is colored *black.* (Adapted from Moise *et al*., 2002)

CHAPTER II

ELECTROPHYSIOLOGICAL AND PHARMACOLOGICAL CHARACTERIZATION OF A GENETICALLY MODIFIED NICOTINIC α3 SUBUNIT IN SUPERIOR CERVICAL GANGLION NEURONS FROM A KNOCK-IN MOUSE EXPRESSING AN α-BUNGAROTOXIN SENSITIVE, HETEROMERIC NICOTINIC ACETYLCHOLINE RECEPTOR

2.0 ABSTRACT

Using gene targeting in embryonic stem cells, we generated mice in which the α3 subunit bears 5 amino acid substitutions (α3/α1[5]) rendering neuronal nicotinic acetylcholine receptors (nAChRs) containing the modified α3 subunit functionally sensitive to α-bungarotoxin (Bgtx). The functionality of nAChRs containing α3/α1[5] subunit was assessed using whole-cell patch clamp technique and rapid drug application on primary cultures of dissociated mouse superior cervical ganglion (SCG) neurons prepared from these knock-in mice. Our data show that: 1) α3/α1[5]-containing receptors were functionally expressed and readily identifiable in dissociated SCG neurons; 2) ACh-evoked responses mediated by α3/α1[5]-containing receptors were rapidly and reversibly blocked by Bgtx (100 nM); 3) α3/α1[5]-containing receptor function was blocked by methyllycaconitine (MLA), but only in the micromolar concentration range,

showing that MLA can serve to discriminate Kin α3 receptors from endogenous Bgtx-sensitive α7 nAChRs, which are normally blocked by MLA in the nanomolar range; 4) 50 μM agonist rank profiles in SCG neurons from homozygous animals showed that cytisine was a more potent agonist than 1,1-dimethyl-4-phenylpiperazinium (DMPP). In combination with *Xenopus* oocyte expression studies, this suggests a predominant contribution of the β4 subunit to the population of functional α3/α1[5] nAChRs expressed in the SCGs of the Kin mice; 5) The α3β2 selective toxin, α-conotoxin MII (100 nM), produced reversible blockage on α3/α1[5] nAChRs, implying that β2 subunits can be incorporated within a fraction of functional receptors; 6) The α3/α1[5]-containing channels retained characteristic inward rectification. Taken together, the results provide direct evidence that the α3/α1[5] subunit can participate in the formation of functional channels. With pharmacological and biophysical properties largely unaltered, the major population of α3/α1[5]-containing receptors in the SCG of our Kin mouse feature a critical gain of function : Bgtx-sensitivity.

2.1 BACKGROUND AND SIGNIFICANCE

The main focus of this study was to fully characterize the biophysical and pharmacological properties of α3/α1[5] receptors in dissociated mouse superior cervical ganglion neuronal cells in a genetically modified mouse line by using

electrophysiological techniques. Understanding the basic electrophysiological and pharmacological properties of α3/α1[5] receptors in mouse SCG neurons is essential for demonstrating the merit of the new α3/α1[5] mice as a new tool for any future studies.

2.1.1 Overview of nicotinic acetylcholine receptors

Remarkably, perhaps, nAChR was the first membrane receptor of a neurotransmitter and ion channel that was characterized as a protein. Its biochemical isolation in 1970 constitutes a landmark in the history of pharmacology. Early in the study of the nAChR, investigators attempted to characterize the receptor using a number of ligands, but the great advance occurred when Lee in 1967 (Lee, Tseng et al. 1967) and Changeux (Changeux, Kasai et al. 1970) in 1970 tested a highly specific toxin, Bgtx, from Bungarus multicinctus venom and found that it caused almost irreversible block of *Torpedo* and *Electrophorus*. The discovery of Bgtx led a great step forward for the research of nAChRs, as it made possible the isolation and characterization of these proteins. In 1983, the nAChR was the first ligand-gated ion channel for which the DNA and protein were further defined by using molecular genetics. For the longest time, nAChR has served as a playground for the neurobiology community, allowing relatively early and easy testing of concepts in neurotransmission. Nicotinic receptors have provided a testing ground for electrophysiology, an arena for sequencing, a test site for neurotoxins, the first electron microscopy images, and an opportunity for cysteine-scanning mutagenesis. As a result of the extensive characterization in the last two

decades, its functional organization and biophysical properties of nAChR have been, perhaps, the best characterized among the receptor families.

The discovery of nAChRs is a very recent story. Converging with a series of pioneering approaches, however, it led to a good deal of success in present state of understanding of this receptor. It is well accepted today that nAChRs are the members of a gene superfamily of ionotropic that are formed by five homologous subunits oriented around a central ionic channel (Figure 3). This superfamily includes, in addition to nAChRs, 5-HT_3 receptors, $GABA_A$ receptors and glycine receptors (Ortells and Lunt 1995). Within this superfamily, it is a significant fact that nAChRs mediate fast excitatory synaptic transmission in all vertebrate peripheral nervous system (PNS) neurons. In the central nervous system (CNS), the nAChRs play multiple and important roles in signal transduction, fast synaptic transmission, axo-axonic transmission and modulation of presynaptic transmitter release. ACh is involved in numerous cognitive and behavioral processes, such as voluntary movement, sensory function, biorhythms, ingestive behaviors, aggressive behaviors, thermoregulation, sleep and arousal, attention span, learning and memory, and sexual function(Jones, Sudweeks et al. 1999). These receptors have highly variable kinetic, electrophysiological and pharmacological properties. This functional diversity allows them to take part in two major types of neurotransmission. Classical synaptic transmission (wiring transmission) involves the release of high concentrations of neurotransmitter, acting on immediately neighboring receptors. In contrast, paracrine transmission (volume transmission) involves neurotransmitters released by synaptic buttons, which then diffuse through the extra-cellular medium until they reach their receptors, which may be distant. Nicotinic

receptors can also be found in different synaptic locations, for example the muscle nicotinic receptor always functions post-synaptically. The neuronal forms of the receptor can be found both post-synaptically (involved in classical neurotransmission) and pre-synaptically where they can influence the release of multiple neurotransmitters. Neuronal nAChRs as ACh receptors are key players in cholinergic nicotinic transmission at the neuromuscular junction, in autonomic ganglia and in several brain areas. Neuronal nAChRs as they are heavily involved in central functional processes, have gained increasing attention for their roles as modulators in the CNS over recent years (Clementi, Fornasari et al. 2000; Weiland, Bertrand et al. 2000).

2.1.2 Pathologies involving neuronal nicotinic receptors

Although best known for their role in physiology of neuromuscular junction, these nAChRs have attracted the increasing attention of academic and industrial scientists because of their relevance to understanding brain functions and their possible involvement in various pathologies. A very hot issue is the role of nicotinic receptors in smoking addiction. Nicotinic receptors have roles in development and synaptic plasticity, and nicotinic mechanisms participate in learning, memory, and attention. Nicotinic-associated disturbances in neurotransmission are being increasingly linked with neurological disorders occurring at all stages of life- development, adulthood, and aging. Decline, disruption, or alterations of nicotinic cholinergic mechanisms contribute to a number of dysfunctions. More comprehensively, neuronal nAChRs are involved in a growing list of pathological conditions associated with frontal lobe epilepsy,

schizophrenia, Alzheimer's disease, autism and Parkinson's disease(Gotti, Riganti et al. 2006). Neuronal nicotinic receptors are also linked to a number of non-neuronal diseases. For example, evidence suggests α7 is linked to the development of small cell lung carcinoma(Plummer, Dhar et al. 2005), Meanwhile, α3-, α4-, α5-, β2- and β4 neuronal nAChR subunits are found in non-neuronal tissues such as skin keratinocytes, bronchial epithelial cells and endothelial cells. The pharmacological manipulation of these receptors profoundly modifies the shape and motility of these cells, which suggests that they could be involved in smoking-associated pathologies such as skin aging, chronic bronchitis and atherosclerosis(Conti-Fine, Navaneetham et al. 2000).

2.1.3 Heterogeneity of neuronal nicotinic acetylcholine receptors: so many and so similar

Over a billion years ago, the family of nicotinic receptor subunits began to emerge by a series of gene duplications from a single common subunit. Today, 5 neuromuscular subunits (α1, β1, γ, δ and ε) and 12 neuronal nAChR subunits have been described, α2-α10 and β2-β4! Two nAChR subtypes are expressed in muscle, the fetal and the adult form that differ only with respect to the γ- and ε-subunit, respectively (Figure 4)(Albuquerque, Pereira et al. 2009). The diversity of nAChRs is much greater in brain, with its large number of possible different subtypes and the expression of multiple subtypes within the same tissue or cell type (Figure 5). Several of the neuronal nAChR

subunits, such as α3, α5 and α7, are also expressed in various non-neuronal tissues, including glial cells, epithelial cells in airways, intestine, and epidermis, endothelial cells, placenta and circulating blood cells (Wessler and Kirkpatrick 2008). In brain, there are two main classes of nAChR subtypes, the homomeric pentamers build from α7–α10, and the heteromeric pentamers consisting either of various combinations of α2–α6 subunits with β2 and β4 subunits, or are a mixture of either α7 with α9 or α10. In homomeric neuronal nAChRs five agonist-binding sites are present, one at each interface between two subunits. The heteromeric neuronal receptors are thought to have two binding sites that are located between an α- and β-subunit each. Exceptions are the α5 and the β3 subunits which are probably not able to form agonist binding sites. Each subunit is expressed throughout the nervous system, and the subunits can combine with each other in heterologous expression systems to form different nAChRs with a broad range of biophysical (i.e., conductance and kinetics of desensitization, Ca2+ permeability) and pharmacological profiles (i.e., agonist and/or antagonist affinities). Growing data suggest that many receptors contain three or more different subunits in neurons. Some pharmacological tools allow the limited identification of subunits in native receptors. The stoichiometry of the individual receptor subtype determines the biophysical and functional properties as well as the pharmacological profile. However, attempts to pinpoint and identify each subtype have not been successful due majorly to the reality that most available ligands can interact with a number of different subtypes, resulting in overlapping pharmacological properties. Unlike skeletal muscle nAChRs, which are constrained to a single pentameric arrangement in adult tissue, neuronal nAChRs vary considerably in their subunit compositions resulting in distinctive pharmacologies, and

physiological functions. In summary, any progress with regard to function of each subunit/subtype has been hampered by their largely unknown pharmacology. Even now that a pharmacological profile for many subunit is being established on the basis of using recombinant technology in heterologous expression systems, many native subtypes in vivo stay enigmatic. Despite of a great deal of interesting work and lots of debate in last 2 decades, we still cannot honestly say we have made great advance on the major fundamental issues: What are the compositions of native nicotinic receptors? Why is there such diversity? Finally, what is their purpose on neurons?

2.1.4 Genetic manipulations and antibodies to study nAChRs

The exact nAChR subtype composition in different brain parts is still not completely known and that highly specific antibodies have not been produced for all subunits yet. Pharmacological manipulations of nicotinic transmission have long been the only way to identify and characterize the role and the functionality of nAChRs *in vivo*. Studies are hampered by the fact that the various ligands are mostly not subtype-specific. More recently, however, the use of genetically engineered knock-out (Ko) and knock-in (Kin) mice has provided a powerful alternative to the classical pharmacological approach (Champtiaux and Changeux 2002). As stated by Champtiaux and Changeux in their review (Champtiaux and Changeux 2002), one advantage to the genetic approach is that the use of Ko mice can pinpoint the genes that mediate the effects of nicotine. The technique of Ko mice shows that a given subunit is *necessary* for a given function. However, the deletion of a gene does not reveal whether variability in this gene can alter

sensitivity to nicotine. In other words, it cannot demonstrate the *localization* for a given subunit in which its expression is *sufficient*, especially for behavioral phenotypes. The generation of Kin mice that have had a hypersensitive or hyposensitive nAChR subunit inserted into the mouse genome can be used to investigate whether variability in nAChR subunit genes can modulate nicotine sensitivity, but this artificial change in the functional properties of the subunit may not reflect what occurs naturally. Antibodies are commonly used biochemical approach these days to localize neurotransmitter receptors in the CNS, to define their cellular and subcellular distributions, thereby providing a neuroanatomical correlate of receptor function. However, it is worth of noting that interpretation of these studies heavily relies on the specificity and selectivity of primary antibodies for their respective nAChR subunit targets. Until recently, determining the specificity of primary antibodies has been problematic. These unexpected findings have major implications especially for the interpretation of nAChR-subunit immunolabelling patterns (Herber, Severance et al. 2004; Shelukhina, Kryukova et al. 2006; Moser, Mechawar et al. 2007). These data raise the question of whether nAChR antibodies can be used reliably. Approaches using probes for *in situ* hybridization on nAChR mRNAs also have problems with regard to their specificity, and false positive results are a common problem.

2.1.5 Call for novel integrated approaches: pharmatope as one candidate

The genesis of the concept of "pharmatope" is credited to Dr. Hawrot, my mentor, who has dedicated over a decade in understanding the structure-based action of Bgtx. After exploiting and discovering a series binding determinants responsible for Bgtx

action on muscle type nAChRs, an audacious attempt was extended to neuronal nAChR subunits normally insensitive to Bgtx by strategically introducing pharmatope sequences bearing Bgtx binding sites into these subunits (Levandoski, Lin et al. 1999; Sanders and Hawrot 2004). Remarkably, the team discovered that the α3 and β4 neuronal nAChR subunits, which are normally insensitive to Bgtx, could be transformed into Bgtx-sensitive variants (Figure 6). These findings provide a step-stone for a more sophisticated approach, our pioneering Kin mouse line, by demonstrating that Bgtx binding to such a pharmatope can produce functional blockade of receptor action.

As I have explained previously, many fundamental questions with regard to neuronal nAChR subunits mechanisms of function in CNS still remain unanswered largely due to lack of powerful selective pharmacological agents. Our lab, using in part with our experiences gained in exploiting structure-based information of Bgtx action plus developing Bgtx sensitive pharmatopes using heterologous expression systems, reasoned constructing toxin-sensitive chimeric subunits in mouse would offer a number of unique experimental advantages: Having strategically labeled but otherwise "normal" tagged nAChRs to dissect neuronal nicotinic receptor composition, distribution and assess the functional involvement of individual nAChR subtypes function; Fluorescent-labeling Bgtx has many practical advantages over staining with antibodies: Bgtx is a relatively small, cell-impermeant protein with a variety of commercially available conjugates. Until we know why nAChR immunoreactivity doesn't knock out, conjugates of the high-affinity Bgtx currently appear to be the most reliable methods of localizing nAChRs(Moser, Mechawar et al. 2007).

2.1.6 Nicotinic α3 subunit: why me?

The success of the Levandoski's work in 1999 transforming Bgtx-insensitive α3 into Bgtx-sensitive α3/α1[5] ultimately led to the Kin mouse project. The α3 subunit was favored also because of its widespread involvement in the peripheral autonomic nervous system. The ganglionic α3 containing nAChRs mediate fast synaptic transmission in sympathetic, parasympathetic and enteric autonomic ganglia. Autonomic ganglia are an important site of neural integration and regulation of autonomic reflexes. Genetic analysis of the function of the α3 subunit indicates that it is essential for autonomic control of some peripheral organs, with the most obvious phenotypic effects on survival, growth, bladder function, and pupillary contraction (Xu, Gelber et al. 1999). Deletion of the α3 gene in inbred mice is lethal for most of the Ko mice, these animals usually die at very early stage.

This subunit is widely distributed in autonomic ganglia as the predominant α subunit and is thought to form heteromeric nAChRs with other α and β subunits (most frequently, α3/β4). The combination is called "ganglia-type nAChRs", in contrast to the nAChRs of the central nervous system (mainly α4β2 combination) (Skok 2002). The α3 subunit is the predominant α gene expressed in most of the autonomic ganglia. The major cytoplasmic loop of the α3 subunit targets specific nAChR subtypes to synapses in autonomic neurons (Temburni, Blitzblau et al. 2000). α3 subunit was also found in the brain and retina (Lindstrom, Anand et al. 1995). The α3-deficient mice are too ill for

meaningful behavioral studies, and no phenotypic features clearly attributable to central nervous system (CNS) dysfunction were readily identified. Thus, a new approach such as a Kin mouse model would be useful for evaluating the function of α3 in central tissues.

2.1.7 Anatomy of SCG: ideal for initial functional characterization of α3/α1[5] nAChRs

The ultimate purpose of generating the Kin mouse is to understand synaptic interactions in the central nervous system (CNS). CNS study is too difficult because of the immense structural complexity of the vertebrate brain and spinal cord. Consequently, much of what is known about synapses has come from studies of a much simpler system, the superior cervical ganglion. The SCG is the largest of the cervical ganglia and has a unique neuroanatomical structure. The α3 subunit was found in each neuron of rodent SCG. The α3 subunit seems to be directly involved in ganglionic synaptic transmission as a predominant ligand-binding subunit mediating response to ACh and nicotinic agonists in a Bgtx-insensitive manner. In addition, the α3β4 nAChRs are considered to be the main nAChR subtype expressed in the neurons of rat SCG(Covernton, Kojima et al. 1994) (Colquhoun and Patrick 1997).

Thus, for the initial functional characterization of the α3/α1[5] receptors, I choose SCG neurons as experimental material. The SCG in mice are very small, glossy, almond-shaped structures that contain sympathetic neurons. These neurons provide sympathetic innervations for the head and neck regions and they constitute a well-characterized and

relatively homogeneous population (Dechant 2002). The anatomy and pharmacological basis of ganglionic transmission are essentially well characterized (reviewed in (Purves and Lichtman 1978)). Moreover, synapses within the ganglion are interneuronal and the organization of the multiple inputs reaching the dendrites of the ganglionic neurons is similar to the connectivity in the CNS. Sympathetic neurons are dependent on nerve growth factor (NGF) for survival, differentiation and axonal growth and the wide-spread availability of NGF facilitates their culture and experimental manipulation. For these reasons, cultured sympathetic neurons have been intensively used as an experimental model in a wide variety of physical and biochemical studies. Dissecting out the SCG from mice and culturing sympathetic neurons is not very complicated and can be mastered fairly quickly.

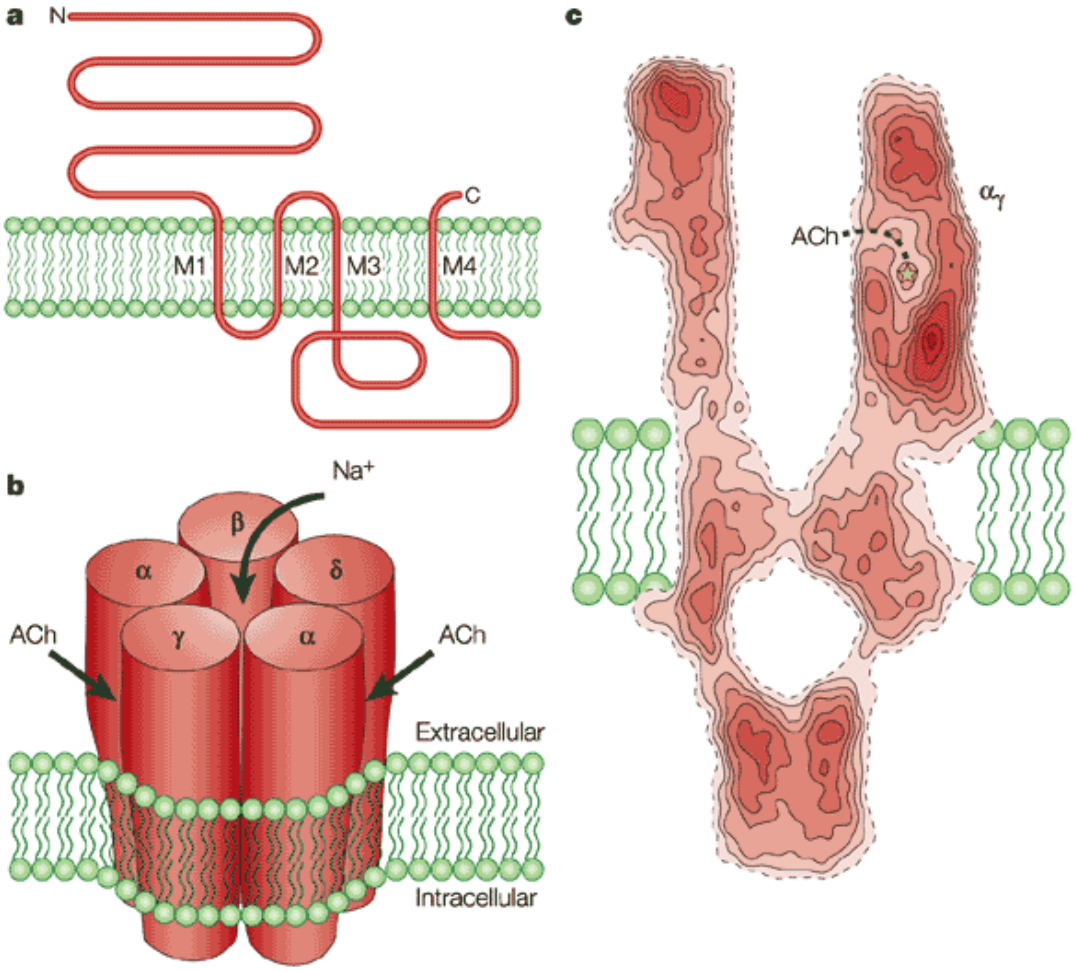

Figure 3. Basic structural features of nicotinic receptors. a) The threading pattern of receptor subunits through the membrane, the extracellular N-terminal domain, four transmembrane regions (M1-M4), and large intracellular loop between M3 and M4 b) A schematic representation of the muscle-type nAChR pentamer , showing the arrangement of the subunits in the muscle-type receptor, the location of the two acetylcholine (ACh)-binding sites (between an α and a γ subunit, and an α and a δ subunit), and the axial cation-conducting channel. c) A cross-section through the 4.6-Å structure of the receptor determined by electron microscopy of tubular crystals of *Torpedo* membrane embedded in ice. Dashed line indicates proposed path to binding site. (Adapted from Karlin, 2002)

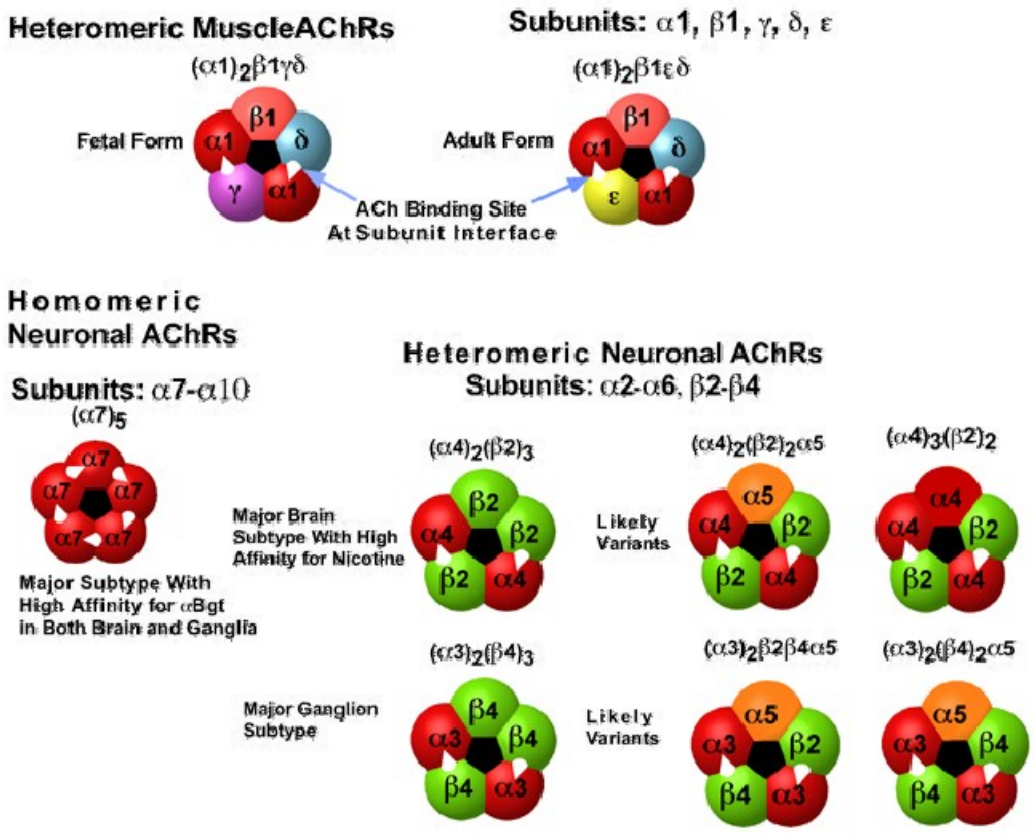

Figure 4. The major putative mammalian neuronal nAChR subtypes. (Adapted from J.M. Lindstrom, 2000)

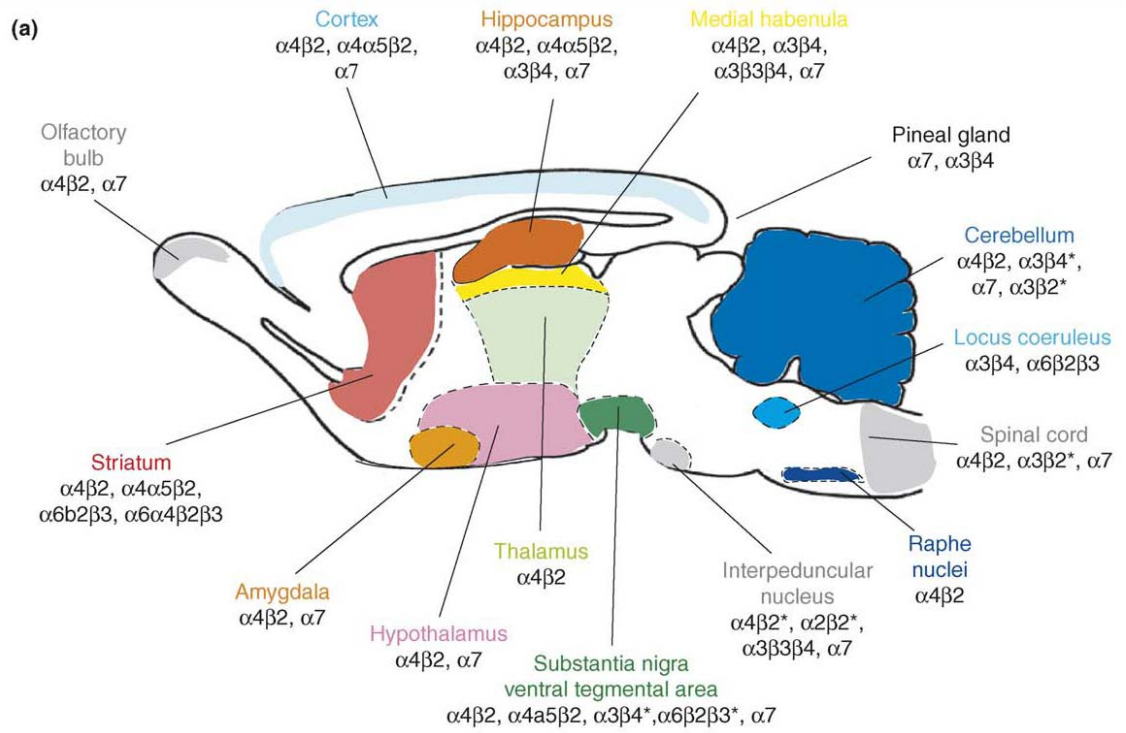

Figure 5. Regional distribution of the main nicotinic receptor sub types in the rodent CNS (Adapted from C Gotti, 2006).

	αBgtx Sensitivity	175					180					185					190					195					200				
														*	*	*	*			*										
Torpedo α1	+++	G	E	W	V	M	K	D	Y	R	G	W	K	H	W	V	Y	Y	T	C	C	P	D	T	P	Y	L	D	I	T	Y
Rat α3	---	G	E	W	A	I	I	K	A	P	G	Y	K	H	E	I	K	Y	N	C	C	E	E	I		Y	Q	D	I	T	Y
α3/α1[5]	++	G	E	W	A	I	I	K	A	P	G	W	K	H	W	V	Y	Y	T	C	C	E	E	I		Y	Q	D	I	T	Y
α3K189Y	+	G	E	W	A	I	I	K	A	P	G	Y	K	H	E	I	Y	Y	N	C	C	E	E	I		Y	Q	D	I	T	Y
α3/α1[4]	---	G	E	W	A	I	I	K	A	P	G	W	K	H	W	V	K	Y	T	C	C	E	E	I		Y	Q	D	I	T	Y
α3/α1[16]	?	G	E	W	V	M	K	D	Y	R	G	W	K	H	W	V	Y	Y	T	C	C	P	D	T	P	Y	L	D	I	T	Y

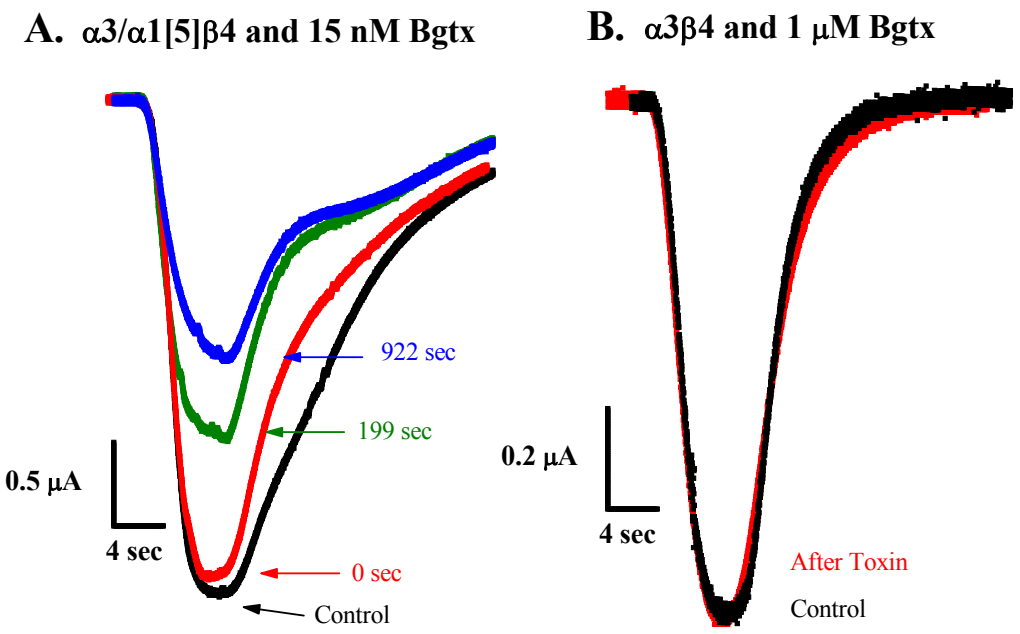

Figure 6. Five residues from the muscle type nicotinic α1 subunit confer Bgtx sensitivity to neuronal α3 subunit. Upper panel shows A Sequence comparison of Bgtx-sensitive α1 and Bgtx-insensitive α3 nAChR subunits. Residues changed in the chimeric subunit constructs are *boxed*. *Asterisks* indicate residues in a position to contribute to Bgtx binding. Superimposed ACh-evoked current traces were obtained from oocytes expressing wild type α3 and chimeric α3/1α[5] subunits in combination with rat β4. 1 μM Bgtx rapidly blocks α3/1α[5]β4 expressed in oocytes. (Adapted from Levandoski, 1999)

2.2 MATERIALS AND METHODS

2.2.1 Mice

All experiments on animals from creation of Kin mice to establishment of their genotypes were conducted using protocols approved by Brown University Institutional Animal Care and Use Committee. Mice were kept on a standard 12 h light/dark cycle at 22°C and given food and water. The mice used for most of my pharmacological and biophysical studies had a mixed BALB/c/C57BL/6 background with one or more generations backcrossed to BALB/c. Thus, most functional data were derived from mice with a mixed BALB/c/C57BL/6 background (as stated in Results 2.3), except some very initial experiments using inbred C57BL/6, outbred ICR or mixed C57BL/6/ICR mice as indicated in the Results or Discussion sections. The main reason to select BALB/c strain is that mixing BALB/c background helped to produce reliable reproducible results for the following electrophysiology studies in the Kin mice. This will be discussed in details in the 2.4 Discussion section.

2.2.2 α3/α1[5] Kin mouse construction

Generation and Phenotypic characterization of Kin mice have been previously described (Caffery, thesis 2007). In brief, we have incorporated the α3/α1[5] mutation into a targeting vector. Using gene-targeting strategy in mouse ES cells we have successfully produced knock-in homozygote mice (Figure 7, provided by Phil Caffery). See 2.3.2 for more details.

2.2.3 Genotyping

A BstZ17I restriction enzyme site was engineered into the mutated region. Germline transmission of the α3/α1 [5] mutant allele was determined by allele specific short-range PCR and then confirmed by a second PCR-based approach, which utilized the BstZ17I restriction site. The diagram in Figure 8, provided by Phil Caffery, illustrates the overall PCR-based genotyping strategy, showing both the relative positions of the allele-specific primers along with an upstream site designed for the restriction-based amplification. All PCR screens utilized the same reverse primer. The gel in Figure 8 shows a typical genotyping result (2% agarose gel) using the restriction-based approach. The image shows 3 of 4 pups, including 1. wild-type (+/+), 2. heterozygous (+/tm), and 3. homozygous (tm/tm) offspring (second +/tm not shown).

2.2.4 α7(-/-) knockout mouse

The α7 knock out genotype α7(-/-) was developed by engineering a 7 kb deletion （exons 8-9）in CHRNA7 (Orr-Urtreger, Goldner et al. 1997). A pair of heterozygote α7(+/-) mutants (B6.129S7-*chrna7tm1Bay/J*) were purchased from Jackson Laboratories (Bar Harber, ME). To produce α3(tm/tm)α7(-/-) double homozygotes, α7(-/-) mice were bred with α3(+/tm) mice. The breeding pair α3(+/tm)α7(+/-) were used to generate α3(tm/tm)α7(-/-) double homozygotes.

2.2.5 Primary SCG neuron culture

2.2.5.1 Dissection of SCG

The detailed protocol is: Wipe working bench with 70% ethanol to reduce chances of contamination. α3/α1[5] homozygote(tm/tm), heterozygote (+/tm) or wild type (+/+) mice are anesthetized with CO_2 and rapidly decapitated with a sharp pair of scissors. Briefly drain excess blood. Place the head facing up on the dissection pad and the severed trachea should be readily visible. Secure the severed head to the dissecting pad using pins. Under the dissecting microscope, use sharp forceps clear away skin and fat around the trachea. This will expose a pair of muscles on either side of the trachea. Use the forceps to cut and remove the muscle to expose the carotid artery. This artery runs alongside the trachea and bifurcates into what looks like a "Y"-shaped ribbon. This bifurcation is a landmark to find the SCG. At the most caudal end of the bifurcation, there is an almond-shaped, glossy looking small mass of tissue that has thread-like pre- and/or post-ganglionic connectives. This is the superior cervical ganglion. Gently detach it and

place in a small culture dish (35 mm) containing Liebovitz L-15 medium. Extract the ganglion on the other side of the trachea following the same protocol.

2.2.5.2 Establishing SCG primary culture

The protocol is: Dissected ganglia are transferred into a 15ml centrifuge tube containing 2~3 ml Hank's Balanced Salt Solution(Ca^{2+}–Mg^{2+}-free)/trypsin (0.5 mg/ml, Worthington, Freehold, NJ). Ganglia are incubated for 50 min at 37°C. The enzymatic solution is discarded and ganglia are transferred to warm growth medium. Dissociation is done by gently trituration with a fire-polished glass pipette (approximately 1/2 mm in diameter) for about 3-5 minutes. Dissociated cells were isolated by centrifugation at 200xg for 5 min and then are re-suspended in growth medium. The growth media consists of Liebovitz L-15 media (Invitrogen) supplemented with vitamins, cofactors, penicillin–streptomycin, 5% rat serum, and NGF (25–50 ng/ml). Neurons are then plated on mouse laminin (Invitrogen)-coated cover-glasses (13mm, Warner Instrument) and maintained in 5% CO_2 at 37°C. Cells were fed with fresh growth medium every 2 days. In order to up regulate the whole cell current, all cultured cells were kept at 30°C for 2 to 3 days prior to any experiments.

2.2.6 Chemicals

All chemical reagents used for electrophysiology were analytical grade. Acetylcholine chloride, nicotine, DMPP, MLA, cytisine, and hexamethonium were obtained from Sigma chemicals. Stock solutions of the chemical agents were made in double distilled water.

2.2.7 Electrophysiology

2.2.7.1 Whole-cell patch clamp

Conventional patch clamp techniques with a whole cell configuration were applied. Briefly, pipettes were pulled from borosilicate standard-walled glass with filaments (1.5 mm outer diameter; .86 mm inner diameter; Warner Instrument Corp., Portland, OR) and fire-polished to a resistance of 2-5 MΩ. Gravity- driven drug solutions were applied with the use of VC-6M Valve Controller (Warner Instrument Corp.). Self-made 6-barreled pipettes were connected to VC-6M tubing. The tip of the glass barrel is 250μm. 6-barreled pipettes are positioned to the recording chamber with a micromanipulator. The tip of the glass barrel was place 20-30 μm away from the clamped cell with the central axis of the barrel in line with the cell before drug application. Drug was applied for 2 seconds for each trial. Otherwise noted, the recording chamber was perfused with external solution throughout the recording. All currents were recorded with an Axopatch 200B amplifier (Axon Instruments, Foster City, CA) in voltage-clamp mode. The built-in series resistance correction and prediction circuitry were set to at least 100%

in all experiments. Signals were low-pass filtered at 5 kHz and sampled at 10-50 kHz. All experiments were performed at room temperature.

Recording solutions were prepared from frozen stocks and stored at 4ºC before use. Currents were activated by the indicated concentration of ACh or other agonists as indicated. Osmolality of recording solutions were adjusted to ~310±10 mmol/kg with intracellular recording solution slightly lower than external. The patch electrodes were filled with the following (in mM): 65 KF, 55 KAc, 5 NaCl, 0.2 $CaCl_2$, 1 $MgCl_2$, 10 EGTA, and 10 HEPES, pH adjusted to 7.3 with KOH. The neurons were perfused continuously throughout the recording at 1 ml/min with perfusion media consisting of the following (in mM): NaCl 140, $CaCl_2$ 1, KCl 2.8, and HEPES 10, pH 7.2 adjusted with NaOH. Atropine was added in perfusion solution to final concentration of 1 μM before recordings.

2.2.7.2 Two electrode voltage clamp

Recordings from oocytes were performed at room temperature (Levandoski et al., 1999). Briefly, plasmids containing rat, wild-type α3, α3/α1[5], β2, and β4 nAChR subunit cDNAs were linearized by restriction enzyme digestion, purified by EtOH precipitation, and used to transcribe nAChR RNAs (Message Machine Kit, Ambion) according to manufacturer's recommended protocol. Oocytes were collected from mature frogs using survival surgery. A brief collagenase treatment was preceded with manual removal of follicular cell layer, and healthy oocytes were selected and incubated in ND96

(96 mM NaCl, 2 mM MgCl2, 2 mM KCl, 1.2 mM CaCl2, 5 mM HEPES, pH 7.5) supplemented with 100 units/ml penicillin and 100 mg/ml streptomycin. cRNA were prepared for injection by mixing equal ratios of α:β and diluting in OR2 medium (115 mM, NaCl, 2.5 mM KCl, 1.8 mM $CaCl_2$, 10 mM HEPES, 0.003 mM atropine sulfate, pH 7.4). Freshly made oocytes were injected with nAChR subunit cRNA and allowed to incubate at 15 °C for 2-6 days prior to recording. Recordings from injected oocytes were done with a Warner OC-725C amplifier at a clamped voltage of -60mV. All drugs for test were diluted in OR2 to desired concentration.

2.2.8 Data analysis and curve fitting

All data were reported as Mean ±S.E.M. All curve fitting was performed using Origin 7.0 (OriginLab Corp., Northampton, MA). Statistical analysis was performed using Student's t-tests and $P<0.05$ was considered significant.

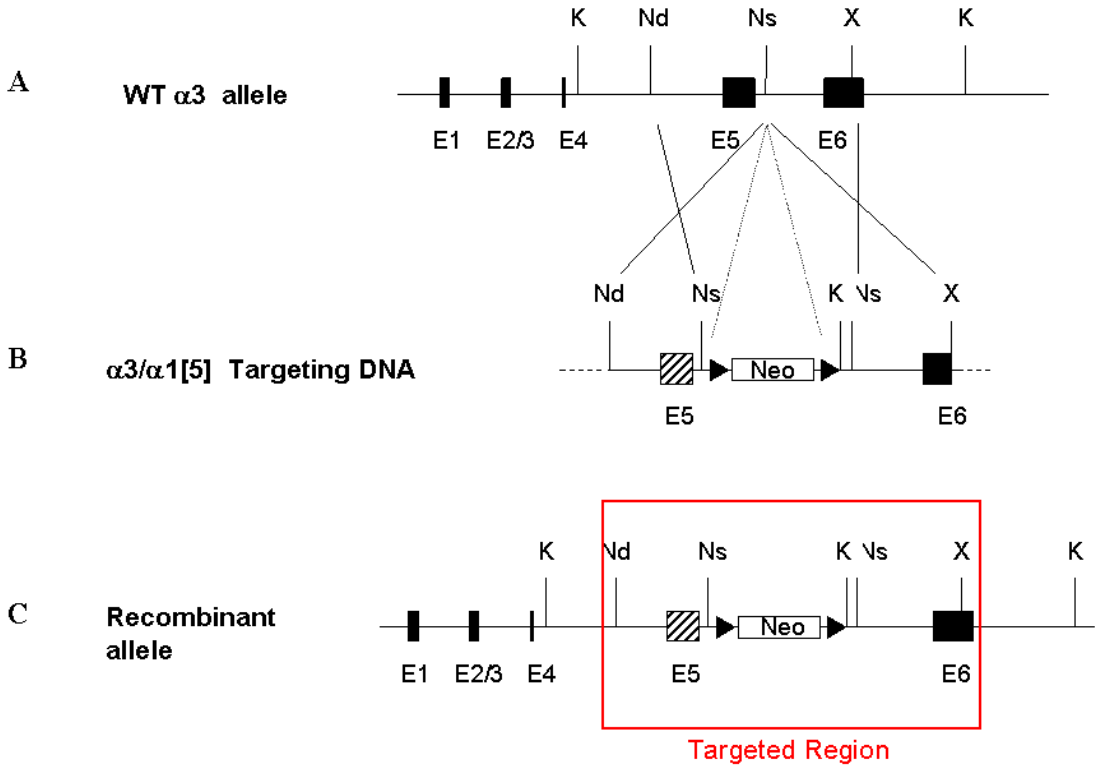

Figure 7. Overview of gene-targeting strategy A) The wild-type CHRNA3 allele, B) α3/α1[5] targeting DNA, and C) the recombinant allele are depicted, along with anticipated regions of homologous recombination and restriction cleavage sites. Wild-type exons are represented as solid rectangles, and the mutated exonV is shown as a hatched rectangle. (Graph provided by Phil Caffery)

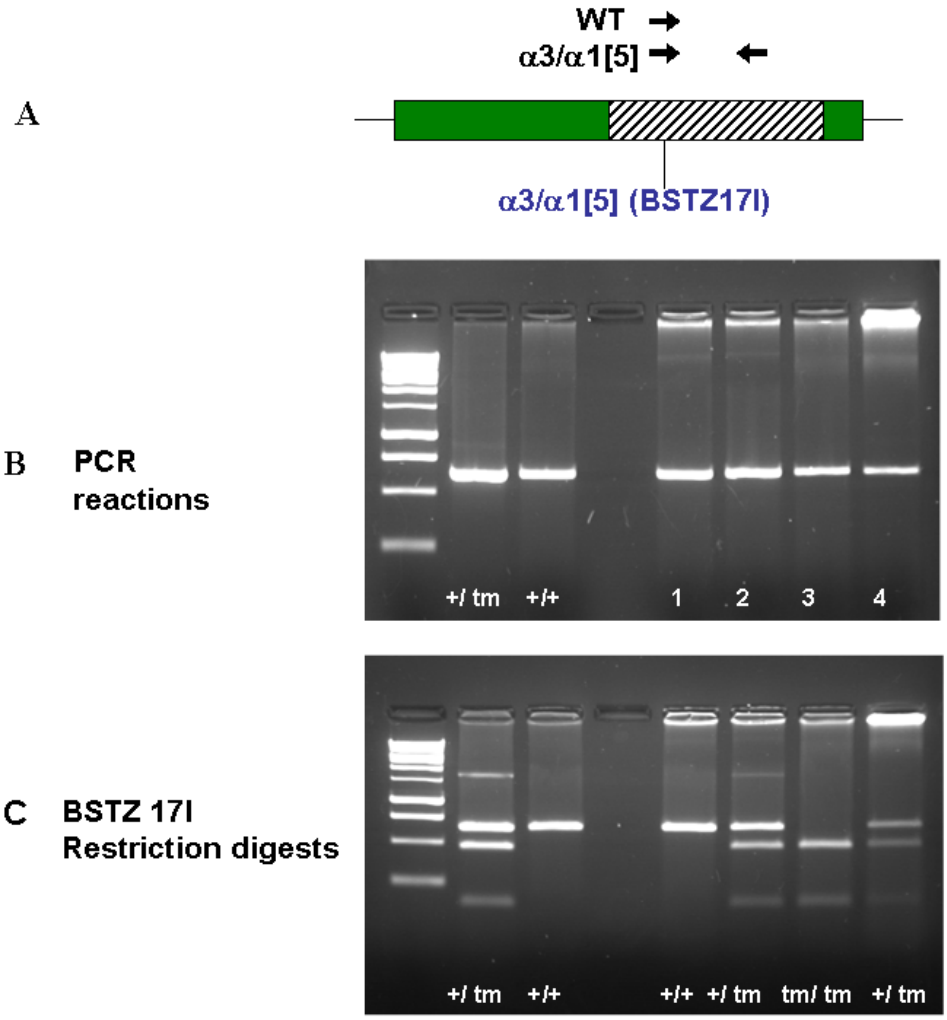

Figure 8. PCR-based allele-specific genotyping A) Overview of allele-specific strategy, showing positions of forward and reverse primers within exonV. B) PCR amplifications of tail DNA from 4 unknown samples (1-4) along with wild-type and α3/α1[5] heterozygous control. C) Gel of same samples following restriction digest with BsTZ17I. (Data collected by Phil Caffery)

2.3 RESULTS

2.3.1 Production of α3/α1[5] Knock-in mouse

Knock-in (Kin) mouse, Chrna3$^{tm1.0(Hwrt)}$, created through homologous recombination-mediated targeted gene replacement following standardized mouse line nomenclature recommendations for targeted mutations (Institute for Laboratory Animal Research). Generation and Phenotypic characterization of Kin mice have been previously described (Caffery, thesis 2007).In brief, we have incorporated the α3/α1[5] mutation into a targeting vector. Using gene-targeting strategy in mouse ES cells we have successfully produced knock-in homozygote mice. Figure 9, depicts the targeting gene as it appears in the mouse genome along with the sites of predicted homologous recombination. Residues critical for Bgtx binding to nAChR α1 were substituted into α3. Blastocyst injection using positive ES cell colonies was carried out at the Brown University Transgenic Facility. Several chimeras were produced and mated with albino C57s, which produced the first F1 pups possessing the α3/α1[5] genotype. F1 generation pups were identified as candidates for genotyping by ES-derived coat color (agouti). Following the removal of the neomycin resistance gene, which was accomplished by mating α3/α1[5] heterozygous males with a commercially available Cre-recombinase-expressing female, 129S1-Cre/HPRT (Tang, Silva et al. 2002). The neomycin resistance gene is flanked by 2 LoxP sequences in the targeting construct, which enables its excision in the presence of Cre-recombinase.

The knock-in genotype was confirmed by restriction digest with BstZ17I restriction enzyme site engineered into the mutated region. Several chimeras were produced and mated with albino C57s, which produced the first F1 pups possessing the α3/α1[5] genotype. The α3/α1[5] Kin mice, which were initially being maintained on a mixed S129/C57 background, had been backcrossed with the inbred C57BL/6 strain for 10 generations. Most the C57-backcrossed homozygotes appear smaller than their wild type littermates and impaired breeding behaviors.

2.3.2 Identification of functional membrane expressed α3/α1[5] in mouse SCG neurons from inbred and outbred mouse strains

The SCG offers great advantages for initial α3/α1[5] subunit characterization as there is abundant evidence that the α3 containing nAChRs are responsible for the fast synaptic transmission between the preganglionic nerve terminals originating from cholinergic neurons in the central nervous system and the principal sympathetic ganglionic neurons. Many studies demonstrated that although there are Bgtx binding sites in the SCG, Bgtx does not bind to synaptic membrane regions nor does it block fast synaptic transmission (Chiappinelli, Cohen et al. 1981; Loring, Sah et al. 1988). More over, studies with α3 knock out null mutants have demonstrated that the α3 subunit is prerequisite for maintaining normal autonomic functions. This evidence makes SCG a classic model system for studying the physiology of α3 containing neuronal nAChRs. The SCG is very accessible and ganglia can be readily isolated following a straightforward dissection. Another major advantage to the SCG is that the principal

neurons in the SCG can be readily maintained in primary tissue culture in the presence of NGF and other essential supplements.

2.3.2.1 C57BL/6 inbred strain: nAChRs from SCG neurons of α3/α1[5] (tm/tm) or α3/α1[5] (+/tm)mice showed no functional Bgtx sensitivity in its initial characterization

Transgenic mouse models have their greatest experimental values when the physiological effects produced by the targeted mutation can be assessed on well characterized genetic background. Therefore, transgenic mice are routinely backcrossed (9-10 times) into inbred strains. The backcrossing strategy produces a congenic mouse strain where ~ 99% of the genome is composed of highly homologous inbred sequence (Bolivar, Cook et al. 2001). We chose to backcross the Kin mice initially maintained on a mixed S129/C57 back ground, into C57BL/6 inbred strain. Because it's strong breeding performance and low "emotionality", C57BL is probably the most widely used of all inbred strains. Substrain C57BL/6 alone accounts for over 14% of occasions on which an inbred strain is used (MGI 4.2, Mouse Genome Informatics, The Jackson Laboratory, Bar Harbor, Maine.).

Initially, with C57 crossed homozygotes, this death was preceded by abdominal swelling and a rapid decline in health. However, backcrossing one or more times into C57BL/6 had increased the average survival of α3/α1[5] homozygotes. The initial whole-cell recordings obtained from acutely dissociated SCG neurons from heterozygous

mice on the C57 genetic background suggested that functional nAChRs could be surface-expressed. However, the specific Bgtx sensitivity in α3/α1[5] homozygote or heterozygote mice in these preliminary studies was problematic. Whole cell current densities showed no significant difference in heterozygous mice before and after SCG neurons were treated with Bgtx. Meanwhile, C57 homozygous mice showed no ACh response in 37 degree cultured or acutely dissociated SCG neurons in this initial characterization.

2.3.2.2 ICR outbred strain: nAChRs from SCG neurons of α3/α1[5] (tm/tm) or α3/α1[5] (tm/+)mice showed functional Bgtx sensitivity

The official definition of oubred is "a closed population (for at least four generations) of genetically variable animals that is bred to maintain maximum heterozygosity" (Festing 1993). Outbred mice are genetically heterogeneous and outbred stocks have been used very successfully in genetic studies as a base population for selection to develop new or improved mouse models of human conditions. Outbred mice can offer a number of advantages over inbred strains in that they have longer life spans, generally fewer back ground lesions, disease resistance, and robust breeding (James G. Fox 2007).

In order to increase the overall health and mortality of homozygotes, α3/α1[5] transgenic mice were out-crossed with an outbred strain, ICR (Taconic, Hudson, NY). Interestingly, α3/α1[5] mice on the ICR strain produced homozygotes whose overall

health was greatly improved and survival was also increased. It is mostly the benefits due to increased heterozygosity from ICR mice. In some cases, α3/α1[5] homozygotes were almost indistinguishable from wild type littermates.

In addition to the immediate improvements in the health and survival of homozygotes, following crosses with the ICR outbred strain, the electrophysiological studies looked encouraging. The preliminary results from electrophysiological studies suggested that α3/α1[5] containing nAChRs were surface-expressed in the SCG neurons. Whole-cell recordings were performed using α3/α1[5] heterozygote, homozygote and wild type littermates to determine if functional α3/α1[5] containing receptors were being surfaced expressed in mouse sympathetic ganglion neurons. Typical whole cell recordings are shown in Figure 10. Unlike C57 homozygotes, ICR derived homozygotes showed detectable ACh responses in acutely dissociated SCG neurons. Furthermore, ACh responses in homozygote mouse SCG neurons were completely abolished following treatment with Bgtx. Bgtx treatment also significantly decreased ACh responses in a heterozygote, but not the wild type littermate. This suggests that α3/α1[5] can be surface expressed on SCG neurons in ICR derived mutants and the expressed receptors bear the functional sensitivity to Bgtx inhibition (Fig 11).

Taken together, the results obtained from mouse outcrosses with ICR outbred strain suggested Bgtx sensitive α3/α1[5] containing nAChRs are capable of surface expression in SCG neurons. Thus, even though functional Bgtx sensitivity is absent in C57 heterozygote mice and C57 homozygote mice could not show detectable ACh response in acute SCG preparations, the results obtained from ICR outcrosses mutants

indicate that α3/α1[5] containing nAChRs in SCG cells can assemble functional receptors conferring functional Bgtx sensitivity.

As general research animals, however, outbred mice have many other disadvantages: background data on characteristics will be unreliable and can change rapidly. For an outbred stock, generally nothing is known about the genetic characteristics of individual animals, i.e., what genes they carry or the extend of their heterozygoity. Each individual is genetically unique. This means that variability observed between animals may be due to their genetic differences. Therefore, in some ways, the experiment is more powerful than if the animals had been genetically identical (Chia, Achilli et al. 2005).

2.3.2.3 BALB/c inbred strain:

Interestingly yet not surprisingly, the reproducible inhibition by Bgtx treatment on heterozygous SCG neurons has been variable in mice carrying ICR background. As mention earlier, each individual mouse is genetically unique. Thus, the production of homozygous Kin inbred mice remained an important goal. In an effort to produce healthy Kin inbred mice with functional Bgtx sensitive α3/α1[5]-containing nAChRs comparable to Kin C57/ICR mice, several new inbred strains were introduced and tested. Among them, backcrossed BALB/c mouse gave the best and most reproducible results. The detailed results are discussed in later sections (2.3.4-2.3.11)

2.3.3 Upregulation of whole cell currents by 30°C treatment

A very important breakthrough came from the protocol used in SCG primary cultures which was tested and validated by Tanya Sanders. ACh response of SCG neurons cultured at 37ºC (3-4 days) and then shifted to 30ºC for 2-3 days can be dramatically upregulated compared to 37ºC treatment (Figure 12). The low temperature induced upregulation of whole-cell-responses appear regardless of the mouse genotype. It has been reported previously that the functional expression of the cloned *Torpedo* nAChR subunits in mammalian fibroblast cells is temperature-sensitive (Claudio, Green et al. 1987). In another report, *Drosophila* nAChR α subunits were unable to reproduce in a mammalian cell line at 37°C, but did so at a lower temperature of 25°C (Lansdell, Schmitt et al. 1997). The author interpreted this as demonstrating that the *Drosophila* nAChR subunits were misfolded when expressed at 37°C. The precise mechanism of low temperature induced nAChRs upregulation still remains unknown. The lack of detectable whole-cell ACh response in acute dissociated or 37°C cultured SCG preparations of homozygous Kin C57 inbred mice and other inbred strains might indicate that α3/α1[5] subunit assembly or receptor trafficking is not efficient for normal levels of membrane expression of α3/α1[5] containing receptors. When treated at 30°C for 1-3 days, all SCG neurons in homozygous mice crossed with BALB/c or DBA inbred strain produced detectable whole-cell ACh response. Thus, the protocol of recordings on acutely dissociated SCG neurons was discarded. In all of the following experiments, all SCG neurons tested were dissociated, 37°C cultured and shifted to 30°C for 2-3 days prior to electrophysiological studies.

2.3.4 Using α3/α1[5] (tm/tm)/α7(-/-) double homozygotes enables an endogenous Bgtx-binding free background

Five nAChR genes are expressed by rodent sympathetic neurons: α3, α5, α7, β2, and β4 (De Koninck and Cooper 1995). Even though the α3β4 subtype is thought to comprise the majority of ganglionic receptors, rodent SCG neurons express significant amounts α7 mRNA (Mandelzys, Pie et al. 1994; Zhou, Deneris et al. 1998). The role of α7 in mammalian sympathetic ganglia is poorly understood. These receptors are not thought to directly participate in ganglionic transmission, but might play a role in modulation of ganglionic transmission. However, CNS studies using α3/α1[5] Kin mice will be further complicated by the presence of endogenous, high affinity Bgtx binding α7 homomeric receptors. In an effort to facilitate the initial characterization of α3/α1[5] Kin mouse on a background lacking endogenous high affinity Bgtx receptors, α3/α1[5] Kin mice were crossed with α7 knockout mice.

2.3.5 Evidence for functional surface-expression of α3/α1[5] containing nAChRs in BALB/c α3(tm/tm)α7(-/-) double mutants

Surface expression analysis of α3/α1[5] containing receptors was performed on SCG neurons from male and female α3(tm/tm)α7(-/-) double homozygotes mice in age from 2 to 4 weeks. ACh evoked currents in 37ºC cultured and 30ºC treated mouse SCG

neurons were examined to investigate the expression level. At holding potential of -60 mV, 100 μM ACh evoked fast-desensitizing, dose-dependent transient inward currents in SCG neurons (Figure 13).

2.3.6 Evidence for α3/α1[5]-containing nAChRs confer functional Bgtx Sensitivity in BALB/c α3(tm/tm)α7(-/-) double mutants

Analysis of Bgtx sensitivity was performed on SCG neurons from α3(tm/tm)α7(-/-) double homozygous mice. This ACh response was completely blocked after 30 min-incubation with 100 nM Bgtx (Figure 13). In contrast, the ACh-evoked currents from SCG neurons expressing the wild type α3 showed no block after incubation with 100 nM Bgtx. In addition, Bgtx had no significant effect on the peak amplitude of ACh responses in SCG neurons from wild type mice. This observation reassured that any observed Bgtx sensitivity was due to α3/α1[5] containing receptors in Kin mouse SCG neurons. Moreover, the results also suggest that α7 does not directly contribute to the ACh evoked whole cell responses in these SCG neurons.

2.3.7 Association kinetics of Bgtx to α3/α1[5] containing receptors in sympathetic neurons of α3/α1[5] knock-in mice

So far, preliminary electrophysiological recordings have shown that α3/α1[5] -containing nAChRs in α3/α1[5] transgenic mice will bind and are blocked by Bgtx. Based on previously published work on recombinant α3/α1[5]β2 and α3/α1[5]β4 receptors expressed in oocyte (Levandoski, Lin et al. 1999), an incubation time of 10 min is sufficient for Bgtx to approach full equilibration, very similar to that for the association of Bgtx with the muscle type of nAChR. Whereas, for recovery from toxin block, half-times ($t1/2$) are 233 min for *Torpedo* α1βγδ and 18 min for α3/α1[5]β4.

To address the association and dissociation rates of Bgtx to α3/α1[5] receptors in native conditions, similar experiments were carried out to measure the onset and offset of Bgtx block. The experiments that form this aim will be important for establishing the experimental conditions for α3/α1[5] as a tool for biochemical applications. For instance, "Toxin-precipitation" would offer a powerful means for isolation of nAChR subunits. Establishing association and dissociation rates of Bgtx to α3/α1[5] receptors will be important to pave the way for future biochemical studies, i.e., toxin-precipitation, or use ^{125}I-Bgtx for autoradiographical analysis to map of the distribution of α3/α1[5]-containing nAChRs in mouse brain sections.

The results of kinetic analysis of Bgtx blockage on α3/α1[5] containing receptors are shown in Figure 14. The control responses to a 1 s pulse of 200 μM ACh were recorded, at time 0. Then the cell was perfused by the external solution with 100 nM Bgtx and the response to a co-application of 200 μM ACh and 100nM Bgtx was recorded again. Between subsequent co-applications at the indicated times, the cell was maintained in 100 nM Bgtx. The data are shown as plots of $I_{\text{co-application}}/I_{\text{control}}$ vs. time in 100 nM

Bgtx, where $I_{\text{co-application}}$ is the peak response evoked by the co-application at the specified time point and I_{control} is the initial peak current to the pulse of 200 μM ACh in Bgtx-free solution. As shown in Figure 14B, following an initial application of 200 μM ACh and further incubation in 100 nM Bgtx between successive test co-applications, the evoked currents of SCG neurons expressing the α3/α1[5] were greatly reduced over a 5-min period. To measure the recovery from Bgtx block, ACh responses were obtained for each cell 1 hour after exposing the cell to Bgtx. 1-hour pre-incubation with 100nM Bgtx is expected to be sufficient for maximal Bgtx blockage. This peak response to ACh pulse is set as control I_{control}. Following the control recording, the recovery was initiated by washout with Bgtx-free external solution. $I_{\text{time-x}}$ is the peak response to ACh pulse of the same dose at the x time point during the washout. The fraction of maximal block ($I_{\text{time-x}} - I_{\text{control}}$)/$I_{\text{control}}$ was plotted as a function of the time of washout.

2.3.8 ACh dose-response relationship reveals an unaltered EC_{50} to ACh in α3/α1[5] BALB/c homozygote mouse

One may argue that replacement of 5 amino acids in the critical region where binding pocket forms may change the pharmacological profiles of α3/α1[5] receptors in neurons where largely unknown biological processes occur. To address this issue, dose response curves for ACh were generated. ACh-induced currents were measured under voltage-clamp mode at -60 mV holding potential. ACh (1 μM - 5 mM) was administered

via a pipette for 2 s. Since repeated applications of ACh in higher doses often caused desensitization of the current, cells were perfused for more than 2 minutes between 2 adjacent drug applications. A lower dose of ACh was used first. The subsequent dose was at least 100 times higher in order to generate the dose-response curve. The data from the same culture were pooled for plotting dose response curves.

The data shown indicate that EC_{50} values of ACh for WT and homozygote littermates are very close and that the EC_{50} of Het slightly higher than its WT littermate (Figure 15). This may suggest that introducing α1[5] does not largely functionally perturb ACh binding to a great extent in α3/α1[5] receptors in BALB/c homozygote mice.

2.3.9 Current-voltage relationship of ACh-induced current reveals characteristic inward rectification of α3 nAChRs in α3/α1[5] BALB/c homozygous mouse

ACh-evoked currents through nicotinic receptors on neurons are carried by small monovalent and divalent cations. A property common to all functional neuronal nicotinic receptors is that they conduct inward current when the membrane potential (V_m) is negative, but pass little outward current when V_m is positive. Physiologically, this inward rectification serves important functions. For presynaptic receptors, inward rectification ensures that the receptors will not depress transmitter release by decreasing the input resistance of the terminal. For postsynaptic receptors, fluctuations in membrane potential near rest change the conductance of the receptors and consequently affect synaptic

effectiveness (Haghighi and Cooper 2000). The factors that cause neuronal nAChRs to rectify have not been fully characterized. Previous studies suggest that inward rectification of neuronal nAChRs can result from a voltage-dependent block by intracellular spermine and possible intracellular Mg^{2+} may also contributes (Mathie, Colquhoun et al. 1990; Sands and Barish 1992; Haghighi and Cooper 1998). Nevertheless, if rectification is not constant, then changes in rectification can alter synaptic efficacy.

To observe the rectification on SCG neurons, I applied voltage ramps to change V_m from −80 mV to +100 mV. 200 μM ACh was applied for 2 s to the patched cell at -80 mV holding potential. The cell was then voltage-clamped at a different potential and the same dose of ACh was applied. The interval of the ACh administrations (5 min) was determined in preliminary experiments to avoid desensitization of the current. I obtained the current-voltage (*I-V*) curve by plotting the peak current ACh application as a function of holding potential. The *I-V* curve shown in Figure16 exhibits a strong inward rectification. Comparable inward rectification has been reported previously for ACh-evoked currents in adult mouse SCG neurons. The *I-V* curve generated here closely resembles that of previously reports (Haghighi and Cooper 1998; Feng, Mellor et al. 2000). This suggests that the inward rectification properties of α3/α1[5]-containing nAChRs are minimally affected by introduction of the mutation in Kin BALB/c mice.

2.3.10 Pharmacology of α3/α1[5]-containing nAChRs to methyllycaconitine

The objective for this aim is focused on establishing the pharmacology of the mutant α3/α1[5]-containing receptors with respect to the well-known α7 antagonist, methyllycaconitine (MLA). The reason for this study is based on the high affinity interaction between Bgtx and homomeric α7 receptors, which are known to be expressed in the autonomic nervous system as well as in the CNS. Studies have shown that MLA potently inhibits Bgtx at low nanomolar concentrations in rat brain membrane preparations (Ward, Cockcroft et al. 1990; Navarro, Xu et al. 2002). Thus, we hypothesize that MLA can be used to discriminate between α3/α1[5]-containing receptors and endogenous neuronal Bgtx binding sites in α3/α1[5] Kin mice by blocking α7 nAChRs. Oocyte studies done previously in our lab showed that α3/α1[5]-containing receptors are inhibited by MLA at high μM concentrations.

I aimed to obtain IC_{50} values for Methyllycaconitine (MLA) block on neurons from WT and α3(tm/tm) homozygote littermates. Firstly, ACh response was measured in drug-free solution to serve as control response. 20-min incubation with desired dose of MLA was followed. The responses to ACh were measured in a mixture of ACh plus MLA. The fraction of the control response ($I_{\text{post-drug}}/I_{\text{control}}$) was plotted *versus* the MLA concentrations. As shown in Figure 17， α3/α1[5]-nAChRs, like wild type α3 nAChRs, are only sensitive to μM concentrations of MLA. The dose inhibition relationships show that MLA sensitivity on mutant receptors falls into the several hundred μM range. This result will enable us to use MLA to inhibit Bgtx sensitive α7 receptors without affecting α3/α1[5].

2.3.11 Rank agonist profile has pharmacological characteristics indicative of α3β4 nAChRs

Considering that nAChRs in SCG neurons are a mixed population (α3α4 and α3β2 are thought to be dominant) with each subtype having distinct pharmacological features, any interpretation of data should be made with extra care. We thus reasoned that using a heterologous expression system would serve as a good place to start for initial pharmacological characterization of α3/α1[5]. The two-electrode voltage clamp technique was used to study oocyte-expressed nAChRs. Single subtype was studied each time. The aim of this study was to characterize the pharmacological properties of currents activated by nicotinic agonists to determine whether different receptor subtypes become apparent. A similar approach has been used successfully to demonstrate that nAChRs on neurons in the medial habenula are different from those on neurons in the interpeduncular nucleus (Mulle, Vidal et al. 1991).

In this series of experiments, oocytes were voltage-clamped at −60 mV. ACh (50 μM) was applied for 5 s while the oocyte was perfused with normal external solution. Subsequently, 50 μM solutions of agonists to be tested were applied to the cells. 5 min perfusion of normal external solution was followed after each drug pulse to ensure recovery from desensitization of nAChRs. The same protocol was applied to whole-cell recording on SCG neurons from homozygotes. The agonist study of α3/α1[5] receptors in mouse SCG shows that the receptors are responsive to these widely used ligands. In addition, when compare to wild type α3β4 or α3β2 expressed in oocytes, the profile looks most similar to α3β4, suggesting α3/α1[5] preferentially assemble with β4 subunit

resulting in a major dominate α3/α1[5]β4 subtype in SCG neurons (Figure 18). This result is also consistent with other evidence showing that the α3β4 receptor is the prevalent subtype of autonomic ganglia neurons (Covernton, Kojima et al. 1994; Colquhoun and Patrick 1997).

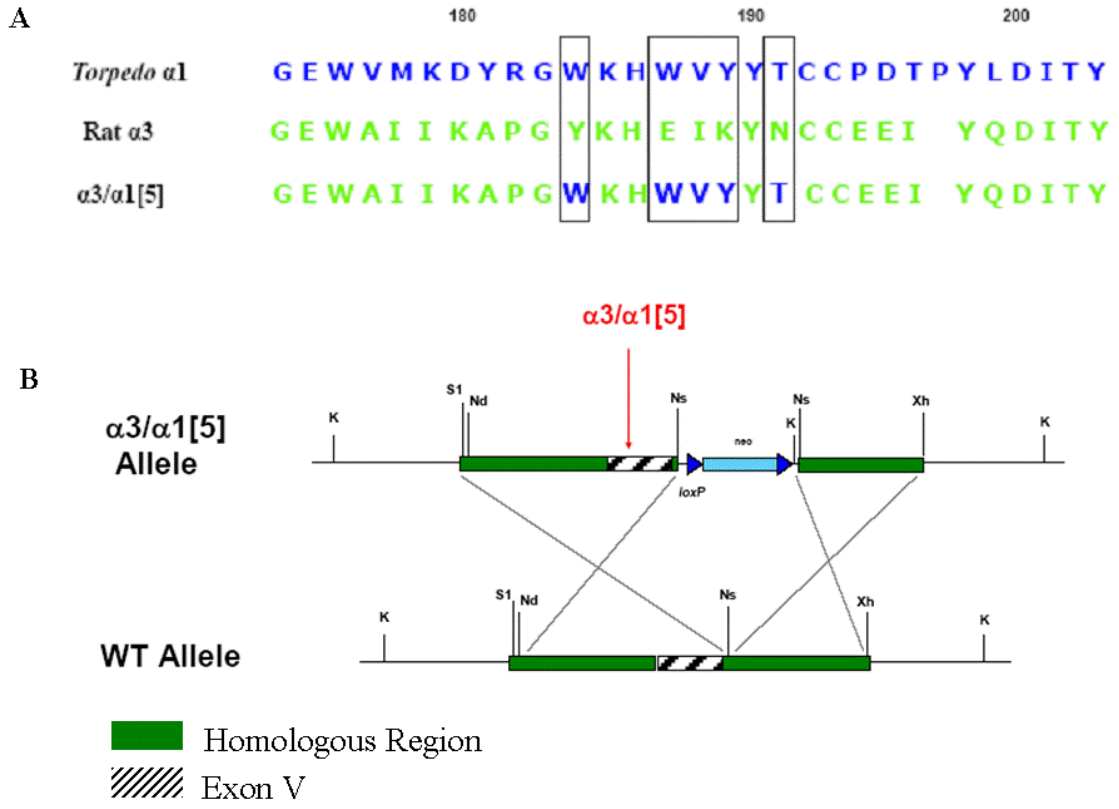

Figure 9. The α3/α1[5] targeting construct overview. A) Protein sequence alignment showing the 5 amino acids in the exonV region of mouse α3 that were substituted with the corresponding residues from *Torpedo* α1. B) The α3/α1[5]-containing recombinant allele and wild type allele. (Graph provided by Phil Caffery)

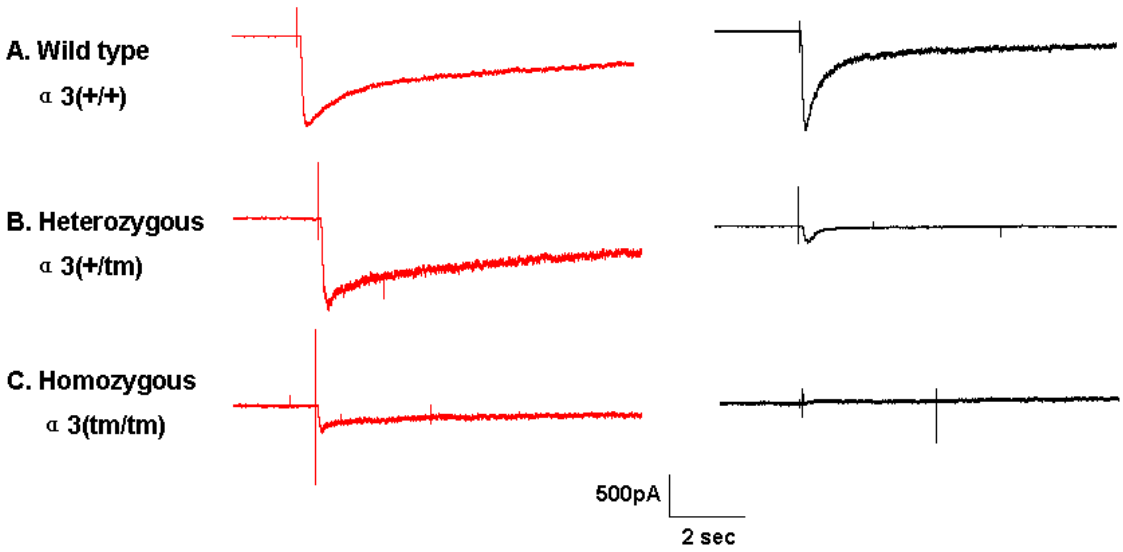

Figure 10. ACh currents were affected differently by 1 hour Bgtx incubation among ICR Wild type, Heterozygous and Homozygous littermates. Each representative trace shows the whole-cell currents obtained from individual SCG neuron having the same membrane capacitance. A shows the representative traces recorded from P25 WT mouse neurons in absence of Bgtx (in red) and treated with 1 hour Bgtx (100 nM) pre-incubation (in black) in response to 200 μM ACh. B shows the representative traces recorded from the P27 α3(+/tm) mouse neurons in absence of Bgtx (in red) and treated with 1 hour Bgtx (100 nM) pre-incubation (in black) in response to 200 μM ACh. C shows the representative traces recorded from P18 α3 (tm/tm) SCG neurons in absence of Bgtx (in red) and after 1 hour Bgtx (100 nM) pre-incubation (in black) in response to 200 μM ACh. In Het SCG neurons, after treatment of 1 hour Bgtx (100 nM) pre-incubation, 200 uM ACh induced currents were remarkably reduced. 1 hour Bgtx (100 nM) incubation abolished all the detectable currents in P18 Homo (tm/tm) SCG neurons.

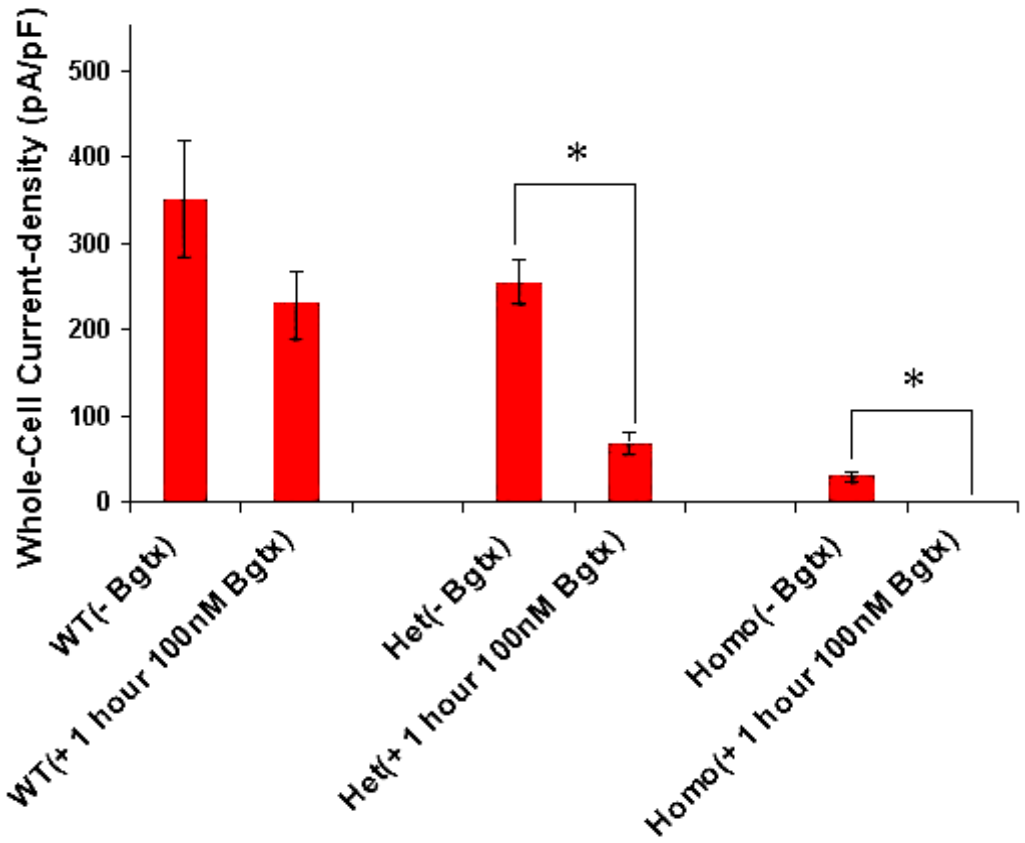
Whole-Cell Current-density (pA/pF)
500
400
300
200
100
0
*
*
WT(- Bgtx)
WT(+ 1 hour 100nM Bgtx)
Het(- Bgtx)
Het(+ 1 hour 100nM Bgtx)
Homo(- Bgtx)
Homo(+ 1 hour 100nM Bgtx)

Figure 11. Bgtx significantly blocked ACh currents in heterozygous and homozygous SCG neurons. Analysis of 200 μM ACh-induced current density of SCG neurons from Wild type (WT), Heterozygote (Het) and Homozyote (Homo) ICR HH35A littermates. Two groups of neurons in absence of Bgtx or with 1-hour Bgtx pre-incubation were examined for each genotype. Each column represents mean ± SEM. The decrease of current density in Het SCG neurons with 1 hour Bgtx (100 nM) was found to be significantly different as compared with Het SCG neurons without treatment of Bgtx ($P<0.001$, t-Test; n=5 and 5, respectively). The same significant difference was also noted in Homo ($P<0.001$, t-Test; n=5 and 5, respectively). No significant difference was noted in WT ($P > 0.1$, t-Test; n = 5 and 5, respectively). These findings show that 1-hour 100nM Bgtx significantly blocked ACh currents in Het and Homo SCG neurons but not WT, suggesting that α3/α1[5]-containing receptors are functionally expressed and have sensitivity to Bgtx.

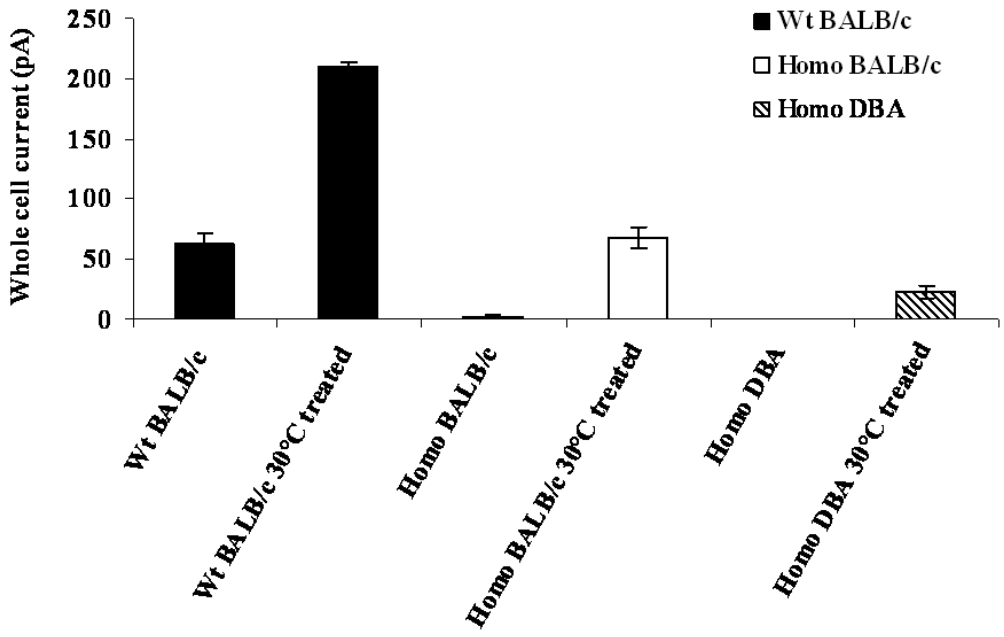

Figure 12. Culturing mouse SCG neurons at 30°C up-regulates whole cell currents regardless of the genotype or its genetic background. 3 different animals were tested as indicated: a wild type BALB/c, a homozygous BALB/c and a homozygous DAB. Currents recorded from cells that were 37°C cultured or 37°C cultured with a following incubation at 30°C for 24-72 hours (as indicated). 30°C treatments increased whole cell current as judged by the gain of whole-cell current density to 100 μM ACh. Each column represents mean ± SEM, n= 3~5.

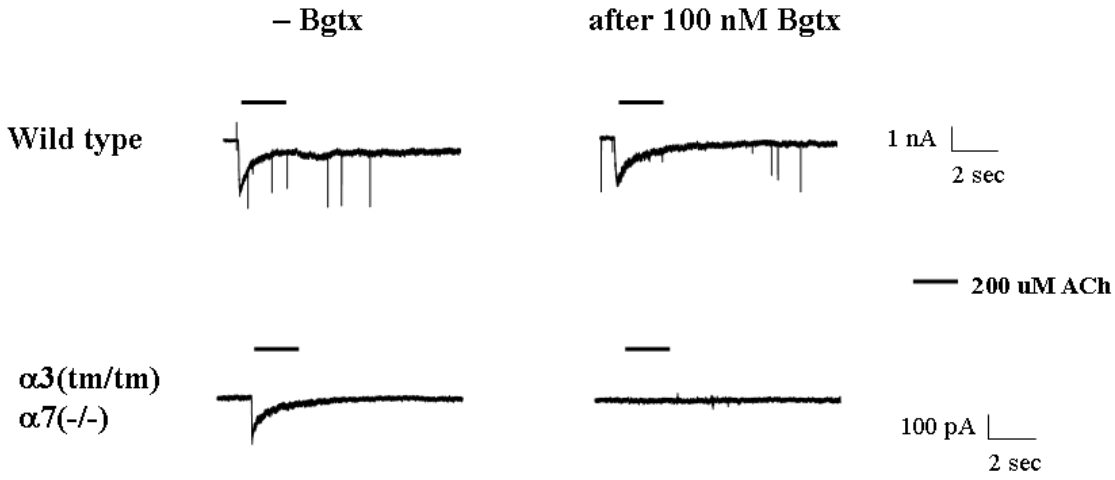

Figure 13. Evidence for functional membrane expression of α3/α1[5] containing nAChRs in BALB/c double homozygous α3(tm/tm)α7(-/-) mouse. Sample traces obtained from two groups of neurons in absence of Bgtx or with 30 min Bgtx pre-incubation as indicated. Bgtx completely blocked ACh induced responses in 30ºC treated double homozygous SCG neurons. In contrast, incubation with 100 nM Bgtx had not apparent effect on ACh currents from wild type SCG neurons.

A

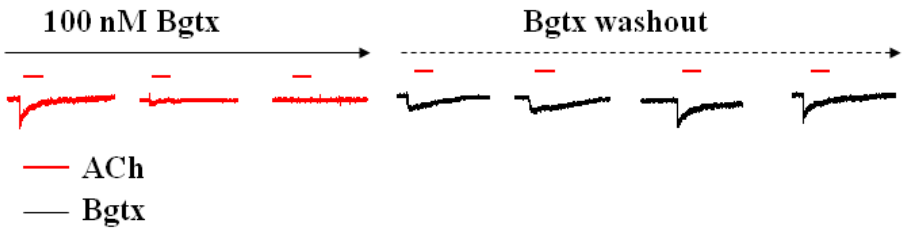
100 nM Bgtx
Bgtx washout
ACh
Bgtx

B

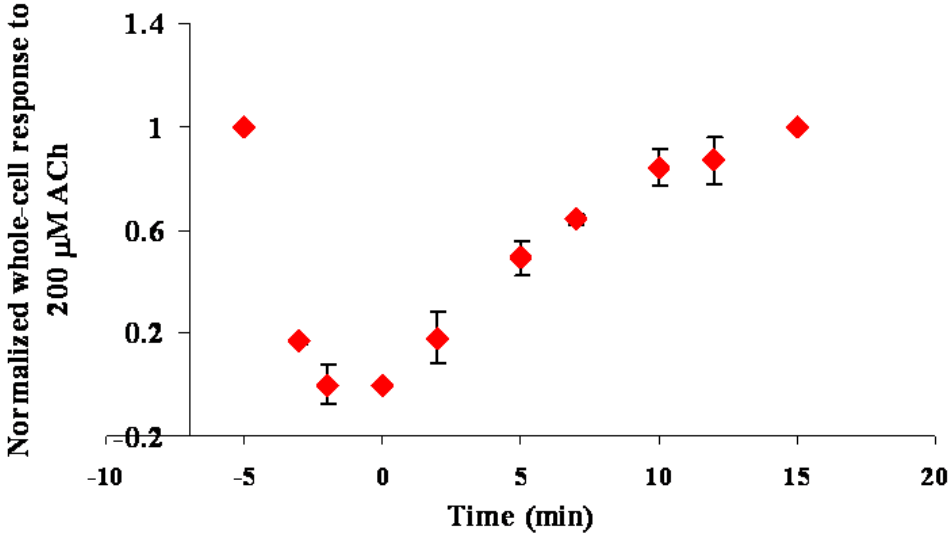
Normalized whole-cell response to 200 µM ACh
1.4
1
0.6
0.2
-0.2
-10
-5
0
5
10
15
20
Time (min)

Figure 14. Kinetic analysis of Bgtx block of α3/α1[5] receptors reveals a rapid and reversible block on α3/α1[5] containing receptors as studied in a α3(tm/tm) BALB/c mouse. A) Functional α3/α1[5] -containing receptors were surface-expressed and blocked by Bgtx. Currents induced by 200 μM ACh during (-5 min to 0 min) and after washout (0 to 20 min) of 100 nM Bgtx treatment. B) Bgtx rapidly and completely blocked whole cell currents within 3 minutes. Currents recovered within 15 minutes following washout. The control responses to 200 μM ACh was recorded, at time -5 min. The current density of the control responses was 11.8± 2.1 pA/pF (n=3) in average. Then 100nM Bgtx was begun, and the response to a co-application of 200 μM ACh and 100 nM Bgtx was recorded. Between subsequent co-applications after time -5 min to 0, the cell was maintained in 100 nM Bgtx. At time 0, the washout began. The data are shown as plots of $I_{test}/I_{control}$ vs. time, where I_{test} is the peak response at that time point and $I_{control}$ is the initial peak current to 200uM ACh in Bgtx-free solution. Error bars indicate SEM, n=3.

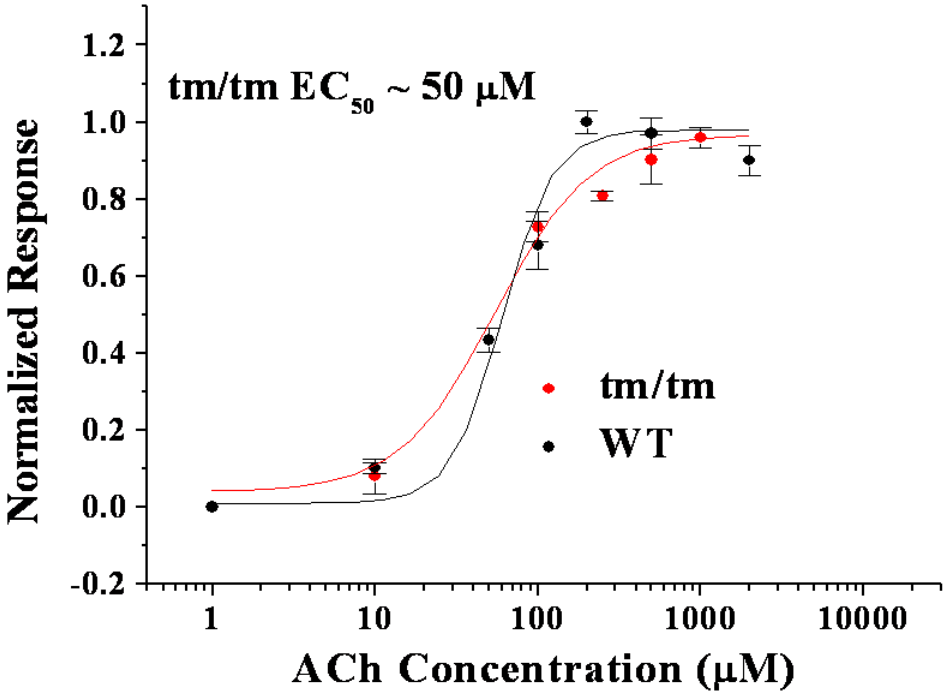

Figure 15. ACh dose-response relationships for α3/α1[5] receptors in BALB/c α3/α1[5] homozygous and wild type mouse SCG neurons . Data were logistic fitted, with EC_{50} of ACh equals 48±2 μM for α3/α1[5] homozygous and 64±3 μM for wild type. All cells were 37 °C cultured and 30 °C treated for 2-3 days Data points are the mean ± SEM (n=3-4) .

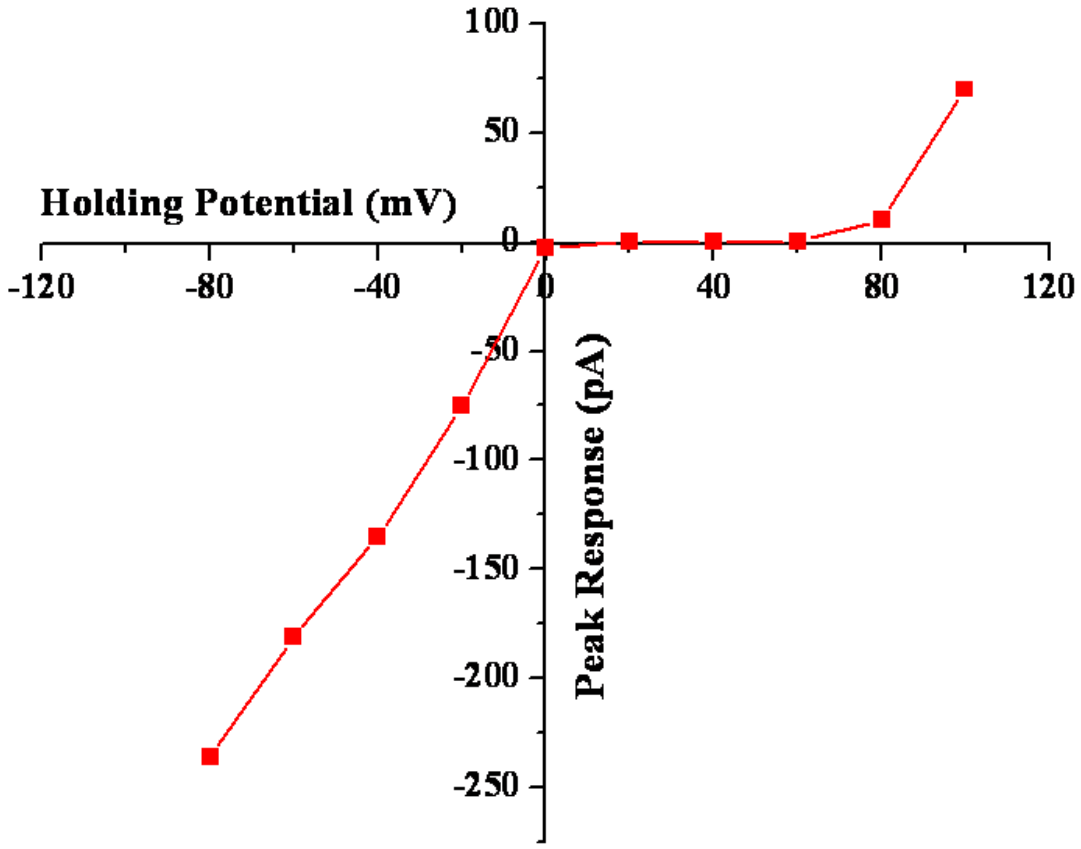

Figure 16. Current-voltage relationships for α3/α1[5] receptors in BALB/c homozygous mouse SCG neuron. Data are the plot of the peak current induced by 200 μM ACh as a function of the holding potential. The currents were linear within the range of –100mV to 0mV. The currents ceased to be inward at a potential ≈0mV, similar to published results for wild type nAChRs in SCG neurons (E Cooper, 2000). Channels exhibited strong inward rectification, and no outward currents were detected at holding potential up to +60mV.

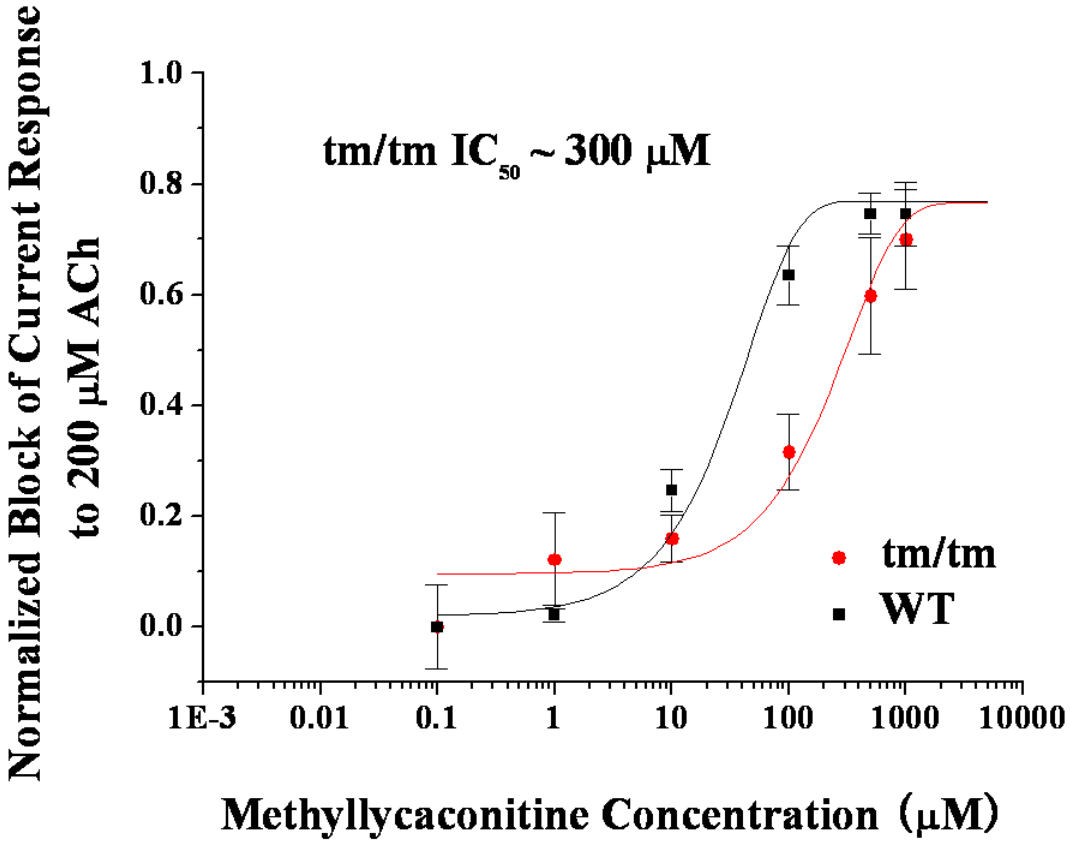

Figure 17. Methyllycaconitine (MLA) blocks α3/α1[5] receptors in a dose dependent manner. Fitted curve shows the dose inhibition relationships for the effect of extracellular MLA on mutant receptors in BALB/c double homozygous mouse (α3(tm/tm) α7(-/-)(in red, IC_{50} = 333±24 μM) or BALB/c wild type mouse(in black, IC_{50} = 40±2 μM) SCG neurons. The cells first received an initial control application of 200 μM ACh followed by co-application of 200 μM ACh plus indicated concentration of MLA. There was 2 min washout before the subsequent drug application. All cells were 37 °C cultured and 30 °C treated for 2-3 days. Data were logistic fitted and data points are mean± SEM (n=4~6).

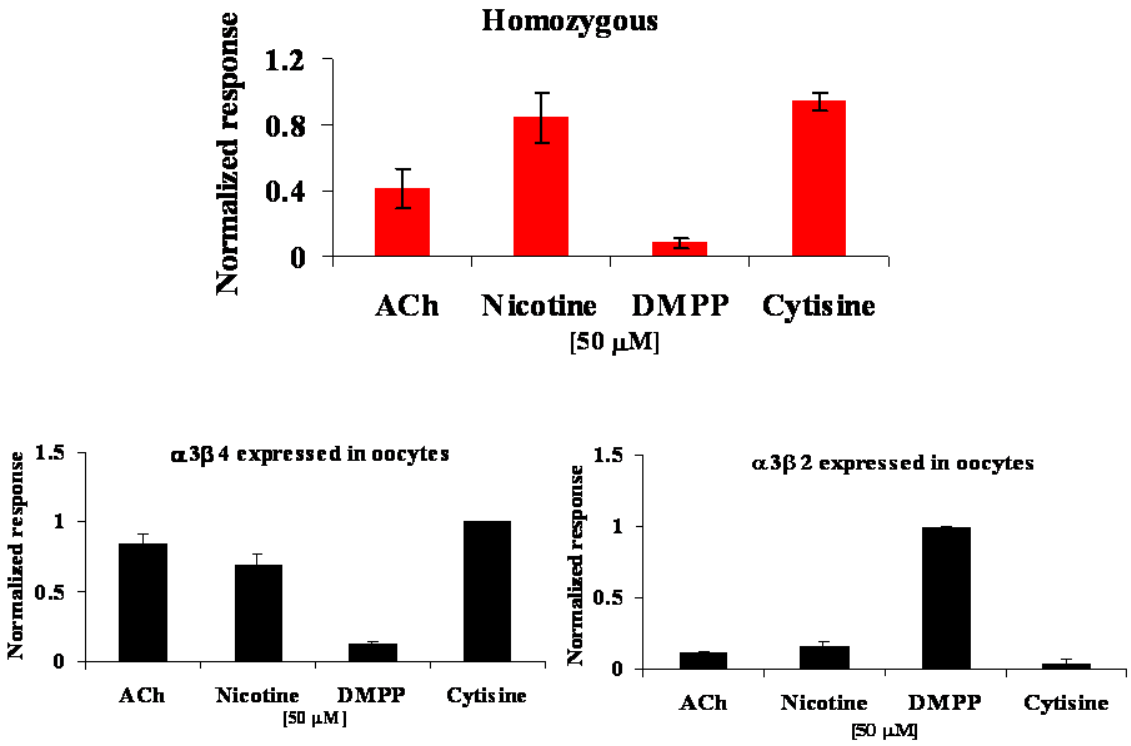

.Figure 18. Rank of agonist profile suggests that α3/α1[5]β4-containing nAChRs predominate in BALB/c homozygous mouse SCG neuron. 50 μM agonist profiles in SCG neurons from BALB/c homozygous animals (in red) show that cytisine is a more potent agonist than 1,1-dimethyl-4-phenylpiperazinium (DMPP). In combination with *Xenopus* oocyte expression studies (in black), this suggests a predominant contribution of the β4 subunit to the population of functional α3/α1[5] nAChRs expressed in the SCGs of the Kin mice. Data points are mean± SEM (n=4~6)

2.4 DISCUSSION

2.4.1 Functional α3/α1[5]-containing receptors membrane expression was demonstrated by electrophysiological recordings

The essential task of characterizing basic electrophysiological and pharmacological properties of α3/α1[5] receptors in mouse SCG neurons has been addressed in chapter 2 in this dissertation. Now we know that it is possible to transform the normally Bgtx insensitive neuronal α3 nAChR subunit into Bgtx-sensitive by substituting 5 amino acids with the corresponding residues derived from muscle type *Torpedo californica* α1 subunit. It is also possible to introduce the mutation into the genome of a mouse to produce a knock-in mouse that carries the pharmatope. I have shown and demonstrated that the Kin mice are capable of expressing the functional chimeric α3/α1[5] subunit in mouse SCG neurons. Those α3/α1[5] receptors in mouse SCG neurons can confer functional Bgtx sensitivity, with pharmacological and biophysical properties of the channel largely unaltered. This initial electrophysiological characterization of α3/α1[5] containing receptors also establishes the experimental conditions for future studies and applications.

2.4.2 Visualization of α3/α1[5]-containing nAChRs labeled with fluorescent Bgtx

Additional evidence of the membrane expression of α3/α1[5] containing receptors came from live surface-staining studies using fluorescence Bgtx. Dr. Cooper and Arjun Krishnaswamy in McGill University did this study, and the results are shown in Figure 19. SCG dissected from α3(tm/tm)α7(-/-) and wild type control mice were incubated for 1 hour in presence of 100 nM rhodamine-conjugated Bgtx. The SCGs from homozygous and wild type mice were then post fixed and prepared for immunohistochemistry. Antibodies against vesicular acetylcholine transporter (VAChT) and the heavy chain of neurofilament (NFM-H) were used for labeling presynaptic varicosities and axons, respectively. The figure shows that Bgtx binding sites are absent in the ganglia of the wild type control. In contrast, somatic and dentritic Bgtx labeled receptor clusters are clearly observed in the ganglia from the homozygous animal. Moreover, the Bgtx labeled receptor clusters are co-localized with VAChT, indicating that they are synapse-associated proteins. The Bgtx labeling experiments thus provided additional convincing evidence that Bgtx sensitive α3/α1[5] containing nAChRs are being expressed in the transgenic mice.These results make Bgtx-labeling a legitimate strategy for other *in vivo* experiments.

2.4.3 No ACh response detected in α3 null mouse SCG neurons

One very common concern with using transgenic mice is that compensatory systems can be activated in the mutants that may mask the expression of the resulting phenotypes. In order to rule out the possibility that the observed ACh responses came from other non-α3 nAChRs as a consequence of the transgene, the α3 null mouse with

deletion of exon 5 was purchased and tested for possible up-regulation of other subunits that might account for whole cell currents observed in α3/α1[5] homozygous mice. The null mice survived to birth but with severely impaired growth and mortality, demonstrating that α3 is an essential component of the nicotinic receptors mediating normal function of the autonomic nervous system. The ACh response test on SCG neurons from α3 null mice was performed by Dr. Tanya Sanders in the lab. In identical experimental conditions as in 2.3.3, where SCG neurons were cultured at 37ºC (3-4 days) and then shifted to 30ºC for 2-3 days to up-regulate the whole cell ACh response, no whole cell currents were ever detected using patch clamping (data not shown). This is consistent with previous reports demonstrating that disrupting the α3 gene eliminates fast excitatory synaptic potentials on postganglionic sympathetic neurons. Other subunits, including α5, β4, β2 and α7 are co-expressed in mouse SCG neurons. However, complete deletion of α3 subunit did not result in functional formation of ACh receptors by other non-α3 subunits. The results indicate that α3 is prerequisite for ACh responses seen in SCG neurons. More importantly, the observation obtained from α3 null mice provides additional evidence that the ACh responses produced in α3/α1[5] homozygous SCG cells were due to the surface expressed α3/α1[5] nAChRs. Moreover, the α3-deficient mice are too ill for meaningful behavioral studies, our α3/α1[5] therefore would be valuable for evaluating the function of α3 in central tissues.

2.4.4 Phenotypic variability of α3/α1[5] homozygotes

2.4.4.1 General health and survival

The initial efforts of producing "healthy" α3/α1[5] homozygotes using S129/C57 heterozygote mice were not successful. The early generations of α3/α1[5] homozygotes in mixed S129/C57 displayed a phenotype resembling that of the α3 knock out. The animals were very unhealthy and severely runted at birth. Most homozygotes died at early stages. Unexpectedly, N1 heterozygote mice, produced by backcrossing α3/α1[5] mice into C57BL/6 inbred strain, gave birth to some homozygotes whose overall healthy and life-span were greatly improved. An outbred strain ICR was also tested to outcross our α3/α1[5] mice. Crosses between α3/α1[5] mice and ICR strain produced even healthier homozygotes that sometimes indistinguishable from the wild type littermates. Later in the efforts of producing less variable homozygotes with well characterized genetic background, so that the mouse model can have the greatest experimental value, several other inbred strains were crossed with our Kin mice and electrophysiologically tested. Notably, backcrossing into C57BL/6 has significantly improved lifespan and the overall health of α3/α1[5] homozygotes. Inbred trains of BALB/c, DBA, FVB and CH3 were also tested. However, C57BL/6 homozygote pups have the shortest life span versus other inbred strains being tested. Among the tested inbred strains, crosses with BALB/c had produced the homozygotes with the best appearance, overall health, life span and breeding behaviors.

2.4.4.2 Whole cell ACh response

There was little ACh response detected from 37ºC cultured SCG neurons in the C57 background. BALB/c, DBA, FVB and CH3 strains produced detectable ACh response from 37ºC cultured SCG neurons in α3/α1[5] homozygotes. We have noticed, however, that the BALB/c strain produces robust ACh responses in cultured SCG neurons with or without 30ºC treatment as shown in Figure 12. Moreover, these ACh responses from BALB/c mutant mice give rise to the largest whole-cell current density vs. other inbred strain DBA, FVB, CH3 and C57 under the same culture condition (personal communication with Tanya Sanders).

2.4.4.3 Functional Bgtx sensitivity

Functional Bgtx sensitivity and membrane expression of α3/α1[5]-containing receptors are demonstrated in BALB/c α3/α1[5] homozygotes. Initially, α3/α1[5] knock-in mice were maintained on a mixed 129/C57 background. However, early efforts of demonstrating surface expression of functional Bgtx sensitive α3/α1[5] receptors are not very successful using C57BL/6 homozygote pups. There was little ACh response detected from 37ºC cultured SCG neurons. BALB/c strain, however, produced robust ACh responses, which were consistently blocked by Bgtx, namely, displaying functional Bgtx sensitivity. The Bgtx sensitivity was also variable in homozygotes produced by ICR outbred strain crosses. Crosses of DBA, FVB and CH3 inbred stains produced

homozygotes with ACh responses of smaller amplitude than those seen with the BALB/c background.

Theoretically, assuming: 1) α3/α1[5] and α3 subunits' transcripts are expressed equally in heterozygous animals carrying one copy of wild type gene and one copy of mutated gene; 2) nAChRs in SCG neurons have a stoichiometry of [α3]2[β4/β2]3, ¾ nAChRs are expected to contain at least one α3/α1[5] subunit in heterozygous mice. In these cases, ¼ of nAChRs in each SCG neuron are expected to be purely α3/α1[5] containing; ¼ to be purely wild type; ½ to be hybrids containing one α3/α1[5] subunit and one α3 subunit. Preliminary whole-cell recording results obtained from ICR heterozygous mice indicated that some ACh responses were sensitive to Bgtx in some cases. Figure 20 shows time dependent Bgtx block on ACh responses in SCG neurons from ICR crossed C57BL/6 heterozygote mice. However, this Bgtx sensitivity was not reproducible in the ICR crossed hererozygote mutants.

2.4.5 Consideration of genetic background

This variability of phenotype as well as Bgtx sensitivity of our transgenic product in different inbred or outbred stains raises the question of whether the genetic background of a mouse plays a role in expression of the transgenic product. Even though it is difficult at this moment to demonstrate that the expression is indeed influenced by other sequences/genes in or near the transgene, numerous strain-dependent variations in transgene expression have been documented else where (Allen, Norris et al. 1990). The

noted strain-dependent phenotypes suggest the presence of the influence of some modifier genes. We shall consider this possibility. The observations suggest that variations we observed were likely attributable to background genes. For instance, animals had been backcrossed to C57BL/6 mice for multiple generations, so their genetic background can be considered identical. Expression level, however, varied much between BALB/c/C57 hybrid homozygotes and genetically uniform C57BL/6 homozygotes. Moreover, in several cases, heterozygous and homozygous mice outcrossed with the ICR outbred strain expressed high levels of Bgtx sensitive ACh responses in acutely dissociated SCG neurons. Figure 21 compared Bgtx sensitivity in α3 (+/tm)α7(-/-) mice with C57BL/6 or ICR crossed C57BL/6 background. These results suggested that the ICR genetic background might have assisted in α3/α1[5] expression.

Strain-related problems have been reviewed by a number of authors (Nelson and Young 1998; Holschneider and Shih 2000). Accumulating data support the premise that naturally occurring nAChR subunit gene variability contributes to phenotypic diversity in strains. It has been shown that polymorphisms in genes that encode the nAChR subunit family contribute to phenotypic variability among mice (Tritto, Stitzel et al. 2002). Numerous studies provide direct evidence for the role of these polymorphisms in regulating nAChR sensitivity to nicotine or ethanol (Owens, Balogh et al. 2003). In one fairly recent report, mouse strain-specific expression of nAChR subunits α3, α4, α5, α7, β2, and β4 was evaluated in the dorsal hippocampus in mouse strains BALB/c, C3H/J, C57BL/6, CBA/J, DBA/2, Long Sleep (LS), Short Sleep (SS), and CF1 (Gahring, Meyer et al. 2003). The author in this study reported strain-related differences in cell type-specific nAChR expression. The results were correlated with published parameters of

strain sensitivity to nicotine as stated by the authors. Attempts to identify the origin of this significant difference in nAChR expression among strains included comparison of the entire subunit gene sequence. Although multiple polymorphisms were identified, clear correlation with strain-related differences in nAChR expression were proven to be too difficult to pinpoint. Nevertheless, these findings suggest that mouse strain-specific behavioral and physiological responses to nicotine are likely to reflect of a complex interplay between genetic factors that shape differences in expression and cellular architecture of nAChRs in mouse CNS.

My studies showed a notable variability in the expression of Bgtx sensitive ACh response in Kin mice carrying different gene backgrounds. At present, however, we have no data that bear directly on the mechanism of variation. Growing data indicate that strain differences in behavioral variables and neuronal markers are much more common than usually thought (Stitzel 2008). In this regard, it is important to emphasize that variation in transgene expression is likely to be extremely common. My main interest has been in characterizing the nature of the α3/α1[5] containing receptors in our Kin mouse model. Clearly, the choice of an appropriate genetic model can contribute to an interpretation of positive results and help to avoid misleading interpretations of negative results. The good news is, although notable variability in the expression of Bgtx sensitive ACh response in different strains tested, BALB/c inbred strain has demonstrated its merit in expressing functional Bgtx sensitive α3/α1[5]-containing receptors in SCG preparations. In keeping strain-specific variations in mind, we will continue using as well as testing BALB/c inbred strain for future CNS studies.

2.4.6 α-conotoxin MII sensitivity and α3/α1[5] β2 receptor

α-conotoxin MII (CTX) binds with high affinity to both α6- and α3β2-nAChRs (Cartier, Yoshikami et al. 1996; McIntosh, Azam et al. 2004). CTX is a competitive antagonist that is highly selective for the α3β2 neuronal nicotinic receptor. Other receptor subunit combinations (α2β2, α4β2, α3β4) are 200-fold less sensitive to blockade by this toxin. The original purpose of CTX study was to investigate the involvement of the β2 nAChR subunit in the expression of the α3/α1[5] containing nAChRs populations in the Kin mice. It would be our great interest to see if CTX can still serve as a probe to dissect β2-containing nAChRs known to express in rodent SCG neurons.

Interestingly, initial results using 100 nM CTX showed that the toxin produced significant reversible blockage (at a level of ≈70%) on ACh responses in a α3(tm/tm)α7(-/-) mouse SCG neurons, implying that β2 subunits were incorporated within a significant fraction of functional receptors (Figure 22). Surprisingly, in my latest studies using two α3(tm/tm)α7(+/+) animals (from different litters) with identical experimental conditions, 100 nM CTX produced no inhibition on whole cell currents, suggesting no functional β2 containing nAChRs in whole cell currents. The cause of this discrepancy is not yet fully understood. In an attempt to explain the different results between α3(tm/tm)α7(-/-) and α3(tm/tm)α7(+/+) mice, one possible interpretation is that β2 can form functional α3/α1[5] nAChRs only in α3(tm/tm)α7(-/-) mice but not in α3(tm/tm)α7(+/+) mice. The 2nd possibility is technical error or an experimental instance, in which CTX showed

inhibition, may simply be artefact. In any case, α3(tm/tm)α7(-/-) double homozygotes need to be tested again in order to solve the CTX puzzle. Meanwhile, the lab has been encountering technical difficulty when trying to co-express α3/α1[5] subunit with β2 subunit in oocytes. Numerous efforts have been made to coexpress α3/α1[5] with β2 subunit *in vitro* without success so far. However, α3/α1[5] can co-express with β4 subunit to form functional receptors in oocytes with functional Bgtx sensitivity. This could indicate that the mutation in α3/α1[5] caused structural perturbations that result in inefficient subunit assembly with β2. In subunit knock-out studies, mice that lacked only the β4 subunit survived but exhibited profound reduction in nicotine-induced whole-cell currents in SCG. These animals maintained sufficient autonomic function, presumably, through β2 subunit redundancy or compensation. In contrast, mice lacking the β2 subunit had apparently normal organ function and normal whole-cell currents in superior cervical ganglion (Wang, Orr-Urtreger et al. 2002). The reason for non detectable functional expression of α3/α1[5] β2 in oocytes and variability of CTX sensitivity in mutant mouse SCG is unknown. The profile of rank order potencies suggesting a major α3/α1[5]β4 subtype expressed in Kin mouse SCG cells also seems to correlate with what is observed in β2 and β4 knock out studies.

2.4.7 Future directions

Research focusing on synaptic structure and protein trafficking in CNS has faced major challenges due to a lack of effective highly specific probes. Many commercially

available anti-nAChR subunits antibodies are against intracellular epitopes and are therefore not suitable for trafficking studies or localization of expressed receptors. The results of SCG studies obtained from our Kin mouse which I have presented in my thesis work indicate that our Kin mouse may provide as an alternative tool for the synaptic architecture and subcellular trafficking studies. The live-surface staining study as demonstrated using fluorescence Bgtx offers a good example and direct evidence that α3 containing nAChRs can be visualized and monitored.

Brain studies will have to be done in the future to demonstrate the regional expression of Bgtx-sensitive, α3/α1[5]-containing neuronal nAChRs in the brains in order to demonstrate the merit of this new mouse tool. nAChRs are also the primary site of action in the brain for nicotine. Owing to a dearth of nAChR subtype-selective ligands, the precise subunit composition of the nAChRs that regulate the rewarding effects of nicotine and the development of nicotine dependence are unknown. The reinforcing properties of many drugs of abuse, such as nicotine and ethanol, are thought to be principally mediated by their interactions with the mesotelencephalic dopaminergic system. Nicotine acts by binding to nicotinic acetylcholine receptors on either the cell soma in the substantia nigra and ventral tegmental area and/or nerve terminals in the dorsal and ventral striatum (Grady, Marks et al. 1992), therefore activating these cells and causing an increase in extracellular dopamine levels in the dorsal and ventral striatum (Pontieri, Tanda et al. 1996). α3 as one of the identified nicotinic acetylcholine receptor subunits is expressed in mesencephalic dopaminergic neurons (Pidoplichko, DeBiasi et al. 1997), indicating its role in nicotine addiction. In view of the lack of selective antagonists, our Kin mouse can offer a unique opportunity to evaluate the contribution of α3 to the

reinforcing action of nicotine and alcohol dependence. α3 is also found in the medial habenula and ventral tegmental area (VTA). These areas of the brain are part of the reward pathway that plays an important role in addiction. The medial habenula is also an area that has been shown to be very sensitive to the neurotoxic effects of nicotine. This mouse model should add valuble atternitive for determining the effect of α3-containing nAChRs in either the medial habenula or VTA on these nicotine-associated behaviors.

nAChRs can regulate the activity of many neurotransmitter pathways throughout the central nervous system and are considered to be important modulators of cognition and emotion (Gotti, Riganti et al. 2006). The differential contribution of single nicotinic acetylcholine receptor subunits in the various physiological functions has been difficult to assess. The successful production of our knock-in mouse opens many new doors for the pharmacological investigation of the role of α3 in nervous system function. Our Kin mouse should help to elucidate the function of the α3 subunit in those important physiological events, the contribution in the pharmacology using its "gain of function"-Bgtx sensitivity.

In summary, we have documented the important features of Bgtx-sensitive α3/α1[5]-nAChRS expression in mouse SCGs that may be generally useful. Together, these features make it possible for future in vivo studies. To a large extent, the sucessful production of α3/α1[5] Kin mouse offer the possibility that similar pharmatope sequences can be similarly inserted into other nAChR subunit genes.

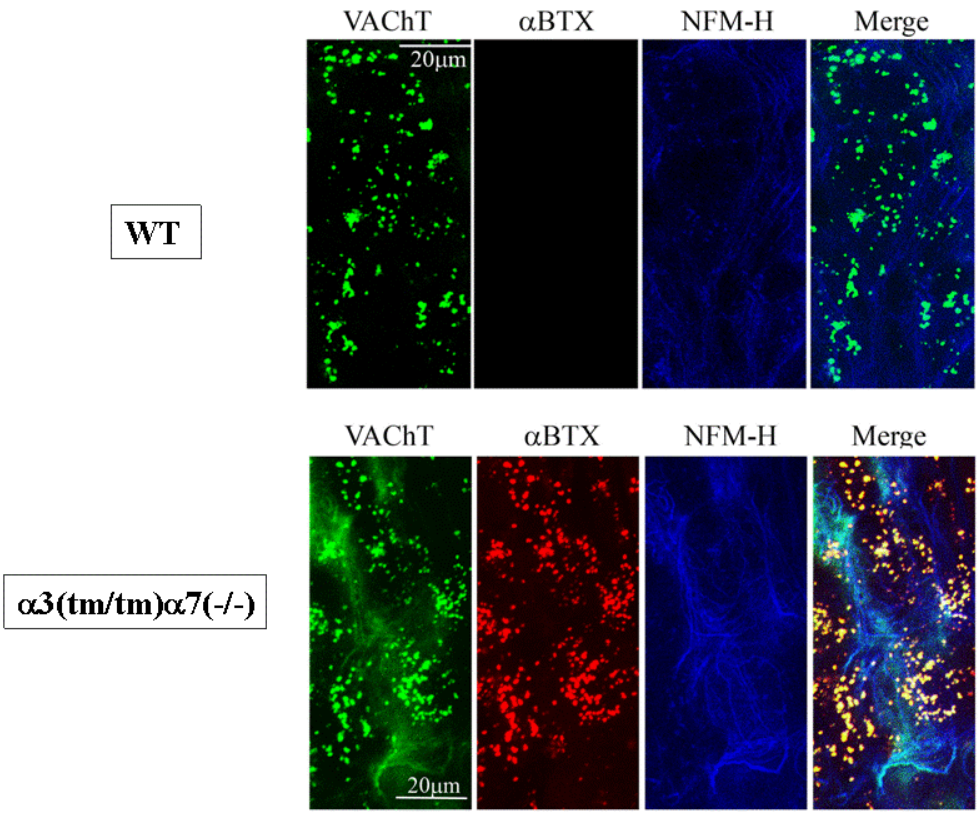

Figure 19. Additional evidences for the functional expression of α3/α1[5]-nAChRs in Kin mouse SCG. Bgtx-labeled receptor clusters were visualized in the SCG from the α3(tm/tm)α7(-/-) and WT mice. Ganglia were incubated in the presence of fluorescently labeled Bgtx (100nM) for 1hr, then fixed and processed for immunofluorescence using antibodies against a cholinergic varicositiy marker, vesicular acetylcholine transporter (VAChT), and the heavy chain of neurofilament (NFM-H). SCG from α3(tm/tm)/α7(-/-) contained Bgtx labeled puncta that co localize with VAChT positive varicosities. The coincidence of these signals indicates that Bgtx positive puncta are clusters of synaptic α3-containing nAChRs (Data collected by Arjun Krishnaswamy & Ellis Cooper, McGill University).

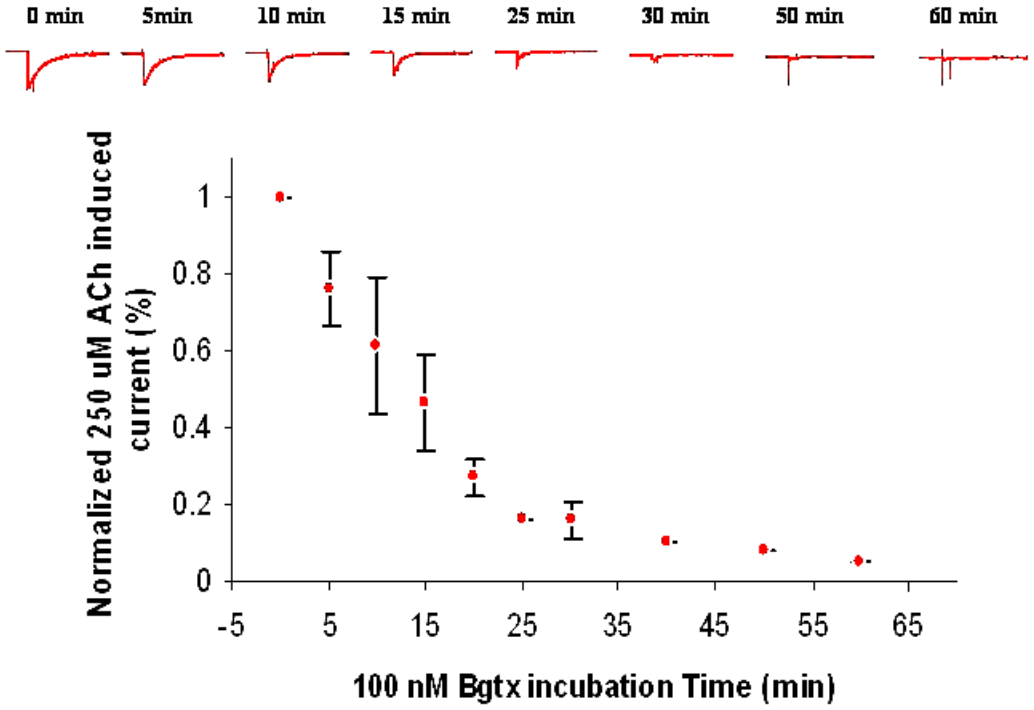

Figure 20. Time dependent Bgtx blockage on ACh responses in SCG neurons from a α3/α1[5] heterozygote ICR crossed C57BL/6 mouse. Typical current traces at different time points in Bgtx solution from one cell are shown in the upper panel. The control ACh (250 μM) response was recorded, at time 0. Then 100nM Bgtx was begun, and the response to a co-application of 250 μM ACh and 100 nM Bgtx was recorded. Between subsequent co-applications at the indicated times, the cell was maintained in 100 nM Bgtx. The data are shown as plots of $I_{\text{co-application}}/I_{\text{control}}$ vs. time in 100nM Bgtix, where $I_{\text{co-application}}$ is the peak response evoked by the co-application at that time point and I_{control} is the initial peak current to the ACh pulse in Bgtx free solution.

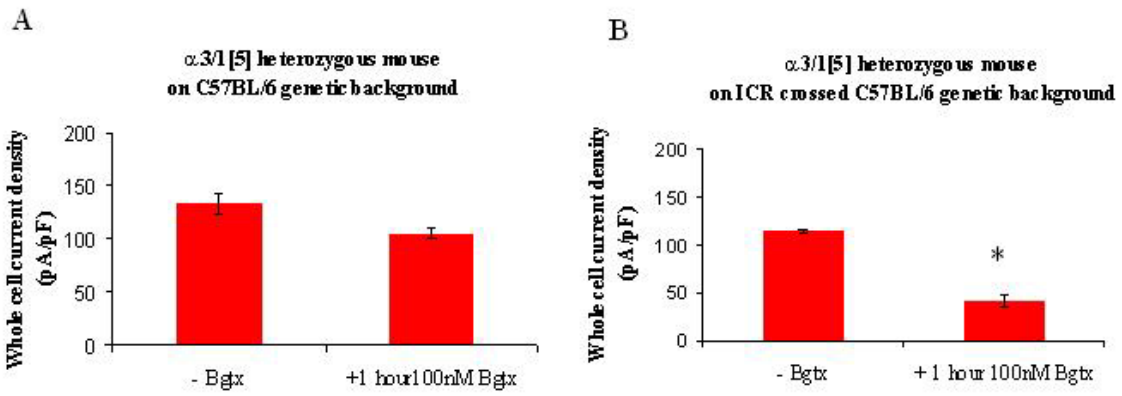

Figure 21. Bgtx sensitivity in α3/1[5] heterozygoute mouse SCG neurons on C57BL/6 (C57) background is different from that of ICR crossed C57BL/6 (ICR/C57) background. Each experiment (A and B) was done with one mouse each. In each experiment, two groups of neurons in absence of Bgtx or with 1-hour Bgtx (+ 1 hour Bgtx) were discretely examined. A) One C57BL/6 α3(+/tm)α7(-/-) was examined. There is no significant difference between the two groups ($P > 0.05$, t-Test; n=4 and 4, respectively). B) For the ICR/C57 α3(+/tm)α7(-/-) mouse, the current density of the neurons with 1-hour Bgtx (100 nM) incubation was found to be significantly different from the current density in absence of Bgtx ($P<0.001$, t-Test; n=4 and 4, respectively). The results show that 1-hour Bgtx incubation can significantly reduce the current density in ICR/C57 α3(+/tm)α7(-/-) mouse but not C57 α3(+/tm)α7(-/-) mouse. The finding suggests that ICR genetic background incorporation may lead to α3/α1[5] containing receptors functional expression which accounts for the observed Bgtx sensitivity in B. The values represent the mean ± SEM.

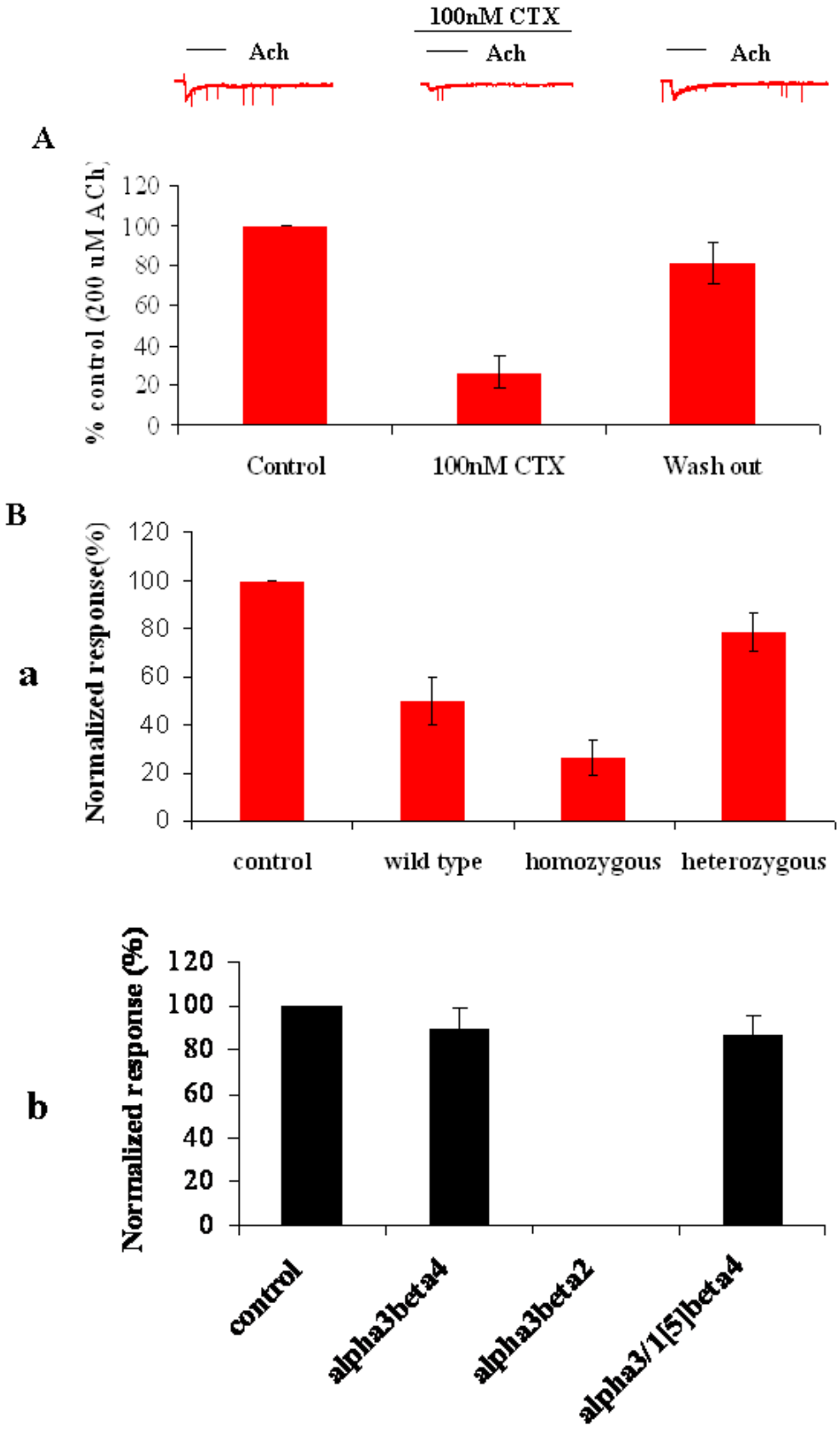
100nM CTX
Ach
Ach
Ach
A
% control (200 uM ACh)
120
100
80
60
40
20
0
Control
100nM CTX
Wash out
B
a
Normalized response(%)
120
100
80
60
40
20
0
control
wild type
homozygous
heterozygous
b
Normalized response (%)
120
100
80
60
40
20
0
control
alpha3beta4
alpha3beta2
alpha3/1[5]beta4

Figure 22. Investigation of the effect of α-conotoxin M II (CTX) on α3/α1[5] receptors expressed in mice (in red) or oocytes (in black). A) CTX reversibly blocked ACh response carried by α3/α1[5] receptors in BALB/c double homozygous mouse(α3(tm/tm)α7(-/-)) SCG neurons . Upper panel shows sample traces induced by ACh before, during and after 10 minutes washout of 100 nM CTX treatment. Histograms show the percentage of current remaining in SCG neurons before (Control), with 1 min treatment of 100 nM CTX and 10 min washout of toxin. The toxin produced a mean blockage of 73.5% on α3/α1[5] receptors, very similar with its reported selective antagonism on α3β2 and α6 nAChR receptors (Cartier, Yoshikami et al. 1996). B) nAChRs in mouse SCG neurons are mixed population with β2 containing subtypes. a. 1 min treatment of 100 nM CTX inhibited ACh response carried by α3/α1[5] receptors in homozygous mouse (α3(tm/tm)α7(-/-)) SCG neurons as well as in wild type and heterozygous littermates. The toxin produced a mean blockage of 73.5% in homozygous mouse, 50.1% in wild type mouse and 21.4% in heterozygous mouse. b. Recombinant α3β4, α3/α1[5]β4 and α3β2 receptors in oocytes. ACh response was recorded first as control followed by 10 min CTX treatment. ACh response recorded right after CTX was as indicated for each nAChR subtype. 10 min treatment of 100 nM CTX completely blocked ACh response of α3β2 but have little affect on α3β4 and α3/α1[5]β4 subtypes. Error bars indicate the SEM, n=4. All SCG cells were 37 °C cultured and 30 °C treated for 2-3 days.

CHAPTER III

SURFACE EXPRESSION AND FUNCTION OF Kv4.2 CHANNLES TAGGED IN THE S1−S2 LOOP FOR EXTRACELLULAR α-BUNGAROTOXIN BINDING

3.0 ABSTRACT

Subcellular targeting and distribution of voltage-gated potassium (Kv) channels play an important role in the regulation of membrane excitability in neurons and cardiac myocytes. To better understand the trafficking mechanisms that regulate these properties, we introduced α-bungarotoxin binding capability, normally found in skeletal muscle type or α7 homo-oligomeric nicotinic acetylcholine receptors, to the Kv4.2 channel in order to facilitate fluorescence imaging in neurons. A short sequence encoding a Bgtx binding site, GGWRYYESSLEPYPDGG, which was derived from the mimotope peptide, HAP, was introduced into the S1-S2 extracellular loop by site-directed mutagenesis, and these HAP-tagged channels were transiently co-expressed with KChIP3 in tsA201 cells for functional activity and assessment of Bgtx sensitivity. We observed that HAP-tagged channels were expressed at levels comparable to wild-type Kv4.2, and that several biophysical parameters of the tagged channels, including time to peak current, rate of inactivation, and recovery from inactivation were minimally affected by the S1-S2 insertion. Surface binding assays using ^{125}I-labeled Bgtx demonstrate that Bgtx binds

specifically to HAP-tagged Kv4.2 in living cells, but not to wild-type channels. Similarly, fluorescence-microscopic imaging of surface expressed Kv4.2 channels shows specific binding of Alexa-Fluor conjugated Bgtx to HAP-tagged Kv4.2 transfected into tsA201 cells or in primary hippocampal neurons. Notably, application of Bgtx had minimal effects on the activation properties of HAP-tagged Kv4.2. Taken together, these results show that the introduced Bgtx binding sequence is functionally well tolerated in an important ion channel, and that the HAP-derived Bgtx recognition sequence provides a highly useful and versatile tag for studies of the trafficking of Kv4.2 channels within neurons.

3.1 BACKGROUND AND SIGNIFICANCE

3.1.1 K^+ channel overview

K^+ channels operate as multimeric, polytopic complexes, composed of pore-forming principal or primary (often called α subunits) subunits plus a number of associated ancillary subunits and scaffolding proteins. Analysis of various K^+ channel sequences indicates several structural elements that are present in most K^+ channels. These include the amino-terminal cytoplasmic domain, the T1 assembly domain, the six transmembrane α-helical domains; the voltage sensor, the pore domain (P-loop), and a

carboxy-terminal cytoplasmic domain (Sansom, Shrivastava et al. 2002) (Figure 23). K^+ channel principal subunits are by far the largest and most diverse of the ion channels. Three groups of K^+ channels have been characterized based on putative membrane topology of their principal subunits. The primary subunits tetramerize to form a single transmembrane pore in all three cases. The first group, typified by voltage-activated and Ca^{2+}-activated K^+ channels, has six transmembrane domains per α-subunit. The second group, typified by the "leak" K^+ channels, has four transmembrane domains in their α-subunits. Finally, the "inward rectifiers" are the simplest structurally and have two transmembrane domains in each α-subunit. Each of these three groups comprises a discrete family, based on sequence homology, which is further divided into subfamilies (Figure 23) (Coetzee, Amarillo et al. 1999).

The action potential constitutes the fundamental unit of information encoded in neurons. The shape of action potential is of critical importance in regulation of neuronal excitability and signaling. Rapidly inactivating A-type K^+ currents shape the action potential by regulating its waveforms and duration. The A-type inactivation leads to reduction or elimination of potassium currents that can be regulated through a dynamic process by a variety of intracellular factors such as neurotransmitters, kinases, second messengers and β-subunits, resulting in a diverse mechanism for control of membrane excitability. Native voltage-gated potassium channels (Kv) are in a form of complex composed of tetrameric core of pore-forming α subunits and additional auxiliary subunits. Binding of auxiliary subunits can change the functional properties of Kv channels at the membrane surface as well as their intracellular trafficking and gating kinetics.

3.1.2 Molecular diversity of Kv Channels

The first molecular components of K^+ channels were identified around two decades ago by molecular cloning methods (Papazian, Schwarz et al. 1987). However, the number of cloned and characterized components has grown so much that reviewing the molecular biology of K^+ channels has become daunting. Progress made in understanding the physiological significance of the enormous molecular diversity of K^+ channel protein subunits has been fairly slow. Over 100 different proteins, subunits of distinct types of K^+ channels, have been identified to date, and the list is growing. In addition to the pore-forming or principal subunits, which determine the infrastructure of the channel, many K^+ channels contain auxiliary proteins that can modify the properties of the channels, often significantly. Early studies in *Drosophila* revealed that the behavioral phenotype associated with the *Shaker* mutant resulted from a K^+ channel defect that eventually led to the discovery of several alternatively spliced, voltage-gated K^+ channel α subunits (Jan and Jan 1997). Subsequent work in Drosophila identified three related voltage-gated K^+ channels, referred to as Shab, Shaw and Shal. These four *Drosophila* K^+ channel genes belong to a subfamily of K^+ channels that includes several mammalian homologues designated Kv1, Kv2, Kv3 and Kv4 corresponding to Shaker, Shab, Shaw and Shal, respectively. The Kv naming system was based on deduced phylogenetic relationships where channels that shared 65% sequence identity were assigned to a particular subfamily (Gutman, Chandy et al. 2003). Presently, a parallel nomenclature designated KCN was developed by the Human Genome Organization to

serve as a mechanism for classifying existing and newly discovered genes within the K^+ channel superfamily (Figure 24).

3.1.3 The Shal-type family

In the super-family of voltage-gated Kv channels of eukaryotes, there are four closely related subfamilies: Kv1 (Shaker), Kv2 (Shab), Kv3 (Shaw) and Kv4 (Shal). The Shal-type family in mammals is composed of three distinct genes: Kv4.1, Kv4.2, and Kv4.3 (Kv4.x). The proteins encoded by these genes are highly homologous within the transmembrane regions, with divergent N- and C- termini. Kv4.x family channels in general are highly expressed in the brain, heart, and smooth muscles. Heterologous expression of these proteins in expression systems demonstrates that they activate at subthreshold membrane potentials, inactivate rapidly, and recover from inactivation quickly compared with other Kv channels. Therefore, they are termed transient currents. Recent data from transgenic and knockout animals as well as expression of dominant negative constructs indicate that these channels participate in the transient outward A-type K^+ current in the somatodendritic compartments of neurons, as well as form the Ca^{2+}-independent A-type K^+ current in cardiac myocytes (or I_{to}). Kv4.x channels can also be identified based on pharmacology. Kv4.x channels, like many other K^+ channels, are sensitive to 4-aminopyridine. More specific blockers for example, the heteropodatoxins are specific for the transient outward current of cardiac myocytes (Sanguinetti, Johnson et al. 1997), a cellular current likely composed at least in part of Kv4.x family channels. The

phrixotoxins are also specific blockers of Kv4.x channels as well as the I_{to} in the heart (Diochot, Drici et al. 1999).

.

3.1.4 The Kv4.2 channel

Kv4.2 is a fast transient (A-type) voltage-gated potassium channel of the *Shal* subfamily that is found in heart and neurons (Dixon, Shi et al. 1996; Fiset, Clark et al. 1997; Kaab, Dixon et al. 1998). Kv4.2 channels are multimeric, primary membrane proteins, that contribute to transient, voltage-dependent K^+ currents in the nervous system (A currents) and the heart (transient outward current) (Bahring, Dannenberg et al. 2001). Regulation of transient outward K^+ currents in cardiac myocytes and in neurons can have profound effects on membrane excitability. In myocytes, Kv4.2 is crucial for recovery from the QT interval and for re-polarization (Fiset, Clark et al. 1997). Moreover, in neurons, Kv4.2 is the primary pore-forming subunit of the I_A transient K^+ current in the dendrites of hippocampal pyramidal cells, visual-cortical pyramidal neurons and spinal cord dorsal horn neurons. Intrinsic membrane properties, in addition to synaptic mechanisms, are known to play a role in the pathologically increased electrical activity associated with epilepsy. Alterations in function and expression of Kv4.2 channels are associated with some animal models of epilepsy and in human temporal lobe epilepsy. Changes in Kv4.2 channels may also occur in Alzheimer's disease. Dysfunctional Kv4.2 can cause prolonged action potential, which is also a common defect found in many cardiac disorders, including hypertrophy, myocardial infarction, heart failure, and arrhythmias.

General biophysical properties of Kv4.2 are (i) rapid sigmoidal activation kinetics; (ii) multiexponential inactivation kinetics; (iii) rapid kinetics of recovery (time constants on the order of 10 to hundreds of milliseconds); (iv) little to no cumulative inactivation during repetitive voltage clamp pulses (Patel and Campbell 2005).

3.1.4.1 Voltage-sensing

The membrane-spanning domain of all voltage-dependent K^+ channels contains two highly conserved portions, the voltage-sensing portion that surrounds the central pore and the pore domain itself. The pore domain, S5, the P-loop, and S6 all together make up the ion permeation pathway, including the selectivity filter (Figure 23). A large body of evidence suggests that the voltage-sensing region of voltage-gated K^+ channels is the fourth transmembrane α-helix, or S4. This region of the protein contains positively charged arginine or lysine residues and is the only transmembrane domain that is appreciably charged. Membrane depolarization causes a movement of the positively charged residues of S4 through the gating canal. This movement of charges through the electric field of the membrane mediates the actual opening of the channel and generates what is referred to as a gating current (Horn 2000). The precise structural basis for voltage-sensing is not completely clear at present. Although all current models invoke the S4 domain as a voltage sensor, the details of how this works awaits further investigation.

3.1.4.2 Channel inactivation

Kv4.2 channels rapidly inactivate. Inactivation of voltage-gated ion channels is the auto-regulatory time-dependent process that shuts down the corresponding conductance in response to a prolonged or sustained membrane depolarization. A relatively fast development of inactivation is a hallmark of all known members of the Kv4 subfamily. Fast recovery from inactivation at hyperpolarized membrane potentials removes Kv4 channel steady-state inactivation in tens to hundreds of milliseconds. Although inactivation of Shaker and Kv1 channels is generally well understood at the molecular level, the mechanisms of inactivation of Kv4 channels, however, remain unsolved.

In heterologous expression systems, Kv4 channels may undergo open- and closed-state inactivation. A current working hypothesis proposes that main internal activation gate of the channel (A-gate) conducts two separate jobs, and therefore, it can control both activation and inactivation. Whether it does one or the other depends on the strength of the electromechanical coupling between the voltage sensor and the A-gate (Long, Tao et al. 2007).

3.1.4.3 K^+ channel interacting protein KChIPs

Recombinant Kv4.2 homomers manifest activation curves that are shifted in the depolarizing direction, and their recovery from inactivation is slower than native A-type K^+ currents. Rat brain mRNA coexpressed with Kv4.2 in oocytes could restore many of the properties seen in native A-type K^+ currents, suggesting that some cofactor was

responsible for this change (Serodio, Kentros et al. 1994). A cofactor came to light in the form of a family of auxiliary proteins known as K^+ channel interacting proteins, or KChIPs. Four KChIPs have been identified to date. The Cytosolic KChIPs (216–256 amino acids) are members of the recoverin-neuronal calcium sensor superfamily that are Ca^{2+} binding proteins. Calcium binding EF-hand proteins KChIPs co-assemble with *Shal* Kv4x α subunits to form a native complex that encodes somatodendritic A-type K^+ current, I_{SA}, in neurons and transient outward current, I_{TO}, in cardiac myocytes. The various KChIPs have a variable amino-terminal region, but a conserved carboxy-terminal region that contains four EF-hand-like calcium-binding motifs. The KChIPs colocalize with Kv4.x subunits through binding to the amino terminus of Kv4.x α–subunits and are thus considered integral components of the native Kv4.x channel complexes (Rhodes, Carroll et al. 2004).

KChIPs 1, 2, and 3 all have similar effects on the physiological properties of Kv4.x channels. The physiological effects of KChIPs include an increase in the density of Kv4.2 currents, a hyperpolarizing shift in the activation curve, an increase in the rate of recovery from inactivation, and a slowing of the time constant of inactivation (Kunjilwar, Strang et al. 2004). Misonou Shibata reviewed that KChIPs profoundly affect the intracellular trafficking and surface redistribution of Kv4.2 in native cells and co-expression KChIPs with Kv4.2 cause fundamental changes in steady-state expression levels, phosphorylation, stability and other properties of Kv4.2 (Shibata, Misonou et al. 2003).

3.1.5 Trafficking and subcellular distribution of Kv4.2 channel

Kv4.2 channel correct functioning depends not only on the regulation of their biophysical properties but also on the fine-tuning of their subcellular localization and number of cell surface copies. The expression patterns of Kv4.2 messages are complicated. In fact, Kv4.2 subunits are expressed in numerous neuronal types throughout the mammalian central nervous system, manifesting selective subtype expression patterns in some cells and overlapping expression in others. Several recent reviews cover biogenesis, specific trafficking signals or mechanisms, in addition to the trafficking of particular subclasses of potassium channels (Ma and Jan 2002; Trimmer and Rhodes 2004; Heusser and Schwappach 2005). In neurons of the central nervous system, Kv4.2 is expressed primarily somatic-dendritically, where it is poised to control potentiation of dendritic excitability and therefore plays an important role in postsynaptic signal integration (Song, Tkatch et al. 1998; Schoppa and Westbrook 1999). The influence of the voltage-gated ion channels on the integrative physiology of excitable cells is determined by the inherent biophysical properties of the channels and their cell surface distribution (Bichet, Haass et al. 2003). The processes that influence trafficking and surface distribution patterns of the channels, therefore will affect their ability to contribute to cellular functions. Clearly, the physiological function of Kv4.2 depends not only on the regulation of biophysical channel properties but also on the fine-tuning of subcellular localization and of cell-surface abundance (Heusser and Schwappach 2005). Potassium channels, as such complex membrane proteins, are hard to study that the mechanisms that specify channel trafficking and distributions are still not well known

(MacKinnon 2003). Thus, it is of great interest to understand the subcellular organization of these channels in order to fully understand their physiological roles.

3.1.6 Review of approaches of studying trafficking and distribution of Kv4.2

Current knowledge of the trafficking and distribution of Kv4.2 is based largely on studies using immunohistochemistry techniques, i.e., antibodies against channel subunit epitopes in fixed cells (Anderson, Adams et al. 2000; Takeuchi, Takagishi et al. 2000; Wong, Newell et al. 2002; Gardoni, Mauceri et al. 2007), or recently, with recombinant Kv4.2-enhanced green fluorescent protein (EGFP) fusion or c-Myc-tagged Kv4.2 constructs in live cells (Rivera, Ahmad et al. 2003; Kunjilwar, Strang et al. 2004; Gardoni, Mauceri et al. 2007). In addition, other common biochemical approaches, i.e., mutagenesis, or indirect channel tagging by labeling Kv channel interacting proteins, have been used to study channel trafficking (Wong, Newell et al. 2002; Pourrier, Herrera et al. 2004; Hasdemir, Fitzgerald et al. 2005).

Even though these approaches have been widely used to study channel trafficking, there are limitations to these techniques. The issue of antibody specificity, in particular, has regained the attention of the neuroscience research community (Moser, Mechawar et al. 2007). The results obtained by using insufficiently characterized commercial polyclonal antibodies should be interpreted with caution (Rhodes and Trimmer 2006; Moser, Mechawar et al. 2007). In addition, when using GFP fusion protein, it is

important to establish that channel function is not adversely affected by addition of the bulky GFP fusion partner.

3.1.7 Constructing chimeric Kv4.2 subunit with Bgtx binding sequence HAP

Studying or manipulating proteins often relies on equipping the protein of interest with an additional functionality. This functionality can either result from the expression of the protein as a fusion protein with an additional polypeptide, from labeling the protein with synthetic molecules, from the incorporation of unnatural amino acids or a combination of these different approaches. Ideally, this new functionality is unique with respect to other proteins or biomolecules and the protein can then, for example, be used for its purification, characterization. There have been various efforts to generate new functionalities useful for protein research as well as to find ways to attach these functionalities specifically to proteins. As stated before, it is our great interest to understand the subcellular organization of these channels in order to fully understand their physiological roles. The mechanisms that specify channel trafficking and distribution, unfortunately, are not well known due to lack of suitable high-affinity probes.

In this chapter of my dissertation, I show we have generated and characterized a new chimeric construct, Kv4.2-HAP. HAP (the high affinity peptide), a mimotope peptide of 13 amino acids in length, binds Bgtx with nanomolar affinity (Harel, Kasher et al. 2001). Fuchs and her collaborators in that study described this synthetic peptide of 13 residues HAP that binds to Bgtx with an equilibrium dissociation constant of 2 nM,

within the range of dissociation constants (0.01–10 nM) for the binding of toxin by intact receptors. The aligned sequences of HAP and *Torpedo* α187–200 have six identical residues and two more residues that are conservative substitutes. α7 subunit also binds Bgtx and α7184–196 and HAP share six identical residues and three more residues that are conservative substitutes.

We introduced this Bgtx recognition sequence into the extracellular S1-S2 loop of Kv4.2, far from the critical gating sensor and from the N- and C- terminus (Figure 25). In comparison with the insertion of GFP, this small extracellular tag sequence should limit potential perturbation of channel structure and function. Bgtx as a small soluble protein also offers unique advantages comaring to other probes, ie, antibodies. (see Chapter I, 1.6)

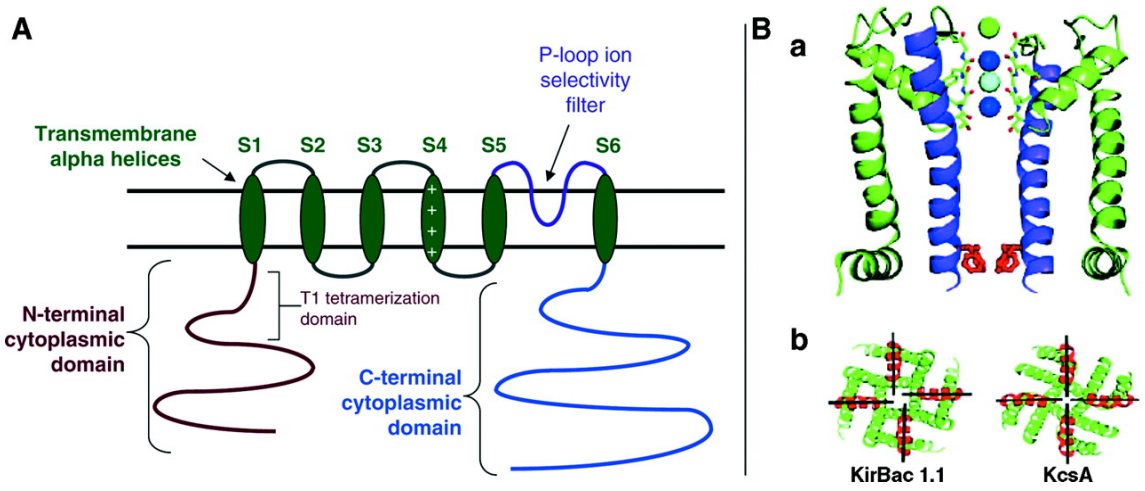

Figure 23. Structure of K^+ channels. A) Schematic drawing of several structural elements present in most K^+channels. See text for discussion. B) A model of the S5, P-loop, and S6 regions of a K^+ channel. a: Ribbon representation of the transmembrane section of two opposing S5/P-loop/S6 structures based on the published crystal structure of two KirBac1.1 monomers. The residues forming the selectivity filter (P-loop), displayed as ball-and-stick, interact with four K^+, colored green and cyan. The inner α-helices, analogous to transmembrane helix S6, are colored purple, whereas the side chains of two hypothetical pore-blocking phenylalanine residues are colored red. The S5 α-helix is colored green. b: Relative positions of the P-loop helices that form the ion selectivity filter are depicted in red in the crystal structure of two K^+ channels: Kir-Bac1.1 and KcsA. This view is from the extracellular side of the channel looking directly down the central ion-conduction pathway. Black lines through the center of each pore helix indicate its orientation relative to the center of the cavity. (Adapted from Birnbaum, 2004)

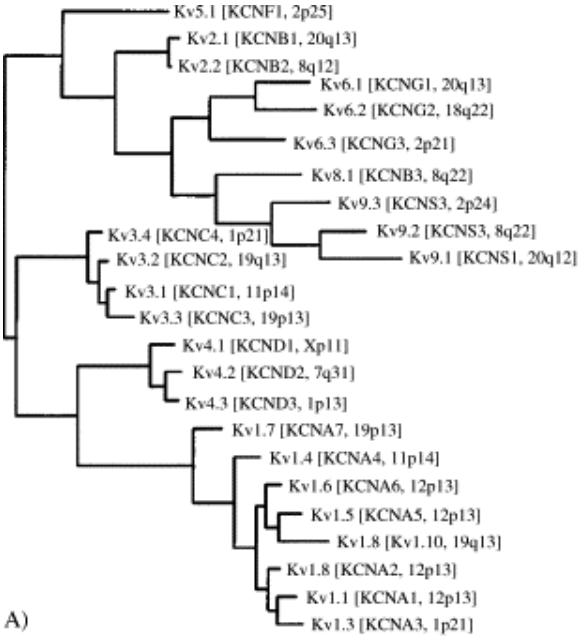

KCNA1-KCNA7	6TM1P K_V channel (Shaker-related)
KCNB1-KCNB2	6TM1P K_V channel (Shab-related)
KCNC1-KCNC4	6TM1P K_V channel (Shaw-related)
KCND1-KCNA3	6TM1P K_V channel (Shal-related)
KCNE1-KCNE3	1TM/ISK accessory subunit
KCNF1	6TM1P K_V channel (modulatory)
KCNG1-KCNG2	6TM1P K_V channel (modulatory)
KCNH1-KCNH5	6TM1P K_V channel (EAG, ERG ELK)
KCNI1	
KCNJ1-KCNJ15	2TM1P K_{ir} channel
KCNK1-KCNK9	4TM/2P (TWIK, TASK, TREK)
KCNL	
KCNMA1	7TM/1P maxi-K_{ca} channel
KCNMB1	β subunit of maxi-K_{ca} channel
KCNN1-KCNN4	6TM1P SK_{ca} and IK_{ca} channel
KCNO	
KCNP	
KCNQ1-KCNQ4	6TM1P K_V channel
KCNR	
KCNS1-KCNS3	6TM1P K_V channel (modulatory)

(C)

Figure 24. Phylogenetic trees of the Kv potassium channels. A) Kv1–6 and Kv8–9 subfamilies; B) Kv7 subfamily; (C) KCN classification system. (Adapted from Gutman, 2003)

3.2 MATERIALS AND METHODS

3.2.1 Preparation of Kv4.2 Mammalian Expression Constructs

HAP and T1 sequences were introduced into Kv4.2 S1-S2 extracellular loop by oligonucleotide-directed mutagenesis using the Quikchange Mutagenesis kit (Stratagene). Mutant sequences were authenticated by DNA sequencing.

Here are the final sequences. The introduced sequences are in bold italics and underlined.

S1-S2-loop-HAP chimera:

ETVPCGSSPGHIKEL***GGWRYYESSLEPYPDGG***PCGER

S1-S2-loop-Talpha1 chimera:

ETVPCGSSPGHIKEL***GGWVYYTCCPDTPYLDGG***PCGER

S1-S2-loop: ETVPCGSSPGHIKELPCGER

3.2.2 Culture and Transfection of tsA201 Cells

tsA201 cells were maintained at 37 °C, 10% CO_2 in Dulbecco's modified essential medium (Invitrogen, Carlsbad, CA) supplemented with 10% fetal bovine serum, 10 µg/ml penicillin, and 10 units/ml streptomycin (all supplements obtained from Invitrogen).

Cells were transfected with Kv4.2 constructs, in combination with KChIP3 (Kv4.2:KChIP3 3:1), using Lipofectamine 2000 (Invitrogen). For non-EGFP-tagged proteins, GFP was co-expressed with the channel to assess transfection efficiency and to identify expressing cells for patch clamp experiments. For fluorescence imaging, tsA201 cells were seeded on poly-L-lysine-coated cover slips and then incubated with fluorensence Bgtx following transfection, as described in 3.2.7. For electrophysiology experiments, cells were resuspended, washed and replated in a recording chamber 36-48 h after transfection. GFP-positive cells were patch clamped, as described below.

3.2.3 Preparation and transfection of primary rat hippocampal neurons

Primary hippocampal neuron cultures were prepared from embryonic day 18 rat hippocampi. Hippocampi were dissociated with Papain solution (10 U/mL). The cells were plated at a density of $3x10^4$ cells cm^2 on glass bottomed Petri dishes (MatTek) pre-treated with poly-L-lysine and laminin (1-2µg/cm^2). Cultures were maintained in 5% CO_2/95% air atmosphere at 37^oC in Neurobasal medium (Invitrogen, pH 7.4) supplemented with B27 (Invitrogen), 0.5 mM L-glutamine, penicilline 100 units/mL and streptomycine 100 µg/mL. Medium was changed twice per week. Neurons were

transfected on after 7-10 days *in vitro* with Kv4.2-HAP construct using Lipofectamine 2000 (Invitrogen) according to the manufacturer's instructions. Cells were analyzed 18-36 hours after transfection.

Because neurons may express α7 nicotinic acetylcholine receptor that bind Bgtx, the transfected neurons were preincubated with the nicotinic receptor antagonist tubocurarine (2 μM) to block binding of Bgtx to the endogenous nicotinic receptors before incubation with 5 μg/ml rhodamine-conjugated Bgtx to label the Kv4.2-HAP channels.

3.2.4 Electrophysiology

Whole-cell patch clamp technique was used to assess the functional expression of Kv4.2, Kv4.2 HAP, and (EGFP-tagged) in transfected tsA201 cells. An Axopatch 200B amplifier (Axon Instruments, Foster City, CA) was used to record ionic currents with the whole cell voltage-clamp technique (Hamill, Marty et al. 1981). Current stimulus protocols and data collection were performed using pClamp 9.0 software (Axon Instruments, Foster City, CA). Pipettes were pulled on a multiple stage puller (Sutter Instruments, Novato, CA) from borosilicate tubing and polished to a resistance of 3-4 MΩ. Cells were bathed in standard extracellular solution containing (in mM): 140 NaCl, 5.4 KCl, 2.8 $CaCl_2$, 0.18 $MgCl_2$, 10 HEPES, 5.6 Glucose, 2 Glutamine (pH 7.4). The pipette solution contained (in mM): 140 KCl, 5 NaCl, 1 $MgCl_2$, 10 EGTA, 10 HEPES (pH 7.4). Leak-subtraction was performed before each recording. Data were filtered at 5

kHz, sampled at 10 kHz and stored online. For the activation phase of Kv4.2-mediated currents the 10–90% rise time was determined. Conductance values (G) at a given test potential (V_m) were calculated from the measured peak amplitude (I) and the mean reversal potential for Kv4.2 ($V_{rev} \approx$ - 40 mV; n =4) using the equation $G = I/(V_m - V_{rev})$. Kv4.2 current inactivation kinetics was fitted with a single-exponential function. The obtained data were further processed using Origin7.5 (Microcal Software, Inc.). Co-transfected cells were identified by fluorescence microscopy using an inverted Axiovert 25 microscope (Carl Zeiss, Germany) equipped for fluorescence detection. All recordings were conducted at room temperature (22-25°C).

3.2.5 Binding experiments

Surface expression of tagged Kv4.2 channels was measured in a ^{125}I -Bgtx binding assay. ^{125}I-Labeled Bgtx (5 nM) was incubated in the presence or absence of unlabeled Bgtx with transfected cells in high-K Ringer's buffer for 2 h at room temperature. Following the incubation, cells were captured on Whatman GF/C filters (25 mm) and washed 4 times with 5 mL of high-K Ringer's buffer. Bound ^{125}I-Bgtx was measured in a γ counter. All measurements were done in triplicate. Controls included cells not transfected and cells transfected with wild-type Kv4.2 and muscle-type nAChR. Specific Bgtx binding was calculated by subtraction of non-specific binding, as measured by ^{125}I-Bgtx binding in the presence of 2.5 μM unlabeled Bgtx, from total binding. For

binding dissociation measurements, Bgtx was displaced by addition of 2.5 μM unlabeled Bgtx, following pre-incubation with ^{125}I-Bgtx to equilibrium over 2 h. Remaining bound toxin was measured over multiple points during a 60 minute period. Data were fit according to a two-component dissociation using

$$y = y_0 + A_1 e^{xt1} + A_2 e^{xt2}$$

with the second exponential term negligible because of the rapid reduction in ^{125}I-Bgtx binding upon addition of unlabeled Bgtx. Bgtx binding association data collected over a 60 minute period were fit according to

$$y = A_1 - A_2 e^{-kob\ x}$$

Where, to calculate an observed k_{ob} from which the apparent k_{on} was calculated according to

$$k_{on} = \frac{k_{ob} - k_{off}}{[radioligand]}$$

3.2.6 Western blot

From tsA201 cells transfected with Kv4.2, Kv4.2-HAP and KChIP cDNAs, total cell lysates were prepared (lysis buffer: 150 mM NaCl, 50 mM Hepes pH 7.4, 0.5% Triton) and insoluble matter pelleted. Equal amounts of the supernatant were separated by 4–15% gradient SDS-PAGE following heat denaturation at 37°C for one hour in SDS-gel loading buffer. Separated proteins were transferred to nitrocellulose membranes. After a blocking reaction (PBS; 0.05% Tween; 5% non-fat milk powder), Kv4.2-antibody (Alomone Labs) was diluted 1:200 and incubated at room temperature for two hours. After washing the membrane, horseradish-peroxidase-conjugated goat anti-rabbit IgG antibody (1: 10,000) was incubated for 1 h. Enhanced chemiluminescence reagents were used for signal detection.

3.2.7 Fluorescence Imaging

To assess Kv4.2-HAP protein expression in live tsA201 cells, cultures were mounted on glass slides and washed with PBS and incubated with Alexa Fluor-Bgtx for 1 h at room temperature. Cells were washed with PBS and fixed with 4% paraformaldehyde. In all cases, fluorescent Bgtx binding was prevented by co-incubation with an excess of unlabeled Bgtx. Cells were imaged using a Zeiss Axiovert 200M Fluorescence Imaging microscope (Carl Zeiss, Inc.) equipped with a Roper CoolSnap CF color camera and a Roper CoolSnap HQ monochrome camera (Roper Scientific, Inc.) controlled by MetaMorph 6.0 software.

For TIRF (total internal reflection fluorescence) imaging experiments on primary neurons, cell-containing MatTek dishes were transferred to the CellR imaging system (Olympus Europe, Hamburg, Germany). The system was equipped with an automated filter wheel for excitation filters and with 488 nm (20 mW) and 532 nm (50 mW) DPSS lasers (Melles Griot, CA, USA) for TIRF imaging. For improved recording stability, the microscope frame and all optical elements were maintained at 34^{o}C using the temperature control incubator (Solent Scientific, Segensworth, UK). Images were collected with a CCD camera (Orca, Hamamatsu, Japan). In TIRF mode, fluorescent molecules are excited by the thin evanescent field formed above the glass substrate due to total internal reflection of the laser beam (attenuated to 5-10%). In Huganir (2004) paper, the author stated that preincubation with tubocurarine completely eliminated endogenous binding background but did not block detection of the Bgtx binding sequence (HAP) tagged GluR2 receptors in transfected primary neurons. To label the HAP tagged GluR2 in neurons, they preincubated the transfected neurons with tubocurarine before incubation with rhodamine Bgtx to eliminate the low endogenous Bgtx binding background. There fore in our study, to block endogenous Bgtx binding, the transfected neurons were preincubated for at least 30 minutes with the nicotinic receptor antagonist tubocurarine (2 μM) prior to incubation with 5 μg/ml rhodamine- or Alex Fluor-conjugated Bgtx to label the Kv4.2-HAP channels. Fluorescence of tagged Bgtx was excited at 532 nm and collected above 560 nm, and fluorescence of GFP was excited at 488 nm and collected between 515 and 545 nm.

3.3 RESULTS

3.3.1 Insertion of Bgtx recognition sequences into the Kv4.2 S1-S2 loop

Two Bgtx binding sequences were designed and inserted individually into the extracellular S1-S2 loop of Kv4.2. This work was performed by Dr. Leonard Moise. One derived from the principal Bgtx binding site on the *Torpedo* nAChR α1 (Tα1) subunit and the other from a high affinity peptide (HAP) sequence derived from a combinatorial phage-displayed library (Balass, Katchalski-Katzir et al. 1997; Harel, Kasher et al. 2001). These sequences were inserted into a location distant from the voltage sensor (S4) and ion selectivity filter to minimize perturbation of the channel structure and function (Figure 24, generated by Leonard Moise). Constructs were generated both with (i.e., Kv4.2-HAP-EGFP) and without (i.e., Kv4.2-HAP) cytoplasmic N-terminal EGFP-tags to facilitate visualization of Kv4.2-HAP. Studies of Tα1 chimera were limited by the low surface expression of this construct (e.g., see Figure 33).

3.3.2 Heterologously expressed Kv4.2-HAP constructs form functional channels

The engineered constructs of Kv4.2-HAP were co-expressed with its auxiliary binding protein, KChIP3 (Rhodes, Carroll et al. 2004), in tsA201 cells. Whole-cell recordings from Kv4.2-HAP transfected cells showed large, depolarization-activated,

rapidly inactivating currents with amplitudes similar to those reported for wild-type channels (Hoffman, Magee et al. 1997; Yeola and Snyders 1997), demonstrating functional expression of Kv4.2-HAP channels on the cell surface (Figure 26). In order to facilitate the study of Kv4.2-HAP channels, an EGFP (enhanced green fluorescence protein) fusion protein construct Kv4.2-HAP-EGFP construct was also prepared and tested. Expression of Kv4.2-HAP and Kv4.2-HAP-EGFP constructs in transfected tsA201 cells were further validated by Western blot analysis using an anti-Kv4.2 antibody (Figure 27).

3.3.3 Introduction of HAP tag sequence into S1-S2 is functionally silent

Any investigation into the normal physiological role of particular ion channels requires that the kinetic properties of heterologously expressed channels closely match those of the native protein. To determine the effect of HAP tag on Kv4.2, we compared the properties of Kv4.2-HAP to those of untagged Kv4.2 in tsA201 cells.

3.3.3.1 Time to peak

In Figure 28, we measured the time required for currents to reach peak amplitude in voltage steps from -30mV to +50mV. The rate of activation for Kv4.2-HAP was

decreased at more hyperpolarized potentials relative to wild-type Kv4.2, but it was nearly identical to wild-type at more depolarized potentials (Figure 28).

3.3.3.2 Peak conductance-voltage relationship

Figure 29 compares the peak conductance-voltage relation (G/G_{max}). The profiles of the voltage dependence of the peak conductance/activation of Kv4.2 and Kv4.2-HAP are remarkably similar. The analysis of current decay is shown in Figure. Although minor differences in inactivation kinetics were observed for Kv4.2-HAP and wild type Kv4.2, the overall profile of the voltage dependence of the inactivation was similar. The current decay fit very well with a single-exponential, and the rate of inactivation increased with strong depolarization.

3.3.3.3 Inactivation time constants

Inactivation time constants τ for Kv4.2 and Kv4.2-HAP were compared and shown in Figure 30.

3.3.3.4 Rate of recovery from inactivation

Traces of the recovery of Kv4.2, Kv4.2-HAP and Kv4.2-HAP-GFP from inactivation are shown Figure 31. Recovery was characterized using a typical two-pulse

protocol where the time spent at the interpulse potential was varied to characterize the recovery time course. Even though the plot shows Kv4.2-HAP recovers more slowly from inactivation than wild type, the differences are minimal.

In summary, the results of functional analysis of Kv4.2-HAP show that the insertion of the HAP tag into the S1-S2 loop of Kv4.2 does not prevent formation of functional channels. The expressed Kv4.2-HAP currents displayed fast inactivation and rapid inactivation with similar characteristics to Kv4.2, thus indicating that insertion of the HAP sequence, within the S1-S2 linker, does not disrupt subunit synthesis, assembly or protein structure.

3.3.4 ^{125}I-Bgtx binds Kv4.2-HAP expressed in tsA201 cells

Specific binding of Bgtx to living cells was measured by Leonard Moise in a ^{125}I-Bgtx binding assay. Transfected tsA201 cells were incubated with radioactive Bgtx, washed to remove unbound toxin, and then the cell associated radioactivity was determined (Figure 33). Specific Bgtx binding was observed for HAP-tagged Kv4.2, but not for Ta1-tagged channels. Controls included cells not transfected and cells transfected with wild-type Kv4.2 and muscle-type nAChR. These results suggest that the HAP tag may serve as a tool for tracking surface expressed Kv4.2 channels.

Bgtx binding affinity for Kv4.2-HAP was calculated by measuring association and dissociation with Kv4.2-HAP using the same ^{125}I-Bgtx binding assay. Association measurements over a 60 minute period yielded an apparent k_{on} value of 8.01 x 10^{5} M^{-1} min^{-1}. An apparent dissociation rate k_{off} was measured by displacement of ^{125}I-Bgtx with excess unlabeled Bgtx and calculated as 7.4 x 10^{-3} min^{-1}. The ratio of k_{off} to k_{on} translates into an apparent equilibrium dissociation constant of 9.2 x 10^{-9} M.

3.3.5 Bgtx has no apparent effect on normal channel function of Kv4.2-HAP

Whole cell recordings were performed to measure the effect of Bgtx on Kv4.2-HAP channel function. The toxin had no significant effect on channel opening (Figure 34), suggesting that the bound toxin has limited functional effect when bound to the S1-S2 extracellular linker.

3.3.6 Surface expressed Kv4.2-HAP in tsA201 cells are visualized using fluorescence Bgtx

Visualization of Bgtx bound to Kv4.2-HAP demonstrated the utility of HAP-tagged Kv4.2 for localization and membrane trafficking studies (Figure 35). tsA201 cells transfected with either wild-type Kv4.2 or HAP-tagged Kv4.2, and co-transfected with a GFP construct to identify expressing cells, were incubated with Alexa Fluor-Bgtx for 1 h at room temperature, washed and fixed. Fluorescent Bgtx bound HAP-tagged Kv4.2 and

was competed off in the presence of excess unlabeled Bgtx. No binding was observed for wild-type Kv4.2. Taken altogether, these results suggest that the insertion of the HAP sequence for Bgtx binding can offer a practical method for tracking and isolating Kv4.2-HAP channels in living cells.

3.3.7 Bgtx binds Kv4.2-HAP and GluR2-HAP expressed in cultured hippocampal neurons

Although the HAP tag with Alexa Fluor-Bgtx enabled the visualization of Kv4.2 channels in living tsA201 cells, it was important to demonstrate a similar utility for this method in neurons, thus providing an essential step in understanding the mobility for these channels. Therefore, we visualized expression and subcellular distribution of HAP-tagged Kv4.2 in rat hippocampal cultured neurons (Figure 36). The experiments were perforemed and data were analysed by Leonard Khiroug and Evgeny Pryazhnikov in University of Helsinki, Helsinki, Finland. Cells were transfected with a construct encoding Kv4.2 with both GFP and HAP and treated with Bgtx (tagged with either Alexa Fluor or rhodamine). In order to avoid Bgtx binding to endogenous nicotinic ACh receptors, cells were preincubated with the receptor antagonist tubocurarine (2 μM) prior to application of Bgtx. To highlight perimembrane fluorescently-tagged molecules, total internal reflection fluorescence (TIRF) excitation mode was used. Images were obtained 18-36 hours after transfection using two fluorescence channels, green for GFP (excitation 488 nm, emission around 530 nm) and red for Bgtx-Alexa or Bgtx-rhodamine (excitation 532 nm, emission above 560 nm). Under this imaging configuration, the GFP image

represents all recombinant Kv4.2 molecules independently of their membrane insertion, while the rhodamine-Bgtx image only shows membrane-inserted Kv4.2 molecules capable of binding extracellular Bgtx (Figure 36a). We found that Kv4.2-HAP-GFP channels were distributed throughout neuronal somata and dendrites (Figure 36a, GFP clusters), but only a few Kv4.2-HAP-GFP channels were located in the plasma membrane (Figure 36a, rhodamine-Bgtx clusters). Analyses of cluster size yielded a significantly smaller value for clusters of membrane-inserted Kv4.2 channels, presumably due to aggregation of intracellular Kv4.2 clusters (Figure 36b). Finally, we found that total cellular and surface distributions of Kv4.2-HAP-GFP expressed in hippocampal neurons appeared similar to those of the previously described GluR2-HAP-GFP (Sekine-Aizawa and Huganir 2004) (Figure 36c). Our data on live transfected hippocampal cultures expressing the Kv4.2-HAP-GFP demonstrate that tagged Kv4.2 channels can surface express in primary neuronal cells. More importantly, we show it was possible to track and monitor the channels in primary neuronal cells.

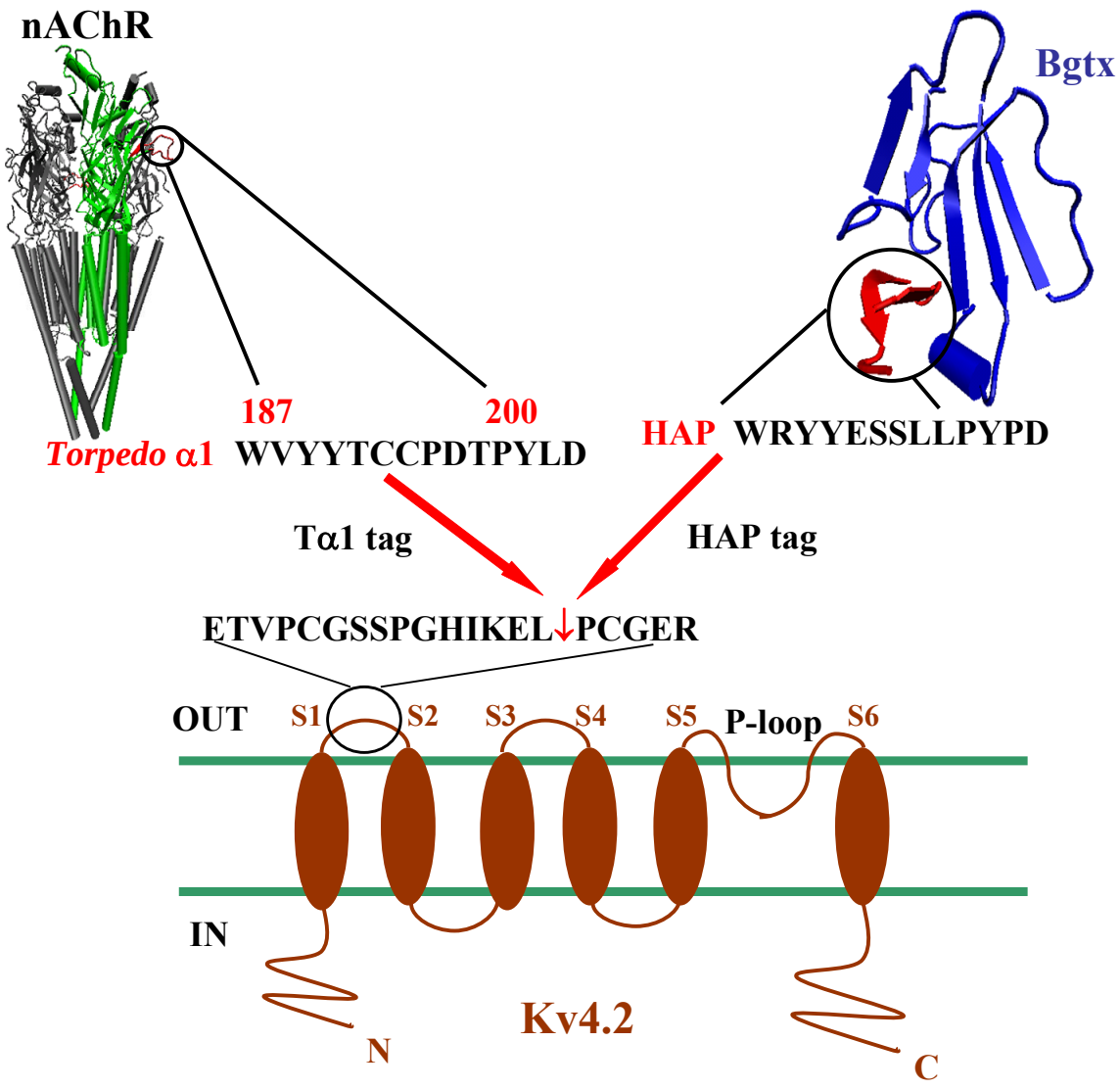
nAChR
Bgtx
187
200
Torpedo α1 WVYYTCCPDTPYLD
HAP WRYYESSLLPYPD
Tα1 tag
HAP tag
ETVPCGSSPGHIKEL↓PCGER
OUT
S1
S2
S3
S4
S5
P-loop
S6
IN
Kv4.2
N
C

Figure 25. Schematic representation of the insertion of the HAP and Tα1 tag into the S1-S2 linker of Kv4.2. The diagrams depicting the structure of the neuronal nicotinic receptor (*left*) next to the structure of Bgtx (*right*) and the topology of Kv4.2 are shown. Two engineered sequences were inserted individually into the extracellular S1-S2 loop. One is derived from the principal Bgtx binding site on the *Torpedo* nAChR α1 subunit (Tα1) with sequence of WVYYTCCPDTPYLD. The other is from a high affinity peptide (HAP) sequence, WRYYESSLLPYPD, derived from a combinatorial phage-displayed library. These sequences were inserted into a location distant from the voltage sensor (S4) and ion selectivity filter (P loop) to minimize perturbation of the channel structure and function. (Figure generated by Leonard Moise)

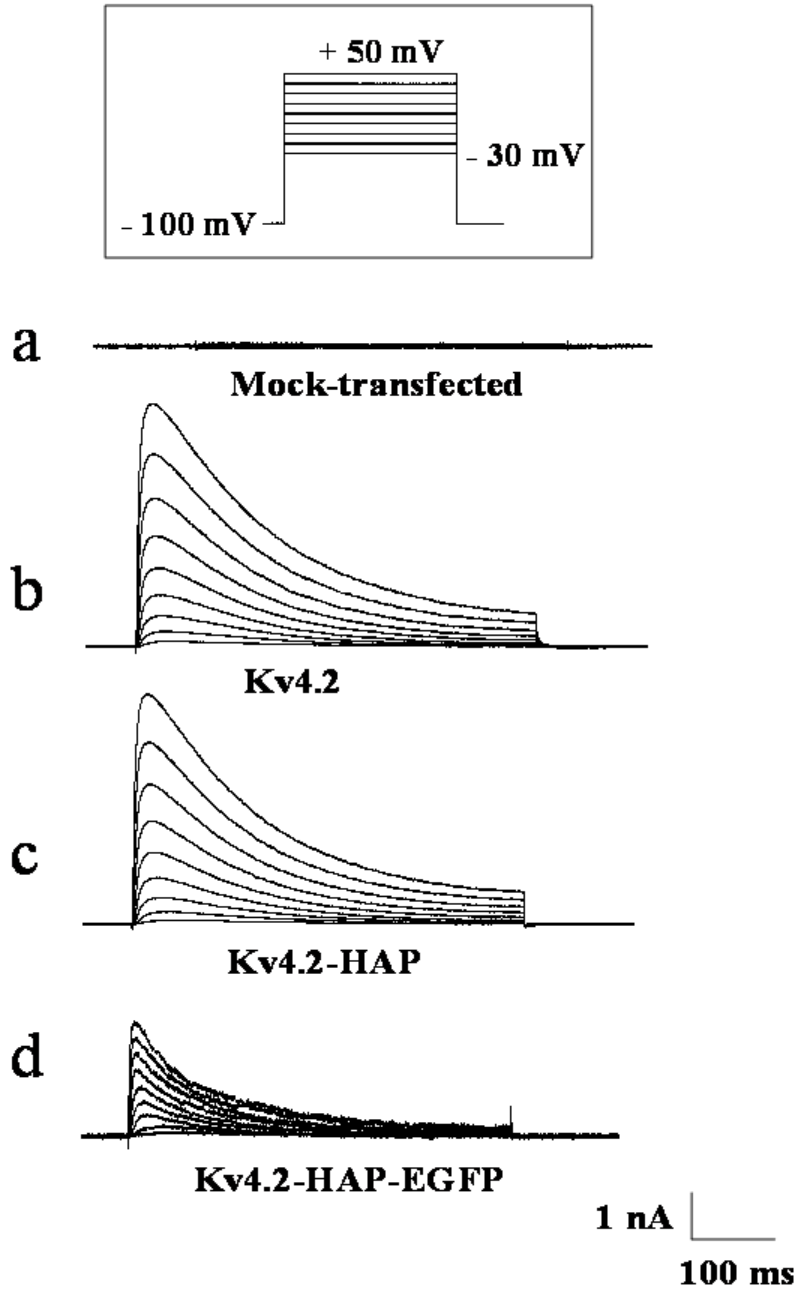
+ 50 mV
- 30 mV
- 100 mV
a
Mock-transfected
b
Kv4.2
c
Kv4.2-HAP
d
Kv4.2-HAP-EGFP
1 nA
100 ms

Figure 26. Heterologous expression of wild-type Kv4.2, HAP-tagged Kv4.2 (Kv4.2-HAP) and EGFP plus HAP–tagged Kv4.2 (Kv4.2-HAP-EGFP) in tsA201 cells. K+ currents in tsA201 cells were elicited by voltage clamp steps delivered at 10-mV increments from a holding potential of -80 mV to step depolarization from -30 mV to +50 mV (*inset*). Each voltage step was 600 ms. Representative traces are from mock-transfected cells (*a*), or cells transfected with Kv4.2 (*b*), Kv4.2 -HAP (*c*), or Kv4.2-EGFP-HAP (*d*). (B) Western blotting of Kv4.2 vs. Kv4.2-HAP and Kv4.2-HAP-EGFP vs. Kv4.2-EGFP. All constructs were detected with anti-Kv4.2 antibody.

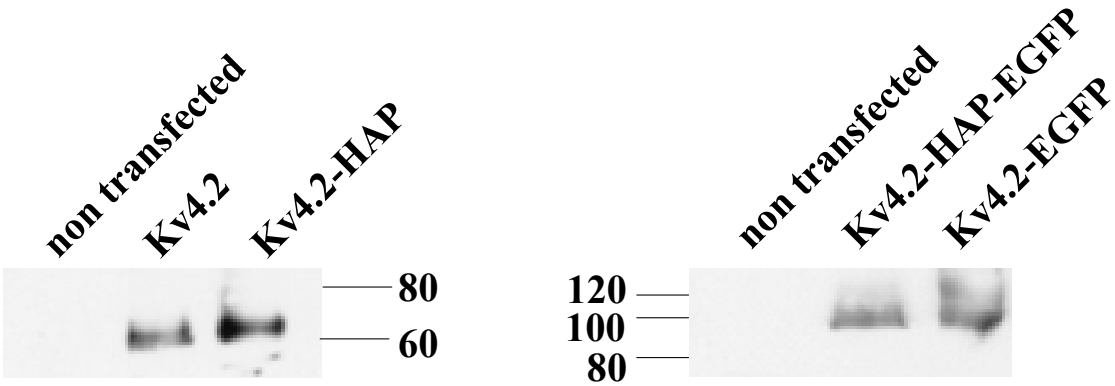

Figure 27. Heterologous expression of Kv4.2-HAP and Kv4.2 -HAP-EGFP in tsA201 cells. West blotting of Kv4.2, Kv4.2-HAP, Kv4.2-HAP-EGFP and Kv4.2-EGFP is shown as indicated. All constructs were detected with anti-Kv4.2 antibody. (Data provided by Lenard Moise)

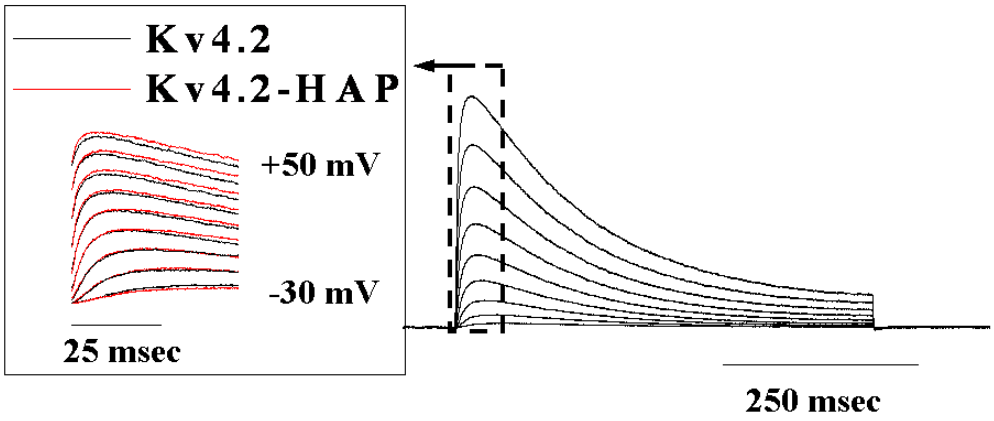
Kv4.2
Kv4.2-HAP
+50 mV
-30 mV
25 msec
250 msec

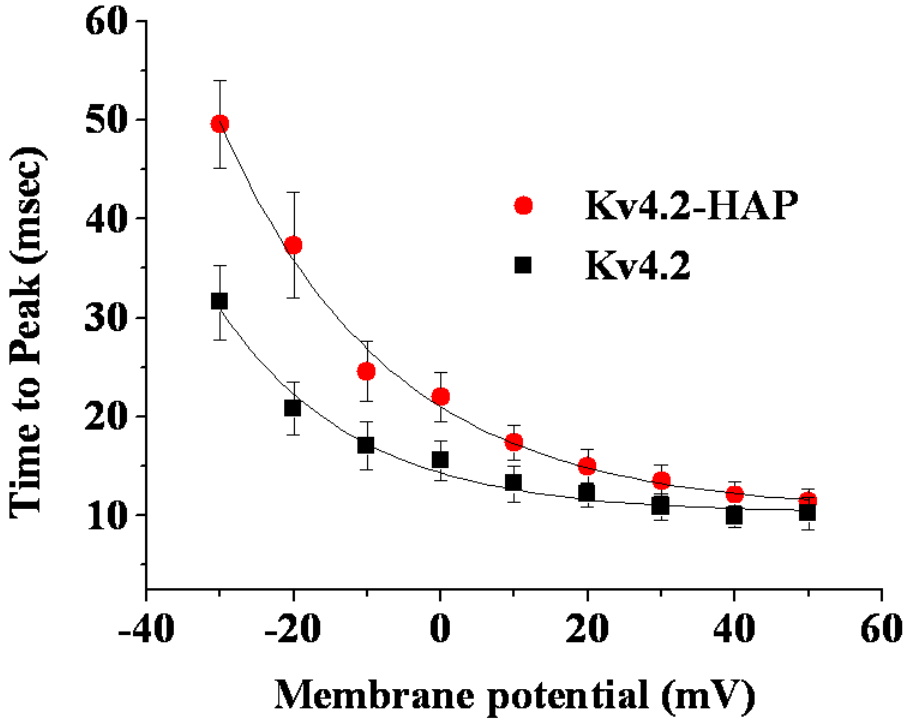
Time to Peak (msec)
Membrane potential (mV)
Kv4.2-HAP
Kv4.2
60
50
40
30
20
10
-40
-20
0
20
40
60

Figure 28. Activation kinetics for Kv4.2 and Kv4.2-HAP: time to peak current analysis. Representative current traces of inactivation for Kv4.2 (■) and Kv4.2-HAP (●) are shown in figure 26. The upper panel shows detailed superimposed peak currents for Kv4.2 and Kv4.2-HAP in response to step membrane depolarization. For Kv4.2-HAP, the time to peak current was slower at more hyperpolarized potentials in comparison to wild-type Kv4.2 but nearly identical at more depolarized potentials. Values represent the Mean ± S.E.M of three to four cells.

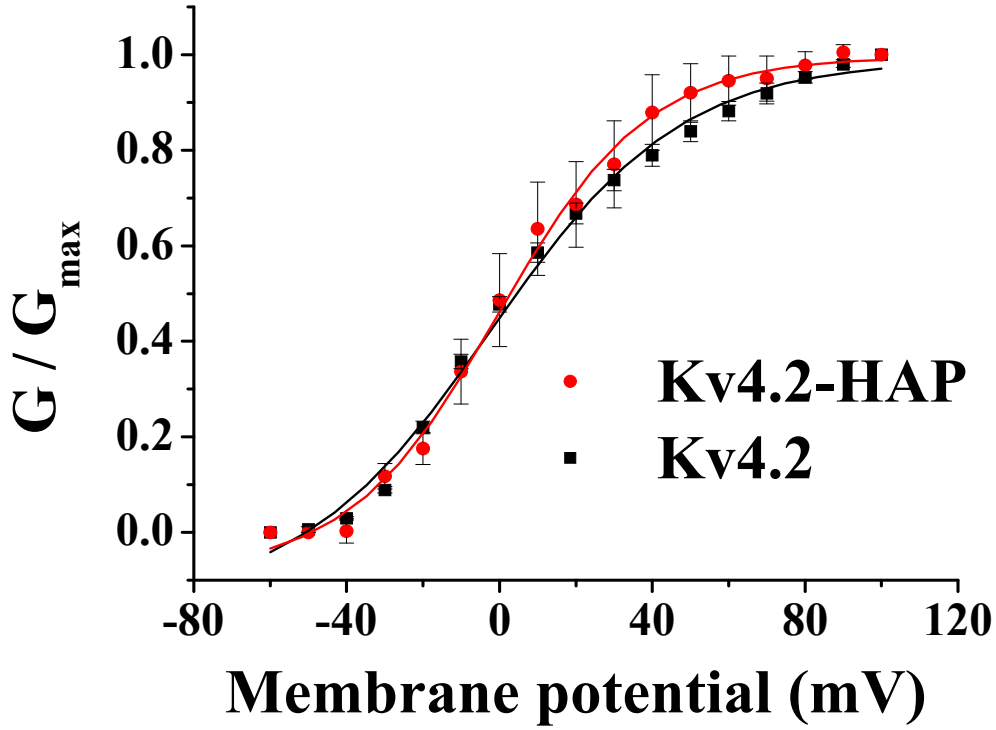

Figure 29. Activation kinetics for Kv4.2 and Kv4.2-HAP: normalized peak conductance-voltage relations for Kv4.2 (■) and Kv4.2-HAP (●). Normalized conductance (G/G_{max}, conductances at the indicated potential divided by G_{max}, the maximum conductance, at +50 mV) plotted as a function of voltage for the currents expressed by Kv4.2 and Kv4.2-HAP. Peak conductance (G) was calculated as $G = I_p/(V_m - V_{eq})$, where I_p, V_m and V_{eq} are the peak current, the test potential and the K+ equilibrium potential, respectively. The continuous lines across the data points are the best-fits to Boltzmann functions. Values represent the Mean ± S.E.M of three to four cells.

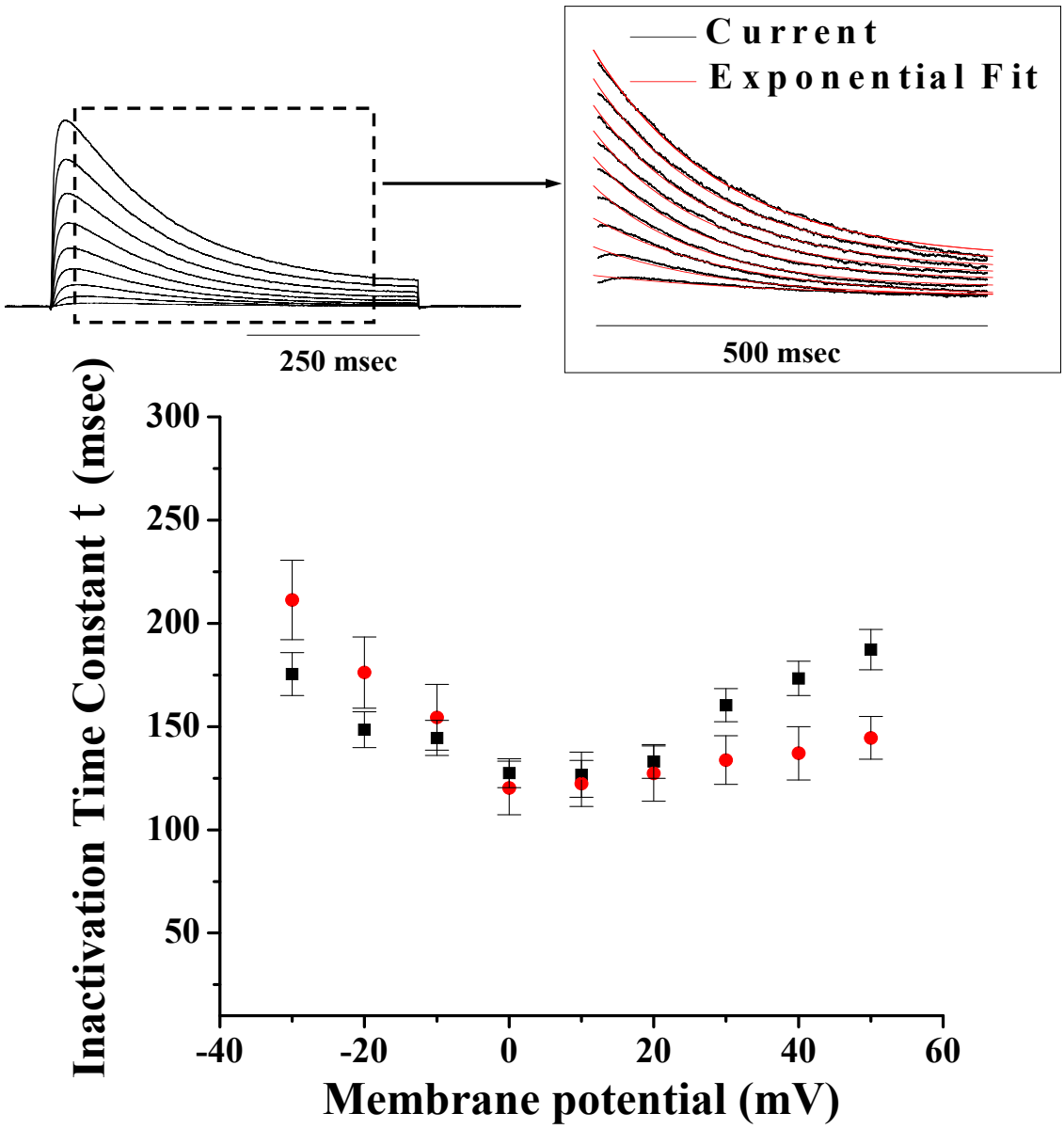
Current
Exponential Fit
250 msec
500 msec
Inactivation Time Constant t (msec)
300
250
200
150
100
50
-40
-20
0
20
40
60
Membrane potential (mV)

Figure 30. Inactivation time constants τ Kv4.2 (■) and τ Kv4.2-HAP (●). The upper panel shows inactivation kinetics of currents in response to step membrane depolarization. The time course of fast inactivation fits mono-exponentially. The continuous lines in red overlaid represent single exponential fits. Note that, the rate of inactivation increases with strong depolarization. Rate of inactivation decreased in the voltage range from –30 mV to 0 mV and increased from 0 mV to +50 mV. Values represent the Mean ± S.E.M of three to four cells.

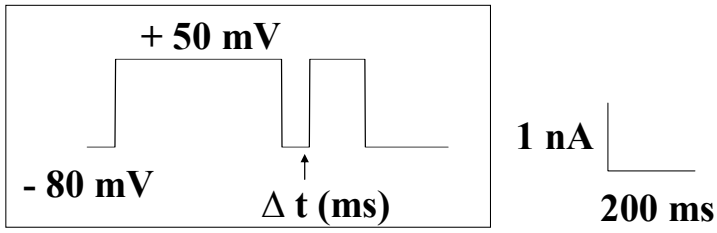

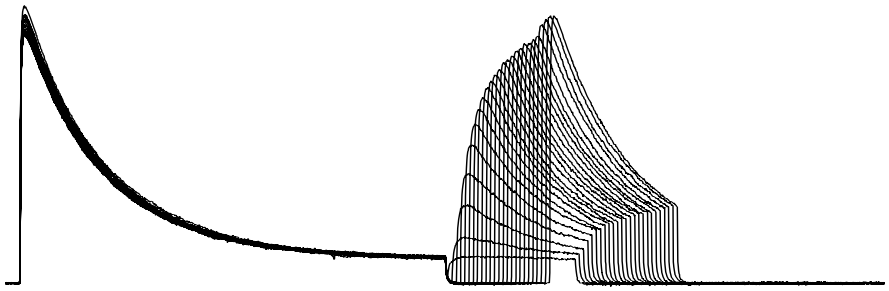

Kv4.2

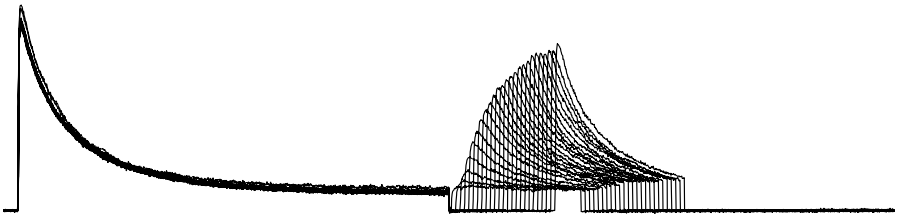

Kv4.2-HAP

Kv4.2-EGFP-HAP

Figure 31. Rate of recovery from inactivation. Representative current traces of the recovery from inactivation for Kv4.2 (*a*), Kv4.2-HAP(*b*) and Kv4.2-EGFP-HAP (*c*) respectively are shown. A paired pulse protocol shown as an insert was applied to transfected tsA201 cells. Each cell was depolarized from -80 to +50 mV by two steps, varying the coupling intervals (Δt) from 5 ms to 245 ms in 10 ms increments. The membrane potential during the interval was also -80 mV. This set of paired pulses was applied once every 15 s.

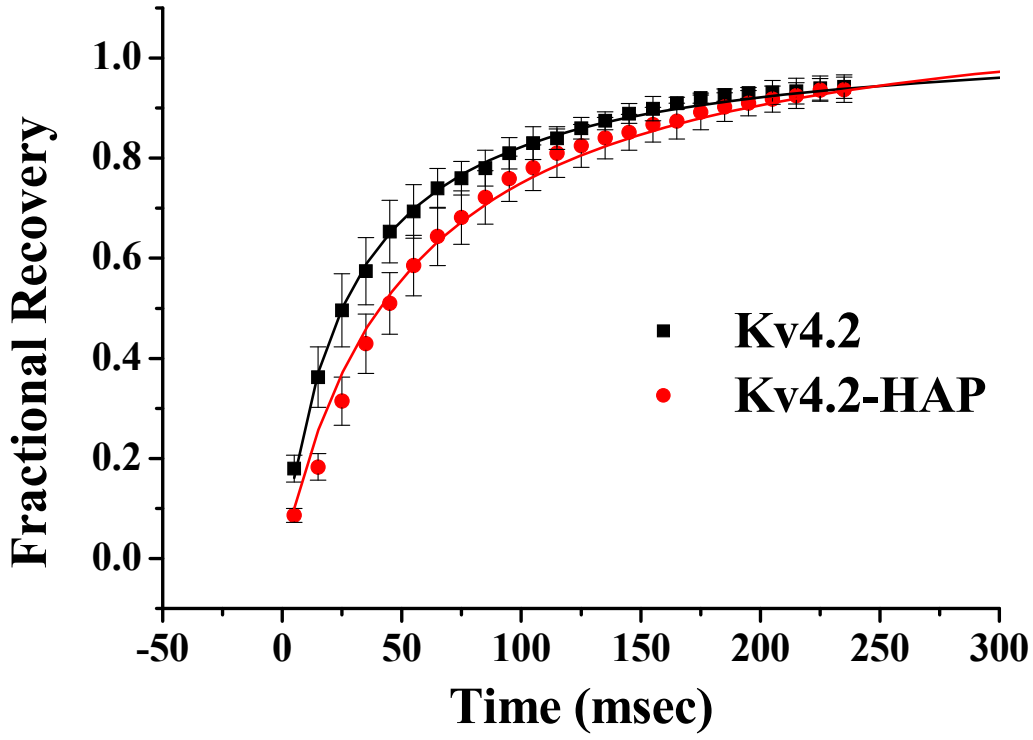

Figure 32. Analysis of rate of recovery from inactivation. The time course of recovery from inactivation is analyzed by normalizing the peak current amplitude of the second pulse to that of the first pulse and plotting as a function of inter-pulse duration. Kv4.2-HAP(●) recovers slightly more slowly from inactivation than wild-type Kv4.2 (■). Values represent the Mean ± S.E.M of three to four cells.

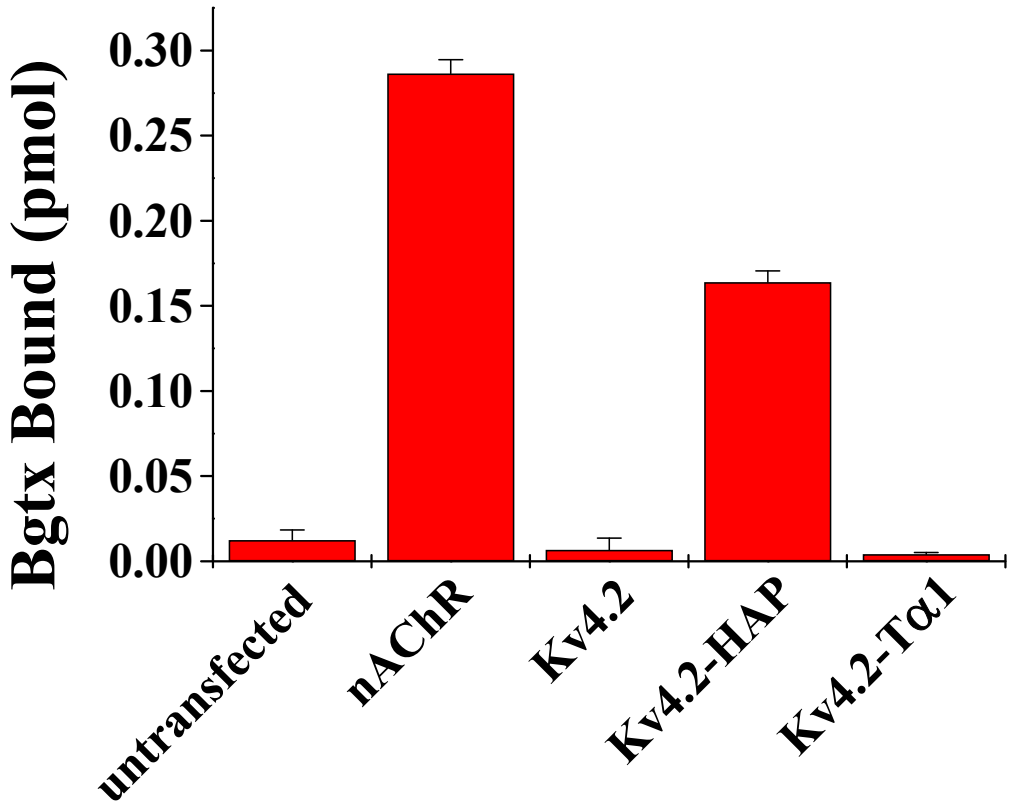

Figure 33. Specific binding of ^{125}I -Bgtx to Kv4.2-HAP. tsA201 cells were incubated with ^{125}I -Bgtx for 2 h. Specific Bgtx binding was observed for Kv4.2-HAP as well as muscle-type nAChR, but not for Kv4.2 or Kv4.2-Tα1. The data shown are representative of three experiments. (Data provided by Leonard Moise)

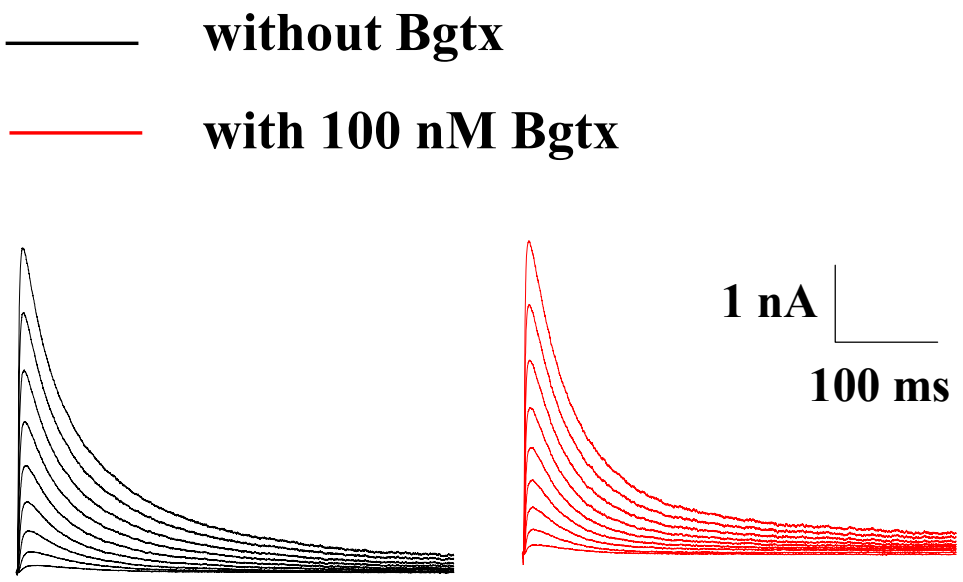

Figure 34. Bgtx had no apparent effect on Kv4.2-HAP currents. The current traces were recorded in the absence (black) or in the presence of 100 nM Bgtx (red). The presence of Bgtx had little effect on the activation of the channels.

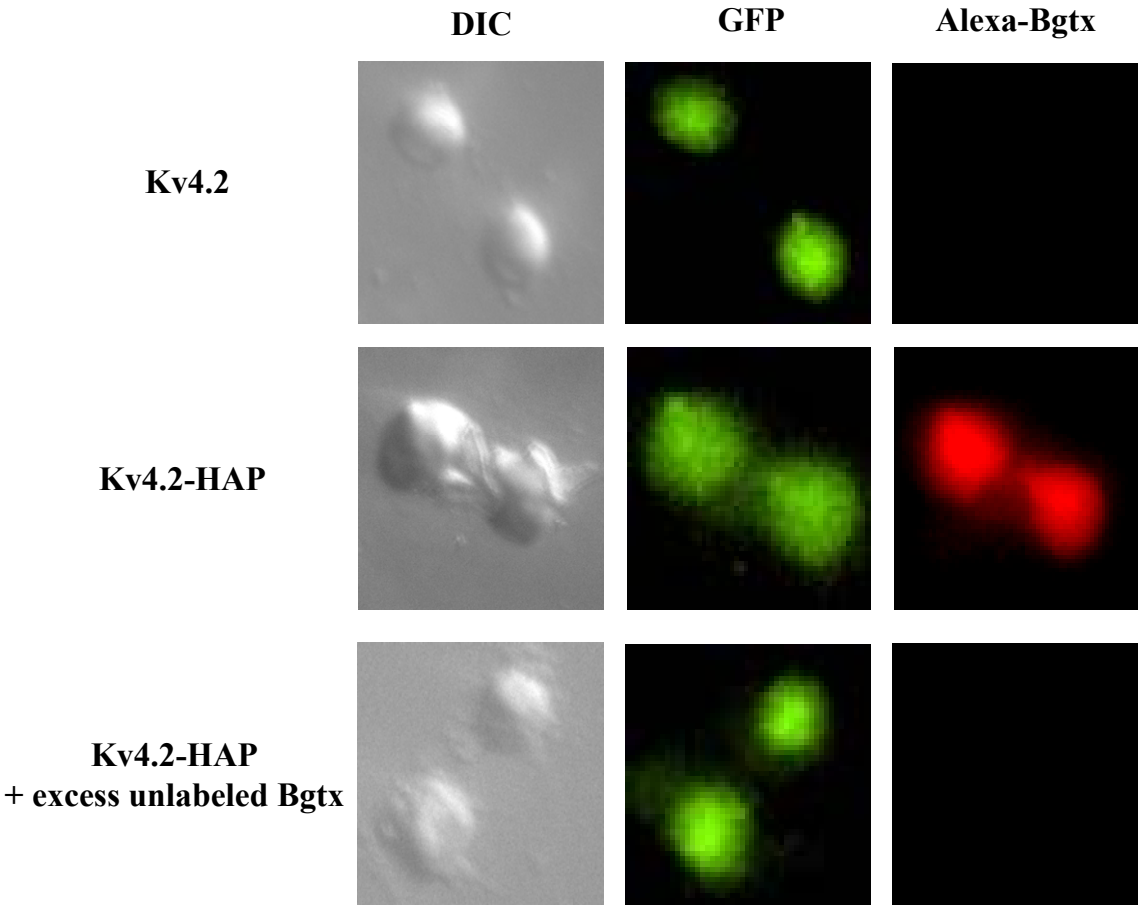

Figure 35. Alexa Fluor-Bgtx binds Kv4.2-HAP expressed in tsA201 cells. DIC, image of differential interference contrast; GFP, fluorescent image of GFP (detecting co-transfected GFP, green); Alexa Fluor-Bgtx, fluorescent image of Alexa Flour-Bgtx (detecting Kv4.2-HAP, red). Wild-type Kv4.2 or HAP-tagged Kv4.2 was co-transfected with GFP in tsA201 cells. Fluorescent Bgtx bound HAP-tagged Kv4.2 and was competed off in the presence of excess unlabeled Bgtx. No fluorescent Bgtx binding was observed for wild-type Kv4.2. (Figure generated by Leonard Moise)

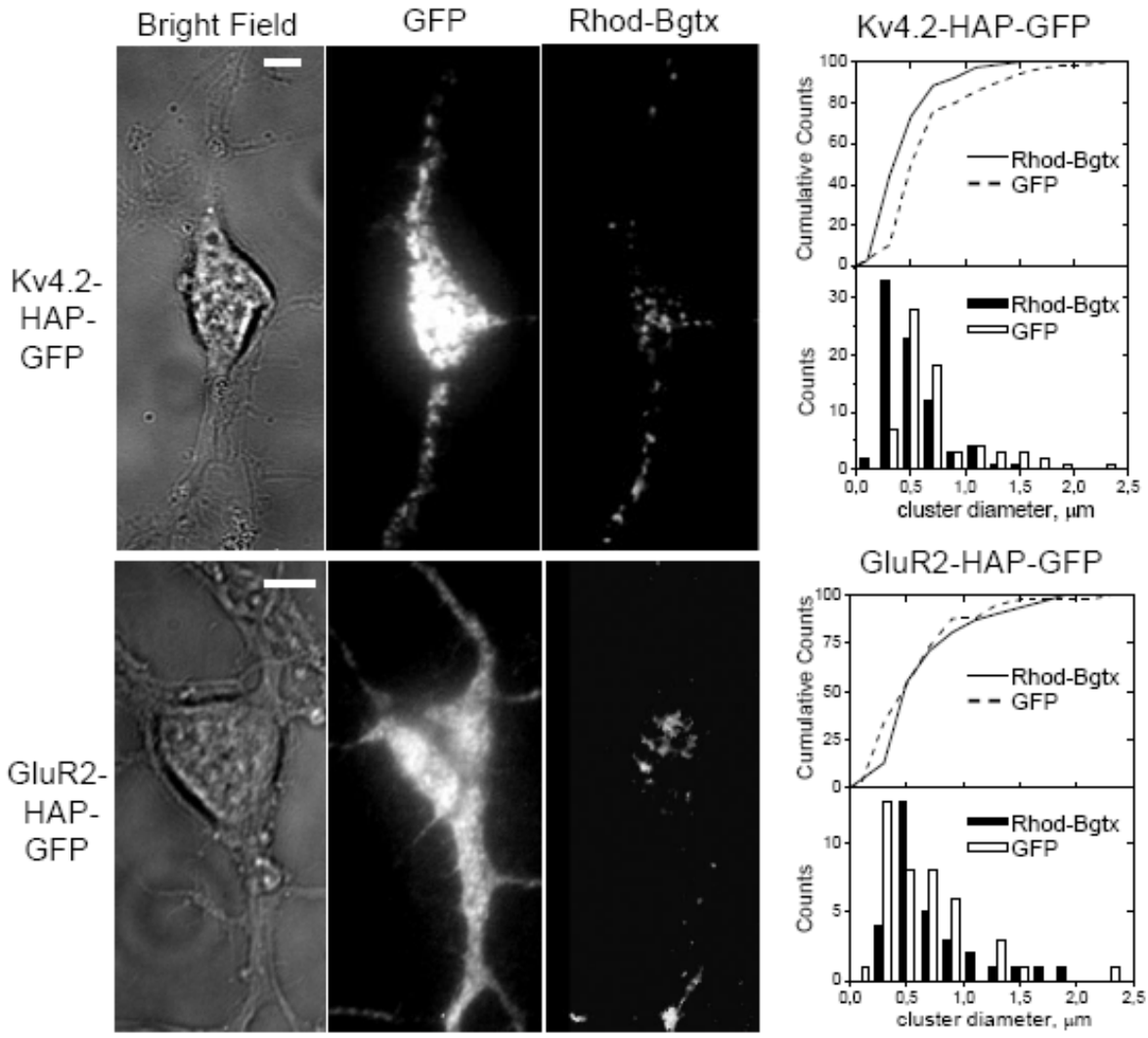
Bright Field
GFP
Rhod-Bgtx
Kv4.2-HAP-GFP
GluR2-HAP-GFP
Kv4.2-HAP-GFP
Cumulative Counts
Rhod-Bgtx
GFP
Counts
cluster diameter, μm
GluR2-HAP-GFP
Cumulative Counts
Rhod-Bgtx
GFP
Counts
cluster diameter, μm

Figure 36. Rhodamine-Bgtx binds Kv4.2-HAP-GFP and GluR2-HAP-GFP expressed in primary rat hippocampal neurons. A) A neuron transfected with Kv4.2-HAP-GFP. Bright Field, bright-field image of the neuron; GFP, fluorescence image of GFP (detecting all Kv4.2-HAP-GFP channels); Rhod.-Bgtx, fluorescence image of rhodamine-Bgtx (detecting membrane-inserted Kv4.2-HAP-GFP). B) Cumulative curves and histograms of Kv4.2-HAP-GFP cluster size distribution obtained for green and red clusters (n=6 cells). C) A neuron transfected with GluR2-HAP-GFP. Bright Field, bright-field image of the neuron; GFP, fluorescence image of GFP (detecting both perimembrane and membrane-inserted GluR2-HAP-GFP channels); Rhod.-Bgtx, fluorescence image of rhodamine-Bgtx (detecting only membrane-inserted GluR2-HAP-GFP). D) Cumulative curves and histograms of GluR2-HAP-GFP cluster size distribution obtained for green and red clusters (n=3 cells). Scale bars: 5 μm. (Data provided by Leonard Khiroug and Evgeny Pryazhnikov in University of Helsinki, Helsinki, Finland)

3.4 DISCUSSION

3.4.1 Kv4.2-HAP channels appear to be functional and efficiently trafficked

In this study, we demonstrate that the chimeric construct of Kv4.2-HAP expresses as well as the wild-type Kv4.2 channel in mammalian cells, and that channel function is comparable to wild-type Kv4.2 channels even in the presence of Bgtx. By using fluorescent Bgtx, we were able to readily detect surface expression of Kv4.2 channels in living cells including transfected primary neurons. Although interior placement of HAP sequence produces Bgtx binding, it produces no detectable pharmacological activity. Taken together, the successful introduction of HAP binding sequence into S1-S2 loop of Kv4.2 extracellularly demonstrates that the HAP construct may serve as a flexible technique for labeling and visualization of channel trafficking in transfected primary neurons.

3.4.2 Rationale for HAP strategy

The rationale of the adoption of interior placement of HAP is based on:

1. HAP is a modification of a peptide selected for Bgtx binding from a phage-display peptide library and corresponds to α87–200 of *Torpedo* acetylcholine receptor. The affinity for Bgtx of HAP is two orders of magnitude greater than that of the lead peptide.

2. Bgtx as a high affinity ligand for muscle type and α7 nAChRs, has been extensively used more than 30 years to study the structure, function, distribution and trafficking of the receptor (Fambrough and Hartzell 1972; Couturier, Bertrand et al. 1990; Levandoski, Lin et al. 1999; Sanders and Hawrot 2004). Similar high-affinity ligands are not available for voltage-gated potassium channels, unfortunately.
3. Recent studies using Bgtx binding sequence have been very successful for ligand-gated ion channels as well as GPCRs as I have stated in chapter 1, but its use in voltage-gated ion channels has not been explored.
4. In those successful studies using Bgtx binding sequence to monitor receptor mobility, including AMPA (Sekine-Aizawa and Huganir 2004) and $GABA_A$ receptors (Bogdanov, Michels et al. 2006), as well as $GABA_B$ receptors (Wilkins, Li et al. 2008), the tag has been placed at N-terminus. HAP insertion site, which is in S1-S2 loop extracellularly, is unique in that it extends the ability to perform trafficking studies to proteins whose N- and C- termini are intracellular or functionally involved and therefore unavailable for tagging.

3.4.3 Use of Kv4.2-HAP vs. Kv4.2 antibodies

Given that all currently commercially available Kv4.2 antibodies label internal epitopes (Anderson, Adams et al. 2000; Takeuchi, Takagishi et al. 2000; Wong, Newell et al. 2002; Gardoni, Mauceri et al. 2007), our extracellular HAP tag is unique in that it can surface-label membrane protein. Thus, quantifying and visualizing the surface

expressed Kv4.2 channels in live cells becomes easily achievable. The relatively small size of Bgtx (~8 kDa) as compared with antibodies may offer a further advantage in tissue penetration and accessibility.

3.4.4 Use of Kv4.2-HAP vs. auxiliary fusion proteins

Kv4.2 plays its key role in the modulation of neuronal function through formation of multi-protein complexes with signaling molecules and auxiliary proteins (Anderson, Adams et al. 2000; Bahring, Dannenberg et al. 2001; Callsen, Isbrandt et al. 2005; Gardoni, Mauceri et al. 2007). Although using tagged Kv4.2 binding proteins (i.e., KChIP, filamin or PSD95) has gained us important insights about channel localization and trafficking (Petrecca, Miller et al. 2000; Wong, Newell et al. 2002; Pourrier, Herrera et al. 2004), factors that target these associated proteins (including localization, expression and clustering) may indirectly affect Kv4.2 participation in these multi-protein complexes. Thus, it is important to be able to visualize the tagged Kv4.2 channel itself.

3.4.5 Structural and functional considerations for location of the HAP tag in Kv4.2

Nearly all tags reported were classically introduced at the C- or N- termini of Kv4.2 channel for the obvious convenience. However, it is becoming increasingly apparent that terminal tails of Kv4.2 contain a variety of regulatory domains. The N- and C-termini of Kv4.2 channel have been shown to be absolutely crucial for channel

expression and interactions with channel signaling molecules and binding proteins (Bahring, Dannenberg et al. 2001; Pourrier, Herrera et al. 2004; Callsen, Isbrandt et al. 2005; Bogdanov, Michels et al. 2006). Thus, any modification of N- and C-termini of the channel, may lead to erroneous results and complicate the interpretation of the findings. In particular, GFP fusion protein, its bulky N-or C- terminal tag could perturb overall channel structure and impede cellular functions. Therefore, it is significant that our engineered HAP insertion site is extracellular (S1-S2 loop) and far removed from the intracellular N- and C-termini (Figure 25). Our observation that application of Bgtx to HAP-tagged Kv4.2 has minimal effect on channel activation suggests that the S1-S2 loop can be sterically constrained with little apparent functional affect. Although the S1-S2 loop of Kv4.2 had previously been modified with an eight tandem repeat Myc tag insertion following Cys221, the effect of antibody binding on channel activity was not reported (Rivera, Ahmad et al. 2003). It is also of interest that the Talpha1 sequence was poorly tolerated after insertion into the S1-S2 region of Kv4.2, while the HAP insertion into the same region, immediately after L219, was well tolerated. It is likely that the reactive vicinal cysteines within the Talpha1 sequence may interact with an extracellular disulfide involving the two endogenous cysteine residues in S1-S2 of Kv4.2. The HAP sequence, in contrast, lacks the native vicinal cysteines and would not be expected to alter the endogenous disulfide pattern of Kv4.2.

3.4.6 Future implications

We have presented functional evidence that Kv4.2-HAP closely resembles those of wild type Kv4.2. Most importantly, Bgtx binds Kv4.2-HAP specifically and we were able to detect and image the tagged channels in live cells including cultured neurons by using fluorescent Bgtx. These findings offer the possibility that Bgtx recognition sequences can be similarly inserted into the extracellular domains of other Kv channels for which appropriate probes are lacking. In cases in which high affinity Bgtx binding is conferred in the absence of pharmacological sensitivity, such constructs would be of considerable utility for studies of channel localization and trafficking given the abundance of commercially available reporter group derivatives of Bgtx. The paradigm employed here, therefore, can be used as a general strategy for the design of chimeras for studying channel trafficking and distribution for other members of the Kv ion channel family.

CHAPTER IV

α-BUNGAROTOXIN IS AN ALLOSTERIC MODULATOR OF A $GABA_A$ RECEPTOR SUBTYPE

4.0 ABSTRACT

Ionotropic γ-aminobutyric acid type A receptors ($GABA_A$Rs) mediate critical inhibitory actions in the brain. α-bungarotoxin (Bgtx) is best known as an antagonist of muscle-type nicotinic acetylcholine receptors at neuromuscular junctions or homomeric α7 in CNS almost irreversibly to antagonize their function. Here, we report a novel interaction between Bgtx and the α1β2 $GABA_A$ receptor. We have investigated the cross-binding properties of Bgtx, on recombinantly expressed α1β2 $GABA_A$ receptor. In two-electrode voltage clamp measurements in *Xenopus* oocytes, we observed that Bgtx reversibly blocks GABA-evoked currents in receptors containing solely α1 and β2 subunits in a dose-dependent manner. In contrast, α1β2γ2 receptors are Bgtx-insensitive. These results introduce a previously unrecognized tool for the analysis of $GABA_A$Rs. The results also suggest that adjacent β2 subunits confer Bgtx inhibition and that this mechanism of toxin inhibition is allosteric.

4.1 BACKGROUND AND SIGNIFICANCE

4.1.1 $GABA_A$Rs overview

The amino acid gamma-aminobutyric-acid (GABA) prevails in the CNS as an inhibitory neurotransmitter that mediates its effects through GABA receptors. GABA is quantitatively one of the most important inhibitory transmitters in the central nervous system. It is estimated that, depending on the brain region, 20 to 50% of all central synapses use GABA as their transmitter (Sieghart 1995). There are two main types of GABA receptors: fast-acting ionotropic $GABA_A$ receptors, and slower-acting metabotropic $GABA_B$ receptors. $GABA_A$ receptors are the predominant type of GABA receptor in the brain. $GABA_A$ receptors are chloride channels and they are members of the Cys-loop pentameric ligand-gated ion channel (LGIC) superfamily and share structural and functional homology with other members of that family. $GABA_A$Rs exist in all organisms with a nervous system, including invertebrates. The textbook model of inhibition holds that $GABA_A$ receptors at synapses on cell bodies or dendrites open an anion conductance, which results in both postsynaptic hyper-polarization (mediated by Cl^- influx) and shunting of excitatory currents. This leads to a transient decrease in the probability of initiation of an action potential. This model may not always be correct because $GABA_A$ receptors can sometimes depolarize neurons, and even cause a net excitatory action: the reversal potential of the mixed Cl^-/HCO_3^- conductance is frequently more positive than the resting membrane potential, especially in some immature neurons prior to the expression of the main Cl^- extrusion system, the KCC2

transporter (Rivera, Voipio et al. 1999). Under some circumstances, $GABA_A$ receptor activation can result in the opening of voltage-gated Ca^{2+} channels, and even in the initiation of action potentials (Cherubini, Gaiarsa et al. 1991).

Molecular cloning identified numerous ligand-gated ion channel GABA receptor subunits. The $GABA_A$ subunits are divided into subfamilies based on the degree of sequence identity. Each subunit has a similar overall transmembrane topology (Figure 37). A ~200 amino acid extracellular N-terminal domain forms the agonist binding sites. All subunits in the superfamily have a 15-residue disulfide-linked loop in the extracellular domain that is the basis of the superfamily name, Cys-loop receptors. Although the specific amino acids in the loop are not well conserved across the superfamily, the loop itself is absolutely conserved. Each subunit contains a similarly sized C-terminal domain with four α-helical, membrane-spanning segments (M1, M2, M3, and M4), a large but variable-sized intracellular loop between the M3 and M4 segments, and a short extracellular C-terminus. The M3–M4 loop is an important site for regulation by phosphorylation and for localization at synapses.

4.1.2 Physiological and pharmacological significance of $GABA_A$Rs

GABA limits the excitability of neuronal activity in all areas of the brain. Excessive GABAergic signaling results in sedation, amnesia, and ataxia, whereas the mildest attenuation of GABAergic signaling results in arousal, anxiety, restlessness,

insomnia, and exaggerated reactivity. Endogenous compounds, such as neuroactive steroids, allosterically modulate receptor function.

A large body of evidence indicates that $GABA_A$ receptors are the targets of a variety of pharmacologically and clinically important drugs. Thus, binding studies and electrophysiological and behavioral experiments medicated that the anxiolytic, anticonvulsant, muscle relaxant and sedative-hypnotic benzodiazepines and some depressant barbiturates enhance the action of GABA on $GABA_A$ receptors. In contrast, some convulsants bicuculline or picrotoxinin or some insecticides, reduce the actions of GABA on this receptor. And finally, some anesthetics produce at least part of their pharmacological effects by interacting with $GABA_A$ receptors. A large series of experiments indicated that, in most cases, the above-mentioned compounds do not interact directly with the GABA binding site but exert their action by binding to additional allosteric sites at $GABA_A$ receptors. This binding induces a conformational change in the $GABA_A$ receptors that in turn influences the binding properties of other binding sites present on these receptors (causing complex allosteric interactions of these binding sites) and modulates GABA-induced Cl^- ion flux (Sieghart 1995). The basic information on the pharmacology of $GABA_A$ receptors has been derived from brain studies or recombinant receptor studies have supported and extended our knowledge on these receptors and provided final evidence for the existence of a multiplicity of $GABA_A$ receptors in the brain.

Recent neurobiological studies on new animal models and receptor subunit mutations have revealed novel aspects of the $GABA_A$ receptors, which might allow

selective targeting of the drug action in receptor subtype-selective fashion. More precisely, the greatest advances have occurred in the clarification of the molecular and behavioral mechanisms of action of the $GABA_A$ receptor agonists already in the clinical use, such as benzodiazepines and anesthetics, rather than in the introduction of novel compounds to clinical practice (Korpi and Sinkkonen 2006). It is likely that these new developments will help to overcome the present problems of the chronic treatment with nonselective $GABA_AR$s agonists, that is, the development of tolerance and dependence, and to focus the drug action on the neurobiologically and neuropathologically relevant substrates. Knowledge of the complex pharmacology of $GABA_AR$s will eventually enable site-directed drug design to further our understanding of GABA-related disorders and of the complex interaction of excitatory and inhibitory mechanisms in neuronal processing (Hevers and Luddens 1998).

4.1.3 Heterogeneity of $GABA_AR$ subtypes and assembly

$GABA_A$ receptors are assembled from a family of 19 homologous subunit gene products and form numerous, mostly hetero-oligomeric, pentamers (Macdonald and Olsen 1994; Rudolph and Mohler 2006). Eight different subunits, some of them with different subtypes, have been described for the $GABA_AR$s (α1–6, β1–3, γ1–3, δ, ε, π, θ and ρ1–3). The assembly of $GABA_AR$ as heteropentamers produces complex subtype heterogeneity in structure, which is the major determinant of their pharmacological profile (Figure 37).

These various subtypes differ in abundance in cells throughout the nervous system and thus in functions related to the circuits involved. Clearly it is the nature, stoichiometry, and arrangement of the subunits that determine details of pharmacological selectivity. Thus, pharmacology can often provide evidence for structural heterogeneity and informs us about the subunit composition of native receptor subtypes. Further specificity of $GABA_A$ receptor expression exists among different neuronal cell types. Some groups of neurons contain a vast number of different subunits, whereas other regions express only a limited number of transcripts. Great heterogeneity of both subunit type and expression patterns of $GABA_A$ receptors occurs throughout the CNS. $GABA_A$ receptor subunits are also differentially expressed within specific subcellular regions within individual neurons, and such selective trafficking and localization of $GABA_A$ receptor subunits contributes to the functional properties of $GABA_A$ inhibition.

Even for the 19 subunit genes, the evidence for some subunits participating in native subtypes varies considerably. In general, different subunit combinations give rise to different subtypes of $GABA_A$Rs with characteristic electrophysiological and pharmacological properties. Although the possible number of combinations of these subunits is huge, only a fraction of them exist in the brain. The functional receptors are formed by the co-assembly of five subunits around the central channel axis (Figure 37). Functional channels are formed following heterologous expression of only $GABA_A$ α and β subunits. The subunit stoichiometry is mainly 2α and 3β subunits, although evidence has been presented for 3α and 2β (Im, Pregenzer et al. 1995). Arguing against the 3-α stoichiometry is the fact that α homomers do not form to any significant extent but β homomers do (Krishek, Moss et al. 1996; Taylor, Thomas et al. 1999). This suggests that

β subunits can assemble at adjacent positions but α subunits cannot. Multiple approaches have demonstrated that following heterologous expression of α, β, and γ subunits, the most common subunit stoichiometry is 2 α, 2 β, and 1 γ subunit. Experiments in heterologous expression systems have also shown that the extent to which the population of expressed receptors uniformly contains the γ subunit may depend on the ratios of α to β to γ mRNA injected in oocytes or cDNA transfected in cells. In receptors expressing the δ or ε subunits, they replace the γ subunit. The pharmacological properties of the receptors and their single-channel properties depend on the subunit isoform composition of the receptors. (reviewed by Akabas, 2004)

Immunocytochemistry data suggest that there is high expression of $GABA_A$ receptor subunits α1,β1,β2, β3, and γ2 throughout the brain, though there are differences in their distribution. γ2 subunit is the most abundant subunit in rat brain and in most regions. The γ2 subunit is required for synaptic localization of $GABA_A$Rs, usually associated with the α1,β2 subunits. α1β2γ2 is the prevalent native combination. The vast majorities, approximately 75 to 80% of $GABA_A$Rs in the CNS, contain α1β2γ2. Recombinant α1β2γ2 receptors have been shown to have a 2α-2β-1γ stoichiometry [denoted (α1)2(β2)2 γ2], and this stoichiometry is supported by coimmunoprecipitation results from rat or mouse brain (Sieghart and Sperk 2002).The relative arrangement and stoichiometry of the subunits in the α1β2γ2 pentameric $GABA_A$ receptor has also been functionally studied using tandem and triple subunit constructs expressed in *Xenopus* oocytes. In these constructs the C-terminus of one subunit is linked to the N-terminus of

another subunit. $GABA_A$ receptor subunits can be concatenated to a trimer that can be functionally expressed upon combination with a dimer. It turned out that many combinations did not result in the functional expression. In contrast, four different combinations of triple subunits with dual subunit constructs, all resulting in the identical pentameric receptor γ2−β2−α1−β2−α1, counterclockwise when viewed from the synaptic cleft. This stoichiometry and subunit arrangement of αβγ $GABA_A$ receptor is generally accepted.

Although progress has been made with respect to identifying native $GABA_A$ receptors, in most cases a direct identification of receptor subtypes *in vivo* currently is not possible, oweing to the lack of highly selective pharmacological tools.

4.1.4 Postsynaptic and extrasynaptic $GABA_A$ receptors

In the mammalian CNS, GABA synapses were long known to generate fast and precisely timed inhibitory activity in the form of inhibitory postsynaptic currents. $GABA_A$ receptors clustered at the postsynaptic terminal are activated by a near-saturating concentration of GABA (>500 μM) that is released from presynaptic terminals. The concentration of GABA in the synaptic cleft remains high for ~500 milliseconds, after which it is rapidly cleared by active transporters and simple diffusion. Activation of postsynaptic $GABA_A$ receptors is characterized by a current that rapidly peaks then decays over the time course of milliseconds. This form of inhibition is designed to allow

high-fidelity rapid and precise transmission of presynaptic activity into a postsynaptic signal.

Another important question surrounding the role of $GABA_A$ receptors is the extent to which they occur at sites other than postsynaptic elements of inhibitory synapses on cell bodies and dendrites. Other possible locations, such as on presynaptic buttons and extrasynaptic membranes on postsynaptic neurons or even on axons, have been demonstrated using a variety of methods (Figure 38). The diffusional inhibitory transmission mediated by $GABA_A$Rs located outside the synapses and activated by GABA present in the extracellular space has triggered a great deal of interest. This form of inhibition is generally referred to as tonic inhibition, while the conductance generated by the $GABA_A$Rs is known as tonic conductance. The physiological and pharmacological importance of perisynaptically and extrasynaptically localized $GABA_A$Rs has recently become increasingly appreciated. Several lines of evidence indicate that the tonic conductance is generated by extrasynaptic GABAA receptors located at the soma, dendrites, or axons (Orser 2006). The best-characterized extrasynaptic $GABA_A$ receptors are those containing $\alpha 6$ and δ subunits in cerebella granule neurons. The functional properties of extrasynaptic receptors were first described in the landmark reports of Brickley et al. (Brickley, Cull-Candy et al. 1999). Immunogold-labeled images showed that δ-containing $GABA_A$ receptors in cerebella granule neurons reside exclusively in the extrasynaptic dendritic membrane (Nusser, Sieghart et al. 1998). The tonic conductance was also absent in many brain areas after deletion of the δ subunit.

The biophysical properties of synaptic and extrasynaptic $GABA_A$ receptors also differ. Extrasynaptic $GABA_A$ receptors desensitize more slowly and less extensively than synaptic $GABA_A$ receptors. The high affinity and slow desensitization suggests that extrasynaptic $GABA_A$ receptors are optimally designed to detect and respond to a low persistent concentration of GABA in the extracellular space.

4.1.5 Selective $GABA_A$ receptor ligands

The $GABA_A$ receptor contains distinct-binding sites for many pharmacologically active compounds, including anesthetics, anticonvulsants, anxiolytics, and sedative-hypnotics. GABA binds to the extracellular N-terminal domain of each α-subunit, near the interface between the α- and β-subunits. Most pharmacologically active compounds do not interact directly with the GABA-binding site, but act as allosteric modulators, either reducing or enhancing the actions of GABA at its receptor. These include such drugs as the synthetic steroid anesthetic, alphaxalone, a positive allosteric modulator of GABA activity, which interacts with δ-subunit-containing $GABA_A$ receptors, and the loop diuretic, furosemide, which interacts with α6 subunit-containing $GABA_A$ receptors to allosterically decrease GABA activity. In addition to distinct-binding sites for neuroactive steroids and furosemide, $GABA_A$ receptors contain binding sites for picrotoxin, sedative-hypnotic barbiturates, ethanol, inhalation anesthetics, and a number of divalent cations. The most extensively studied of the allosteric modulators of GABA

on $GABA_A$ receptors are the benzodiazepines, and widely prescribed for the treatment of anxiety disorders for many decades. Most of the known pharmacological heterogeneity of $GABA_A$ receptors concerns the sensitivity of the benzodiazepine site that is formed at the interface between the α and γ subunits (Pritchett, Sontheimer et al. 1989; Korpi, Mattila et al. 1997). Receptors lacking the γ_2 subunit or containing the α4 or α6 subunits are practically insensitive to benzodiazepine site agonists (Seeburg, Wisden et al. 1990). The two GABA binding sites are formed at the interfaces between the α and β subunits. Only a few different structural classes of ligands are known for the GABA binding site, reflecting the strict structural requirements for $GABA_A$ receptor recognition and activation. To date these GABA binding site agonist compounds display little subunit subtype specificity with gaboxadol forming a class on its own as a "superagonistic" GABA mimetic (Saarelainen, Ranna et al. 2008). A few compounds have been identified which neither bind to the benzodiazepine nor the GABA binding sites and yet still show subtype-selective antagonistic activity, these include furosemide, otherwise known as a $Na^+/K^+/2Cl^-$ cotransporter blocker, that selectively blocks α(4/6)β(2/3)γ2 receptors (Korpi and Luddens 1997), and clozapine, an atypical antipsychotic drug, that inhibits furosemide-insensitive α1 containing receptors (Korpi, Wong et al. 1995). Drug discovery efforts have taken a number of paths with the goal of producing efficacy with reduced side effect liability. Major attempt is to synthesize compounds with selective affinity for different $GABA_A$ receptor subunits.

4.1.6 Bgtx binds to one subtype of $GABA_AR$ with adjacent β3 subunits

In a recent report, Bgtx was shown to bind to one subtype of $GABA_AR$ with adjacent β3 subunits but not to heterooligomeric receptors composed of α-, β-, and γ-subunits (McCann, Bracamontes et al. 2006). As far as published reports go, this is the only document in the literature showing Bgtx cross reactivity to $GABA_AR$. In studies on both muscle and neuronal cholinergic synapses, a guiding assumption has been that Bgtx binds only to nAChRs. Bgtx binding to $GABA_ARs$ in McCann's report bears us particular interest also because we have collected enough evidence in support of their observation. These authors expressed rat $GABA_AR$ β1, β2, β3, α2, or γ2 subunits in HEK cells and then stained cells live or after fixation and permeabilization. They found that only cells that expressed $GABA_AR$ β3 detectably bound Bgtx. Moreover, Bgtx also functionally blocked chloride conductance mediated by homooligomeric β3 and α1β3 $GABA_ARs$. Based on previous studies of $GABA_AR$ subunit composition and stoichiometry, α1β3γ2 receptor is in the order α1-β3-γ2-α1-β3 whereas α1β3 receptor is α1-β3-β2-α1-β3. Even though they lacked direct evidence, the authors reasoned that a lack of effect of Bgtx on α1β3γ2 receptors could indicate that Bgtx binds to an interface between adjacent β3 subunits.

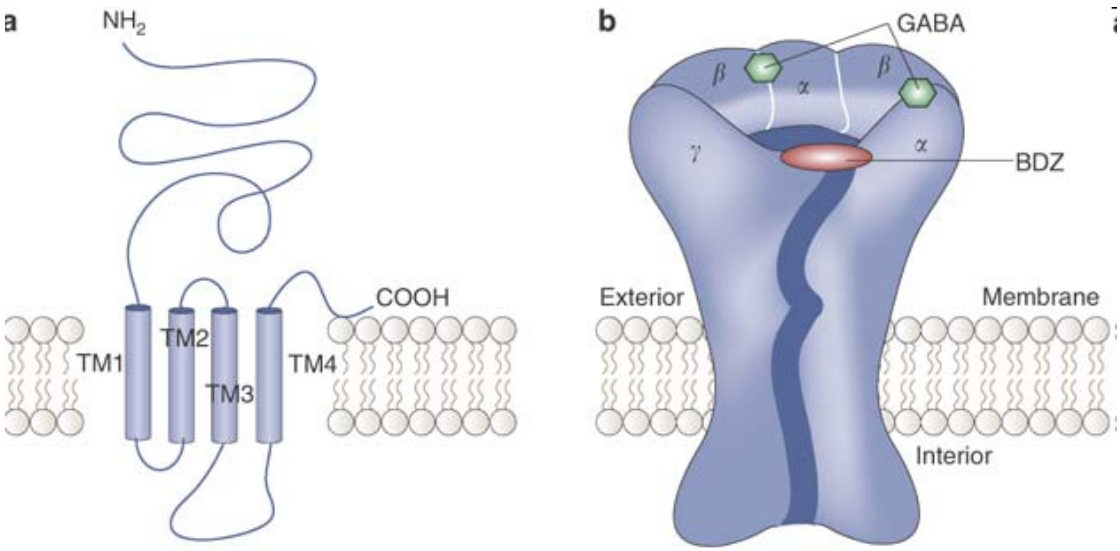

Figure 37. Schematic of a $GABA_A$ receptor. a) Proposed membrane topology and structural domains of a $GABA_A$ receptor subunit. Each subunit contains a large extracellular agonist-/antagonist-binding N-terminal domain, four transmembrane domains and a large cytoplasmic loop between M3 and M4. The second membrane-spanning domain (M2) forms the wall of the channel pore. b) Vertical cross section showing the pentameric arrangement of subunits (2α, 2β, and 1γ) necessary to create the central chloride permeable channel. The recognition sites for GABA are indicated at the interface between the α- and β-subunits, and for the benzodiazepines at the interface between α- and γ-subunits. (Adapted from Grigoriadis, 2009)

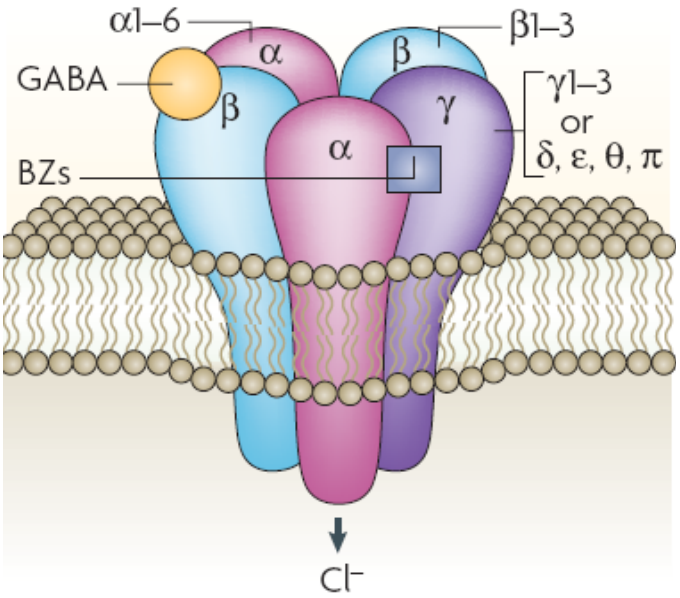
α1–6
β1–3
GABA
α
β
γ1–3
or
δ, ε, θ, π
β
α
BZs
Cl⁻

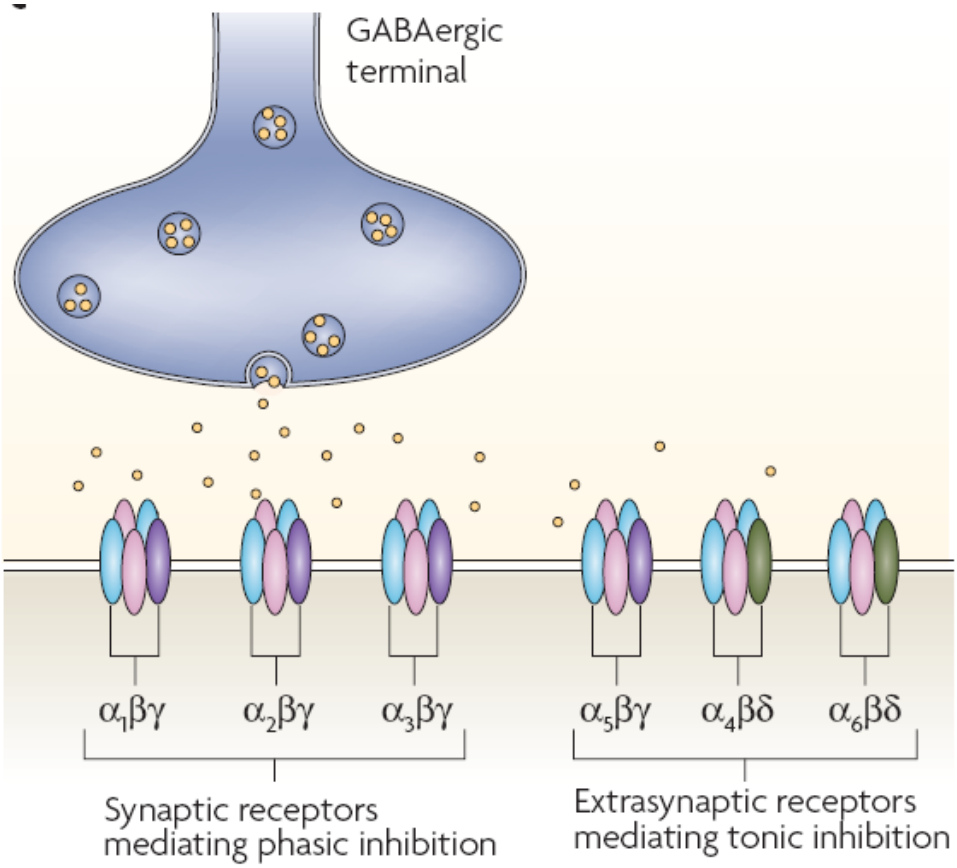
GABAergic
terminal
α1βγ
α2βγ
α3βγ
α5βγ
α4βδ
α6βδ
Synaptic receptors
mediating phasic inhibition
Extrasynaptic receptors
mediating tonic inhibition

Figure 38. Heterogeneity of $GABA_AR$s. Five subunits from seven subunit subfamilies (α, β, γ, δ, ε, θ and π) assemble to form a heteropentameric Cl- permeable channel. Despite the extensive heterogeneity of the $GABA_AR$ subunits, most $GABA_AR$s expressed in the brain consist of two α subunits, two β subunits and one γ subunit; the γ subunit can be replaced by δ, ε, θ or π. $GABA_AR$s composed of α (1–3) subunits together with β and γ subunits are thought to be primarily synaptically localized, whereas $\alpha5\beta\gamma$ receptors are located largely at extrasynaptic sites. Both these types of $GABA_AR$ are BDZ sensitive. By contrast, receptors composed of α (4 or 6)$\beta\gamma$ are BDZ insensitive and localized at extrasynaptic sites (adapted from Jacob, 2008).

4.2 MATERIALS AND METHODS

4.2.1 Oocyte isolation and expression of $GABA_AR$

Oocytes were harvested from mature *Xenopus laevis* females by survival surgery according to the National Institutes of Health guide for the care and use of laboratory animals. Small pieces of ovary were incubated for ~1 hour at room temperature with gentle agitation in 1 mg/mL collagenase Type I (Invitrogen, Carlsbad, CA) in ND96/Ca^{2+}-free medium containing 96 mM NaCl, 2 mM KCl, 1 mM $MgCl_2$ and 5 mM HEPES, pH 7.4. Oocytes were washed several times with ND96 to remove all traces of collagenase followed by several washes in ND96 recording solution containing 1.8 mM $CaCl_2$. Oocytes were manually selected and individually defolliculated.

Wild-type $GABA_AR$ cDNAs encoding the rat α1, β2 and γ2 subunits that were subcloned into pGEMHE were kindly provided by Dr. David Weiss, University of Alabama, Birmingham. Capped cRNAs were prepared by *in vitro* transcription from *Nhe*I-linearized cDNA template using the mMessage mMachine T7 kit (Ambion, Austin, Texas). On the day following their isolation, oocytes were injected with cRNAs mixed in a ratio of 1:1:10 for α:β:γ receptors and 1:1 for α:β receptors (10-200 pg/nl/subunit) using a Drummond microinjector (Drummond Scientific, Broomall, PA). Oocytes were maintained in antibiotic-supplemented ND96 medium (100 U/mL penicillin, 100 μg/mL streptomycin) at 15 ºC for electrophysiology experiments 2-8 days after injection.

4.2.2 Electrophysiology

GABA-evoked currents were measured using the two-electrode voltage clamp method with a Warner OC-725C. Electrodes of resistance 0.5–2.0 MΩ were filled with 3 M KCl, and recordings were performed in a Warner RC-3Z chamber with an OC-725 bath clamp headstage attached. The flow of various drug solutions into the chamber was regulated by solenoid valves driven by a Warner BPS-8 controller. The flow rate of the perfusion fluid was adjusted to 5 ml/min by gravity feed. Experiments were performed at room temperature.

4.2.3 Drug concentrations and method of application

GABA was prepared as a 10 or 100 mM stock solution in OR2 solution (115 mM NaCl, 2.5 mM KCl, 1.8 mM CaCl2,10mM HEPES, 0.003 mM atropine sulfate, pH 7.4). Bgtx first was dissolved in distilled water at 100 μM and then diluted to the final concentration in the OR2 solution. Drug pulse was applied for 5 s and washed out with OR2 solution for 2 min to insure the full recovery of the receptors. To test toxin block, oocytes were incubated in a solution containing the desired Bgtx concentration for 5-10 min after collecting initial responses evoked by a control dose of GABA. The oocyte was then challenged by a co-application of GABA and Bgtx. To measure recovery from toxin

block, GABA responses were collected from each oocyte prior to and after exposing the oocyte to Bgtx. Perfusion to wash out the Bgtx was commenced, and cell responsiveness to GABA was determined at various times. For measurement of the rate of Bgtx association, oocytes were incubated in 75 nM Bgtx. In measurements of Bgtx dissociation, oocytes were incubated in 250 nM Bgtx.

4.2.4 Statistical analysis on GABA response curves

All values are expressed as means ± SEM. Concentration/response curves were fitted by logistic nonlinear fit, using Origin 7.0 (MicroCal Software, Northhampton, MA).

4.3 RESULTS

4.3.1 Bgtx selectively blocks α1β2 $GABA_A$Rs

In initial studies, we found that in two-electrode voltage clamp measurements of GABA-evoked currents in *Xenopus* oocytes, Bgtx blocked heterologously expressed $GABA_A$ receptors assembled of α1 and β2 subunits only but had no effect on receptors containing a γ2 subunit (Figure 39). An excess of γ-subunit is co-injected with α1 and β2 subunits to insure α/β/γ assembly (Boileau, Baur et al. 2002). Figure 39 illustrates this result by comparing GABA-evoked currents before and after bath incubation of oocytes with 1 μM Bgtx for 10 minutes. GABA-gated current was effectively inhibited by Bgtx for $GABA_A$ receptors assembled of α1 and β2 subunits. Little effect of Bgtx was observed on $GABA_A$ receptors assembled of α1, β2 and γ2 subunits, with as much as 1 μM Bgtx, a concentration greater than 1000-fold its K_d for muscle-type nAChRs (Katz and Miledi 1973; Fertuck and Salpeter 1974). In contrast, both receptor subtypes exhibit no change in GABA-evoked currents following a 10 minute mock treatment (Figure 39). Both α1β2 and α1β2γ2 receptors can be blocked by prototypic $GABA_A$Rs antagonist picrotoxin or bicuculline (Figure 39, 40).

4.3.2 Determination of GABA EC_{50} values

GABA dose-response relationships were determined for α1β2 and α1β2γ2 receptors expressed in *Xenopus* oocytes. α1β2γ2 receptors had an EC_{50} value higher than α1β2 receptors. The EC_{50} values for α1β2 and α1β2γ2 receptors were 7.2± 0.2 μM and 22.0±0.7 μM, respectively. The obtained GABA EC_{50} values for α1β2 and α1β2γ2 receptors are in close agreement with published data (Figure 41).

4.3.3 Determination of IC_{50} value for Bgtx block of $\alpha1\beta2$ $GABA_A$Rs

In addition, the Bgtx blockage of $\alpha1\beta2$ receptors is also dose-dependent as shown in Figure 42. The data were fit to the logistic equation from which was calculated an IC_{50} value of 100 nM.

4.3.4 $\alpha7$ nAChRs antagonist MLA does not block $\alpha1\beta2$ $GABA_A$Rs

In the brain, much of Bgtx binding is thought to largely correspond to homomeric $\alpha7$ nicotinic nAChRs (Drisdel and Green 2000). We tested whether MLA, a $\alpha7$ nAChRs highly selective antagonist with nanomolar sensitivity, would also affect $\alpha1\beta2$ $GABA_A$Rs. As shown in Figure 43, the GABA current was affected little by 10 μM MLA.

4.3.5 Characterization of macroscopic kinetics of Bgtx block

At muscle type nAChRs, Bgtx blocks the cholinergic currents rapidly and the block is essentially irreversible (Rosenthal, Levandoski et al. 1999). The rate of onset of Bgtx block of $\alpha1\beta2$ $GABA_A$ receptors was determined by measuring the fractional block of GABA-evoked currents over a range of times of Bgtx exposure at 75 nM (Figure 44). The onset of Bgtx block is well fit to a bimolecular association model under pseudo-first-

order conditions. We calculated for k_{app} a value of 2.9 ± 0.9 x 10^5 M^{-1} s^{-1}, which is about double the value observed for Bgtx association with muscle-type nAChRs (Endo, Nakanishi et al. 1986). The data indicate that an incubation time of 5 minutes is sufficient to achieve full equilibration for Bgtx concentrations greater than 75 nM. The high affinity of Bgtx suggested by 100 nM of its IC_{50}, when considered together with the fast association rate, suggests that the rate of dissociation of Bgtx would be fast. In experiments designed to measure the reversibility of Bgtx (250 nM) binding upon washout of toxin by continuous perfusion, we found that majority of Bgtx dissociated within 5 minutes (Figure 44).

4.3.6 Bgtx-mediated inhibition is non-competitive

To elucidate the pharmacological mechanism of block by Bgtx, we assessed the GABA dose-response curve with or without Bgtx. If the Bgtx block was competitive, one would expect its concentration-response curve to be rightward shifted when the channel was inhibited by Bgtx. GABA 0.1– 500 μM was applied alone and concurrently with 100 nM (IC_{50}) Bgtx as shown in Figure 45. Applications of increasing concentrations of GABA or GABA with or without Bgtx result in sigmoidally shaped concentration-response curves with GABA 500 μM eliciting a maximal GABA-evoked response. There was no apparent rightward shift of the dose-response curve. Bgtx reduced the maximum response without dramatically altering the EC_{50}s for agonist (EC_{50}s for the GABA concentration-response relationship for GABA alone and the concentration-response relationship for GABA and Bgtx 100 nM were 6.0±0.6 μM and 9.1±1.4 μM,

respectively.). The results suggest that suggesting that Bgtx may have only a slight effect, if any, on GABA binding. The Bgtx binding site is more likely to be structurally separate from GABA binding site, and thus Bgtx inhibits GABA-evoked responses most likely by an allosteric mechanism.

4.3.7 Bgtx inhibition is abolished by introduction of the γ subunit

Benzodiazepine (BZD) potentiation of GABA-activated currents in recombinant $GABA_A$ receptors requires the presence of the γ subunit (Pritchett, Sontheimer et al. 1989). As illustrated in Figure 46, co-injection of α1 and β2 subunits resulted in GABA receptors showing no BDZ potentiation due to lack of binding pocket for BDZ located between γ2 and α1 subunits. These BDZ insensitive receptors, however, were blocked by Bgtx (Figure 46A). When we co-injected γ2 subunit along with α1 and β2 subunits, the assembled α1β2γ2 receptors showed characteristic BDZ potentiation but had no Bgtx sensitivity (Figure 46B).

4.3.8 Bgtx is likely to bind to α1β2 receptor at β2-β2 interface

In McCann's (2006) studies, Bgtx blocked homooligomeric β3 and heterooligomeric α1β3 receptors but not α1β3γ2 receptors. In addition, Bgtx binding site in that study was located in the N- terminus of β3 subunit. McCann suggested Bgtx binds to an interface between adjacent β3 subunits. Our results also show that introduction of

the γ subunit either removes or masks the determinants of Bgtx binding in α1β2 receptors. Although subunits composition of the recombinant $GABA_A$ receptor composed of only α1 and β2 subunit has yet to be fully unveiled, [α1]2[β2]3 in a order of α1-β2-β2-α1-β2 is mostly favored. Based on previous studies, the well accepted composition of α1β3γ2 receptors is [α1]2[β3]2[γ2]1 in the order α1-β3-γ2-α1-β3 (Baumann, Baur et al. 2001; Baumann, Baur et al. 2002; Boileau, Pearce et al. 2005; Gonzales, Bell-Horner et al. 2008). Noncompetitive inhibition of Bgtx suggests that the binding site on the α1β2 receptor is distant from the GABA binding pocket, which is located at α1β2 subunit interface. To reconcile all the data, we reasoned that Bgtx might bind at location that is a non α1β2 interface and such location should be absent in the structure of the α1β2γ2 receptor. Therefore, Bgtx is likely to bind to the α1β2 receptor at β2-β2 interface.

4.3.9 α1β2 receptor stoichiometry does not depend on the availability of receptor subunits

We also considered the possibility of existence of two populations of α1β2 receptors—[α1]2[β2]3 and [α1]3[β2]2. We injected cRNAs ratios of (α1:β2) 20:1, 1:1, and 1:20 to see if excess α1 or β2 subunits would result in different subunits combination. Interestingly enough, similar Bgtx blockage was obtained for α1β2 receptors for all cRNAs microinjection ratios (Figure 47), suggesting a single population of α1β2 receptors. This result is in accord with the generally accepted idea that stoichiometry of recombinant α1β2 receptors does not depend on the relative availability of receptor

subunits. Thus, our findings support a stoichiometry of [α1]2[β2]3 for recombinant α1β2 $GABA_A$Rs.

4.3.10 Molecular modeling of α1β2γ2 and α1β2 $GABA_A$Rs

Molecular modeling of α1β2γ2 and α1β2 $GABA_A$Rs was performed by Leonard Moise. Leonard modeled α1β2γ2 and α1β2 $GABA_A$R structures on the atomic structure of the acetylcholine binding protein (AChBP), which is structurally similar to the $GABA_A$ receptor and other members of the ligand-gated ion channel superfamily(Baumann, Baur et al. 2002; Cromer, Morton et al. 2002; Trudell 2002). Figure 48 illustrates how Bgtx might interact with the α1β2 receptor at a β2-β2 interface distinct from the GABA binding pocket.

4.3.11 $GABA_A$R mediated responses are not affected by Bgtx in Rat ventral tegmental area (VTA)

Suggested by the findings from recombinant α1β2 $GABA_A$Rs, the previously unrecognized Bgtx sensitivity may complicate some functional bran studies. Native $GABA_A$Rs are known to express in rodent ventral tegmental area (VTA). In the VTA, previous histological studies indicate expression of α1–3, α5, β1, γ3 and δ subunits in the neurons, while the α1–3, β1–3, γ2 and δ subunits in the processes (Pirker, Schwarzer et al. 2000). Using a combination of single-cell PCR and *in situ* hybridization, α2–4, β1, β3

and γ2 subunits were found in VTA dopaminergic neurons (Okada, Matsushita et al. 2004).

In an attempt to examine the Bgtx effect on native $GABA_A$Rs, whole cell patch clamp recordings were performed on GABA neurons in VTA. The study was done by Esther Penick using rat brain slices (Figure 49). Preliminary results provided by Esther show that GABA responses in rat VTA were not apparently affected by Bgtx batch-application in comparison to control GABA responses. In contrast, bath applied picrotoxin blocked the Bgtx-insensitive currents. The results indicate that the $GABA_A$Rs which give rise to whole-cell GABA response seen in Figure 49 are Bgtx-insensitive and the predominant receptors may not contain a β–β interface.

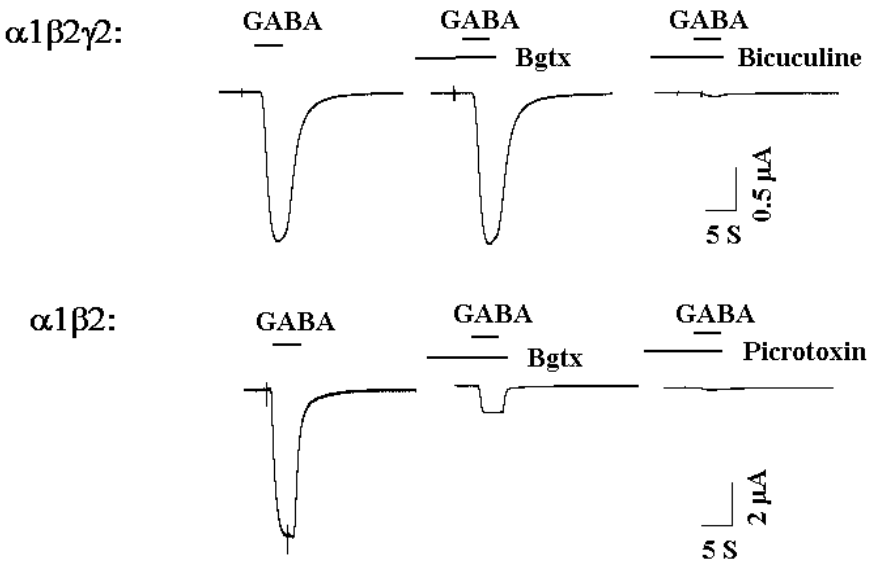

Figure 39. Bgtx blocks α1β2 receptors, not α1β2γ2 receptors. Typical recordings show functional expression of recombinant α1β2γ2 and α1β2 receptors in oocytes. Bgtx pre-incubation selectively blocked GABA response elicited by α1β2 receptors but not α1β2γ2.

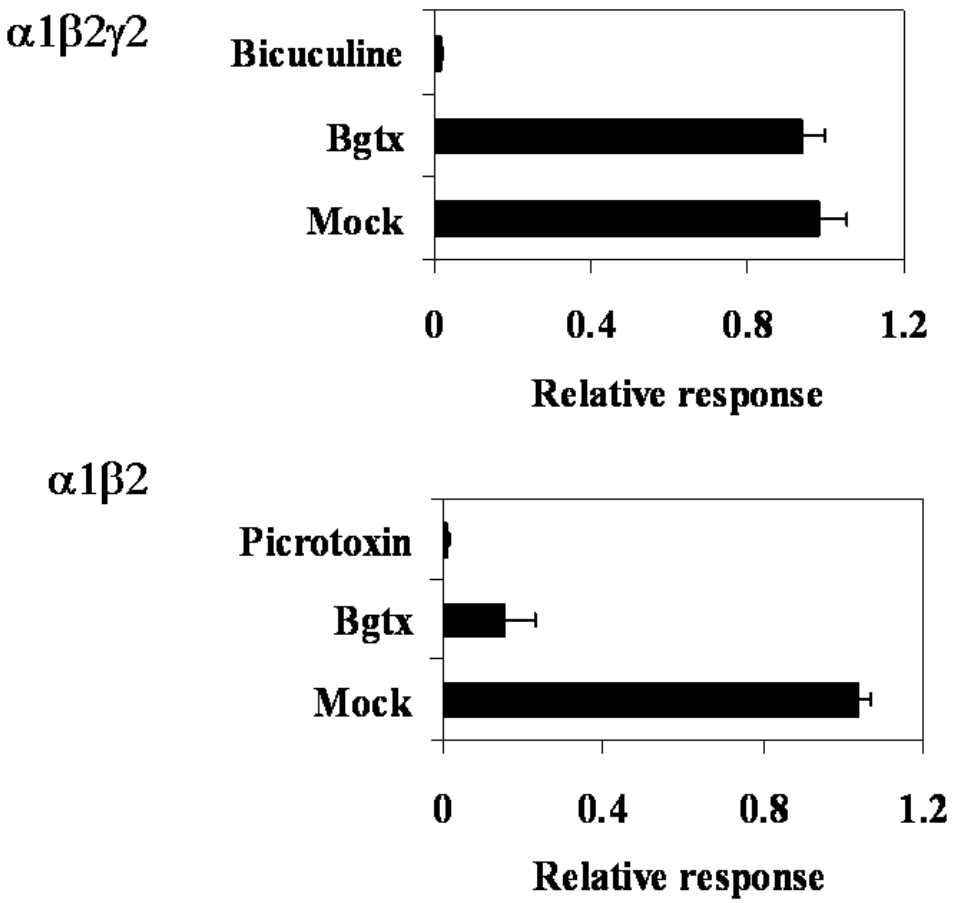

Figure 40. Bgtx selectively blocks α1β2 receptors. Bgtx (1 μM) had no or little effect on GABA current elicited by α1β2γ2 $GABA_A$Rs when compared to "mock" incubation. However, pretreatments with Bgtx (1 μM) blocked α1β2 receptors up to 95%. Both receptors can also be blocked by antagonist bicuculline (100 μM) or picrotoxin (100 μM). Data are averaged from at least 4 oocytes, bars show mean ± SEM.

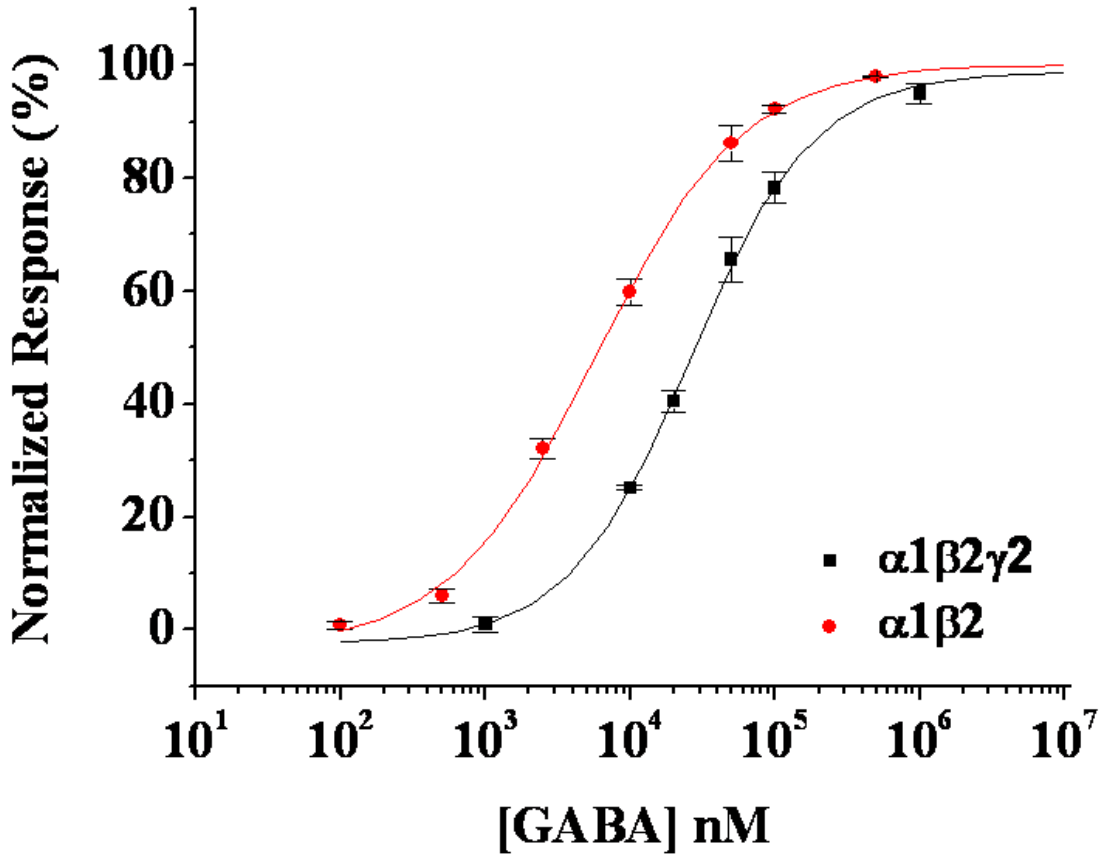

Figure 41. GABA dose-response curves for α1β2γ2 and α1β2 receptors. The EC_{50} values for α1β2 and α1β2γ2 receptors were 7.2± 0.2 μM and 22.0±0.7 μM, respectively. Data are averaged from at least 4 oocytes, bars show mean ± SEM.

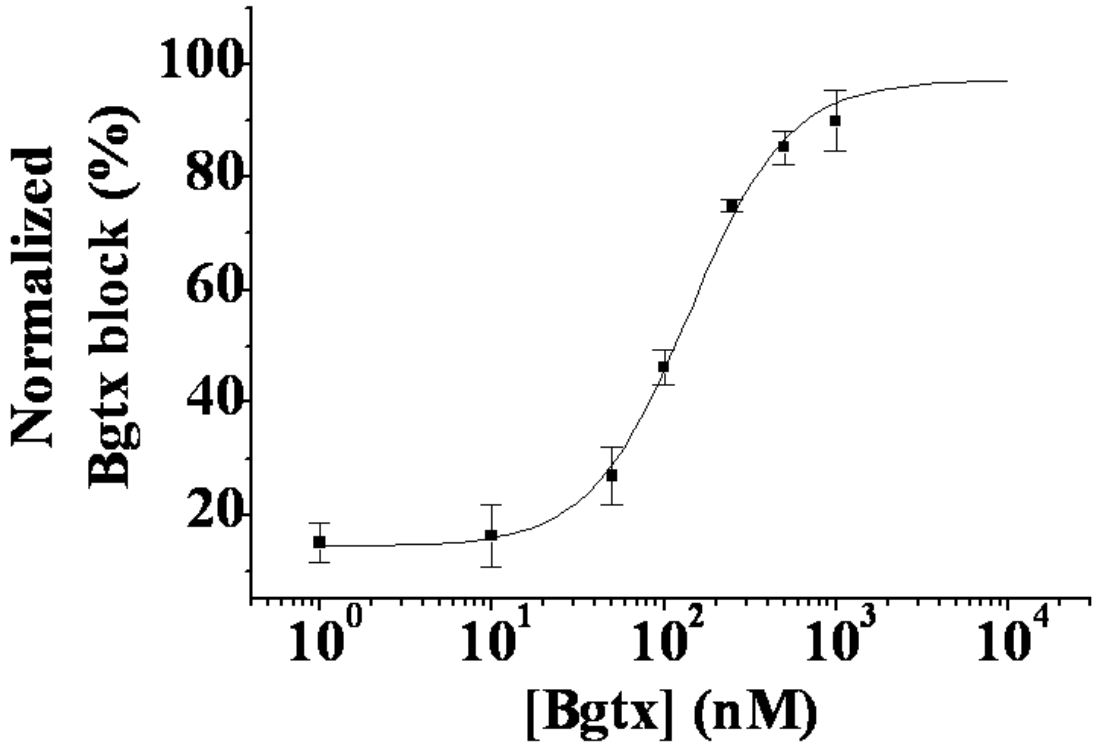

Figure 42. Dose–inhibition curve of Bgtx for α1β2 receptors on the peak amplitude of GABA currents. The fraction of the control response ($I_{post\text{-}toxin}/I_{pre\text{-}toxin}$) is plotted against the Bgtx concentration. $IC_{50} \approx 100$ nM. For technical reasons, Bgtx concentrations >1μM could not be applied, and thus maximum blockage of the receptors could not be determined reliably. The IC_{50} of under such conditions is therefore estimation only. Data are averaged from at least 4 oocytes, bars show mean ± SEM.

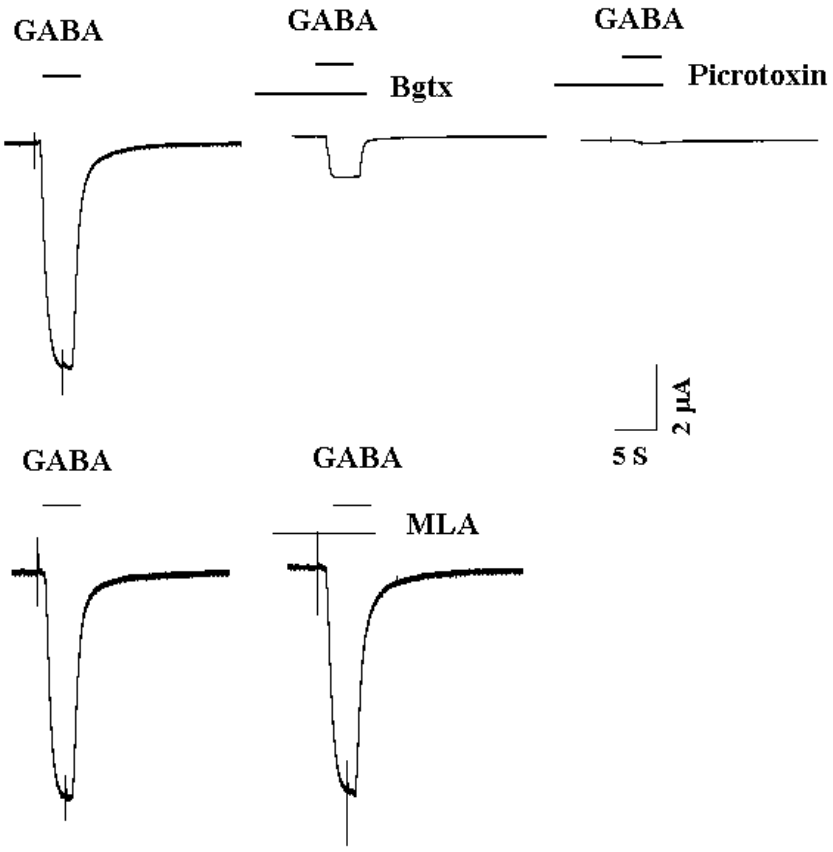

Figure 43. 10 μM MLA, native Bgtx sensitive α7 nAChRs highly selective antagonist, had no effect on GABA currents carried by α1β2 receptors.

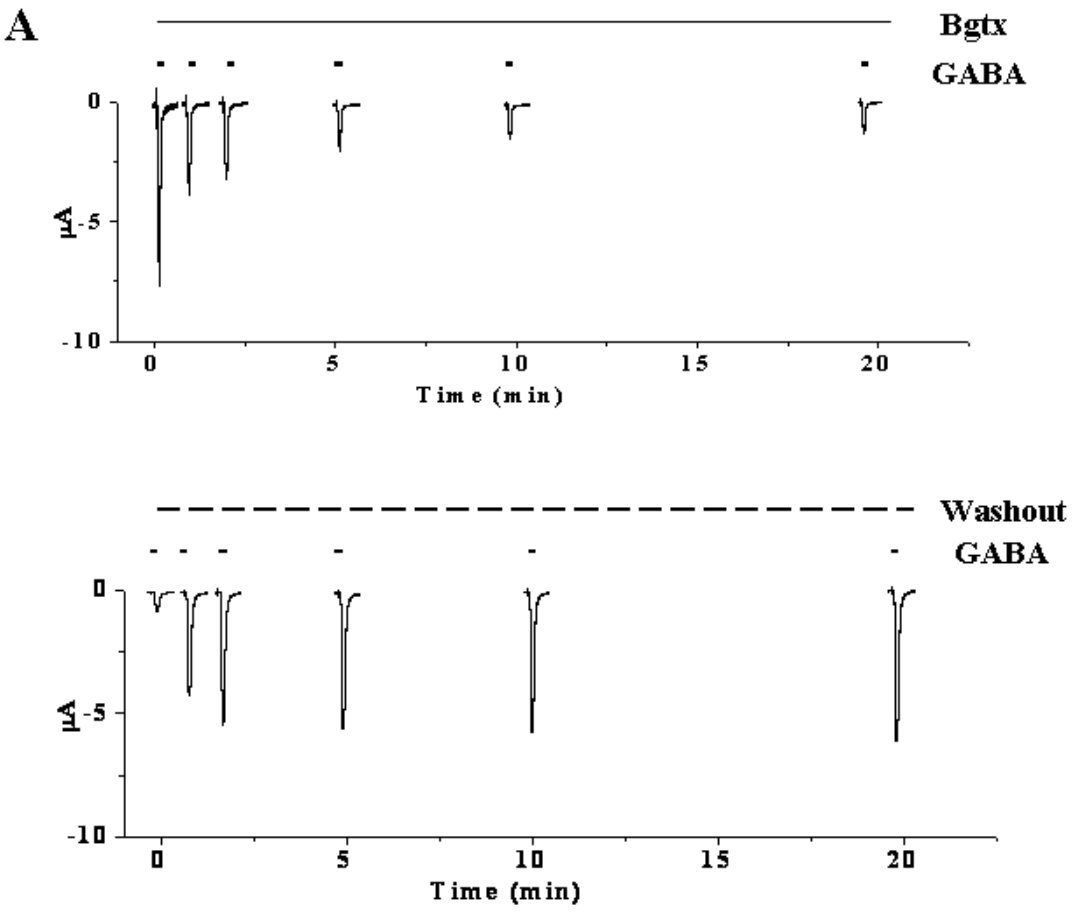
A
Bgtx
GABA
0
-5
-10
μA
0
5
10
15
20
Time (min)
Washout
GABA
0
-5
-10
μA
0
5
10
15
20
Time (min)

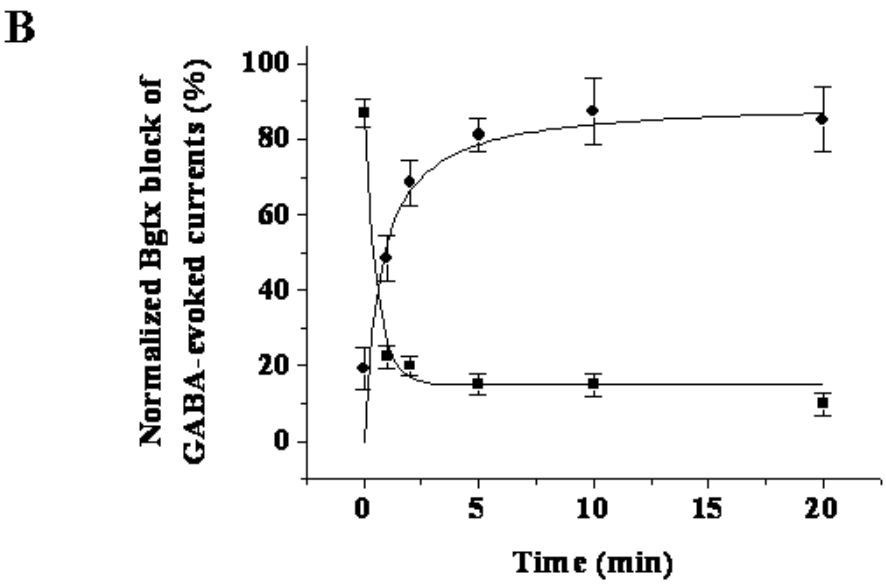
B
Normalized Bgtx block of GABA-evoked currents (%)
100
80
60
40
20
0
0
5
10
15
20
Time (min)

Figure 44. Rapid association and dissociation of Bgtx blockage on α1β2 $GABA_A$Rs. A) Oocytes expressing α1β2 receptors were challenged by a control pulse of GABA (5 μM). After pre-incubation in Bgtx (75 nM) over a range of times, oocytes were challenged again by co-application of 75 nM Bgtx and 5 μM GABA. Lower panel of A shows after the maximum blockage in Bgtx (250 nM), oocytes expressing α1β2 receptors were challenged with GABA at several time intervals following washout. This blockage is also reversible in that GABA currents can recover following Bgtx washout. B) For Bgtx association (●), normalized block defined as 1- ($I_{co\text{-}application}$ /$I_{control}$) is plotted against time in 75 nM Bgtx, where $I_{co\text{-}application}$ is the peak response evoked by co-application of 5 μM GABA and 75 nM Bgtx after Bgtx incubation and $I_{control}$ the peak response evoked by 5 μM GABA before Bgtx incubation. For Bgtx dissociation (■), normalized block defined as 1- ($I_{application}$ /$I_{control}$) is plotted against time following washout of 250 nM Bgtx, where $I_{application}$ is the peak response evoked by 5 μM GABA following washout and $I_{control}$ is the peak response evoked by 5 μM GABA before 20-min Bgtx (250 nM) incubation. Bgtx association with the α1β2 $GABA_A$ receptor equilibrates in about 5 minutes. The currents can reach fully recovery in 5 minutes following washout. Bars show mean ± SEM from n = 4–6 oocytes.

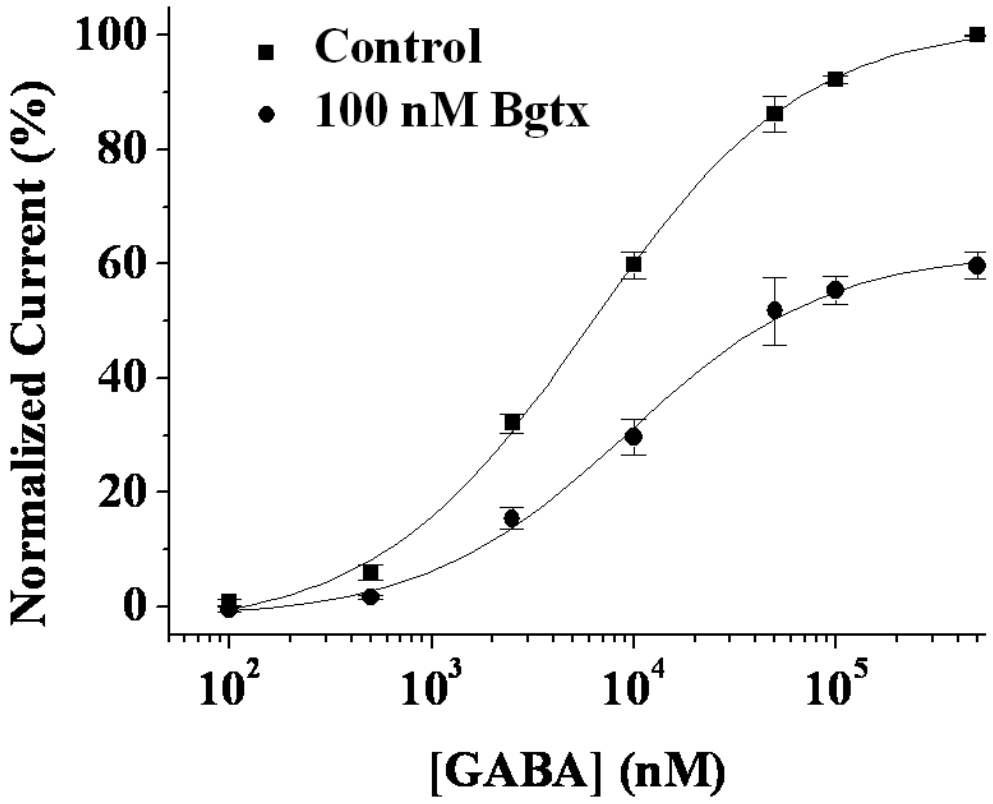

Figure 45. Noncompetitive blockade of Bgtx on α1β2 $GABA_A$Rs. In the presence of Bgtx (100 nM), the GABA dose–response curve was not apparently shifted (GABA EC50=6.0±0.6 μM in absence of Bgtx, GABA EC50=9.1±1.4 μM in presence of Bgtx). Increasing the concentration of GABA did not overcome the partial block achieved with the concentration of Bgtx used. Bars show mean ± SEM from n = 4–6 oocytes.

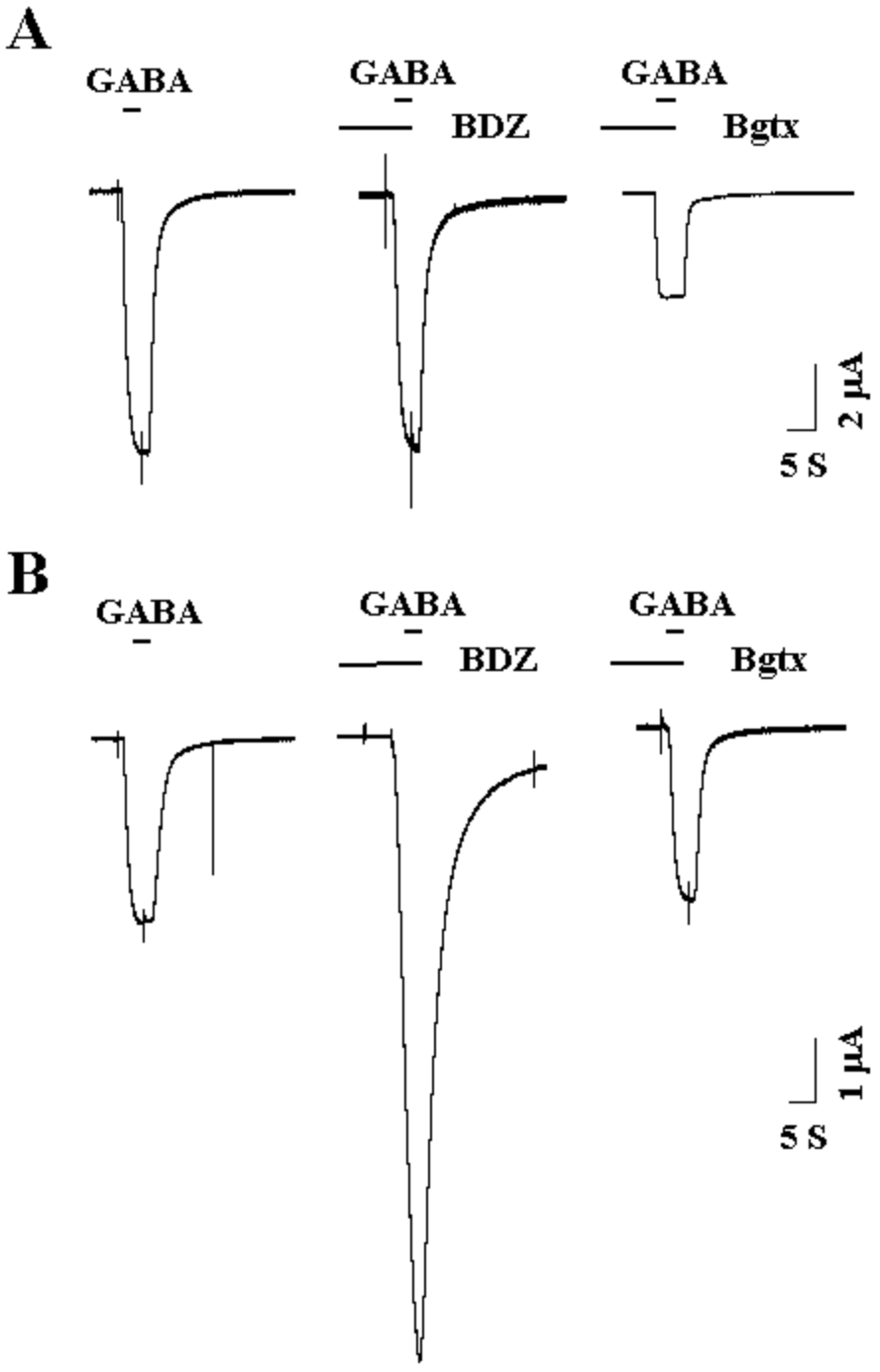
A
GABA
GABA
BDZ
GABA
Bgtx
2 µA
5 S
B
GABA
GABA
BDZ
GABA
Bgtx
1 µA
5 S

Figure 46. Introduction of the γ subunit removes Bgtx sensitivity. A) Channels formed by α1, β2 subunits were not potentiated by benzodiazepine (BDZ), but blocked by Bgtx. B) Channels formed by α1, β2 and γ2 subunits were potentiated by BDZ, but not sensitive to Bgtx. Functional block by Bgtx was observed only for $GABA_A$Rs predicted to contain adjacent β2 subunits.

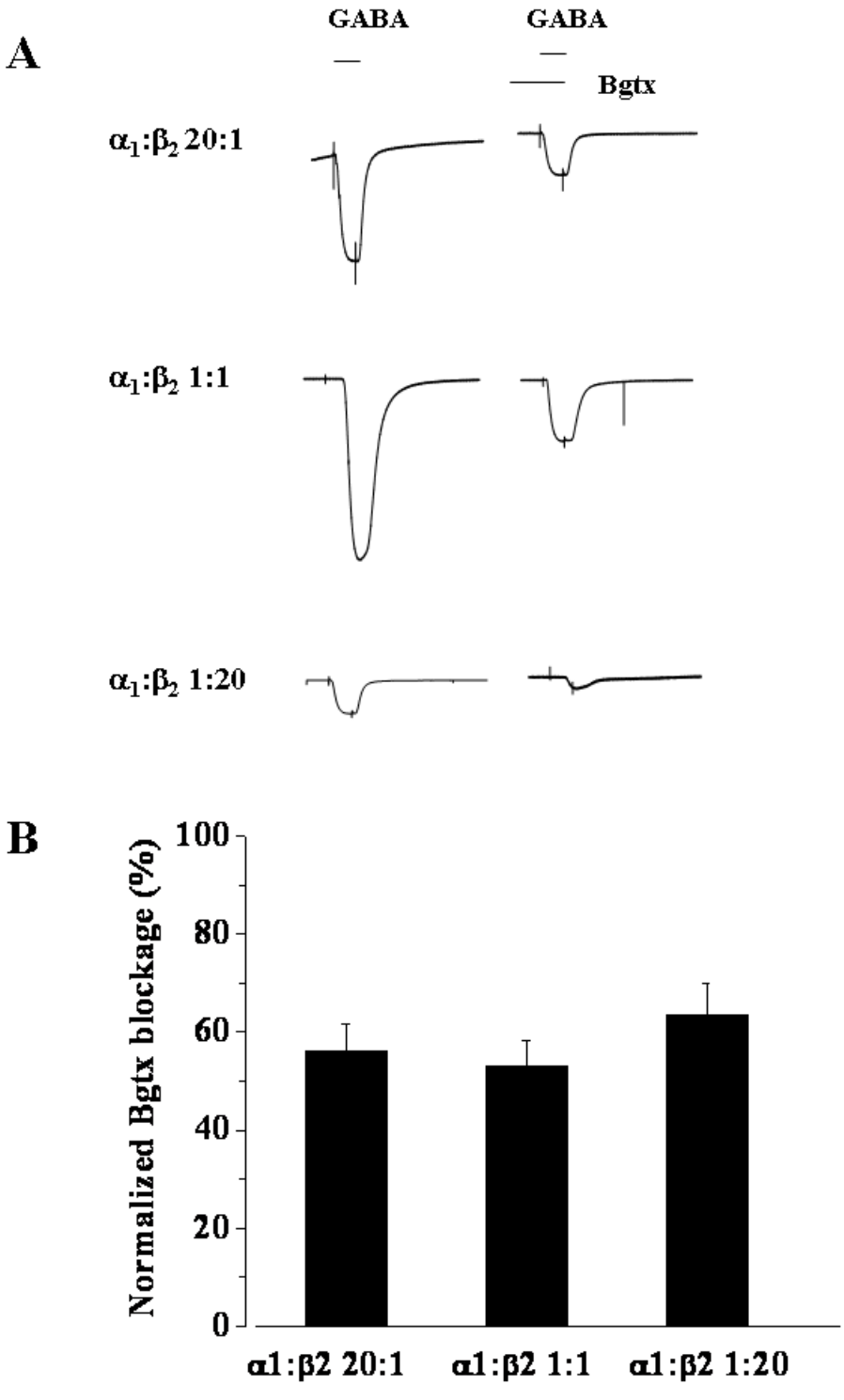
A
GABA
GABA
Bgtx
α1:β2 20:1
α1:β2 1:1
α1:β2 1:20
B
Normalized Bgtx blockage (%)
100
80
60
40
20
0
α1:β2 20:1
α1:β2 1:1
α1:β2 1:20

Figure 47. GABA evoked currents from α1β2 $GABA_A$Rs for 3 injection ratios of α1 to β2 subunit show unitary Bgtx blockage. A) 3 different α1 to β2 injection ratios (20:1, 1:1 and 1:20) all resulted in the functional expression. Measurements were in each case done before and after application of Bgtx with IC_{50} concentration of 100 nM. B) 100nM Bgtx elicited similar blockage on all GABA currents from different α1 to β2 subunit injection ratios. Bars show mean ± SEM from n = 4–6 oocytes.

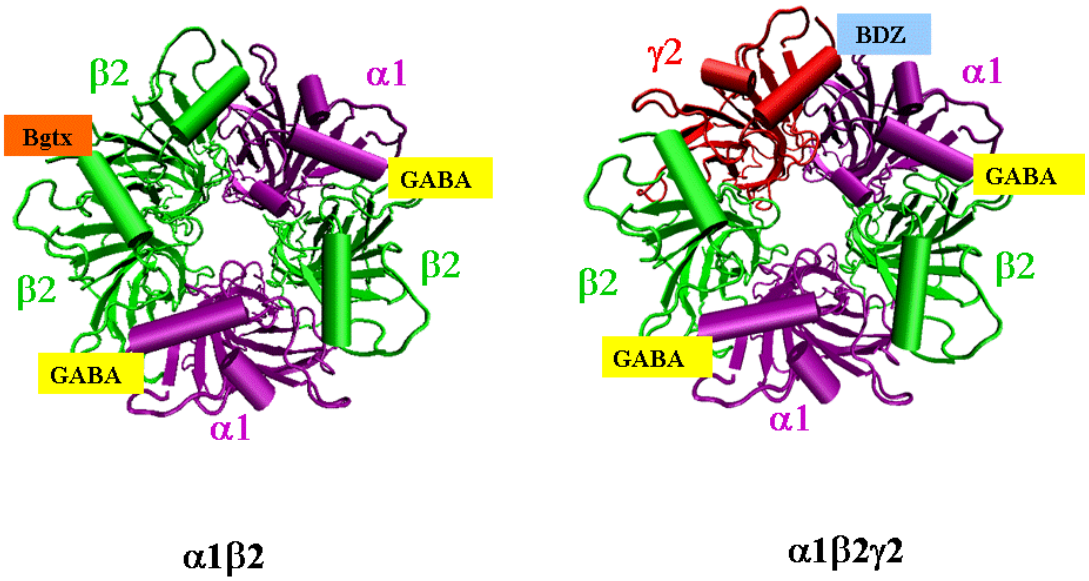

Figure 48. Predicted structure, subunit stoichiometry and arrangement for α1β2 and α1β2γ2 $GABA_A$Rs. View from the 'top' of the protein, looking down through the central pore towards the membrane. The subunits are shown in secondary-structure ribbon representation, α subunit (purple), β subunit (green) and γ subunit (red). Two molecules of GABA are shown as indicated in the putative binding site at each of the two β2–α1 subunit interfaces; BDZ, at γ2–α1 subunit interface; Bgtx, at β2–β2 interface. (Data provided by Leonard Moise)

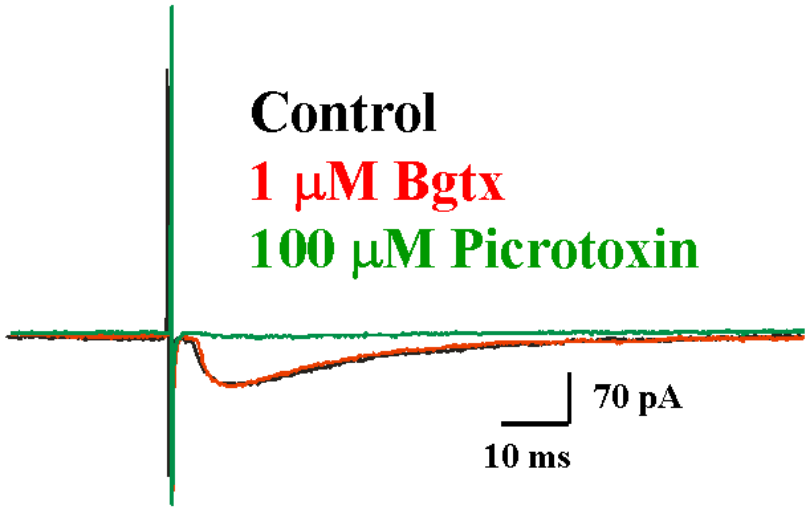

Figure 49. Native $GABA_A$Rs expressed in rat VTA are Bgtx-insensitive. Whole cell patch clamp recordings were performed on GABA neurons in VTA using rat brain slices. Preliminary results show that GABA responses in rat VTA were not apparently affected by Bgtx batch-application (red) in comparison to control GABA responses (black). In contrast, bath applied picrotoxin blocked the Bgtx-insensitive currents (green). Traces are superimposed.(Data provided by Esther Penick & Julie Kauer, Brown University)

4.4 DISCUSSION

4.4.1 Bgtx selectively blocks recombinant $GABA_A$ α1β2 receptors

Our results clearly indicate that Bgtx selectively recognizes and blocks recombinant $GABA_A$ α1β2 receptors but has no effect on $GABA_A$ α1β2γ2 receptors. In light of the newly discovered inhibitory effect of Bgtx on certain $GABA_A$ receptors, the previously thought Bgtx specificity to nAChRs has been challenged and the findings may complicate the interpretation of some studies on neuronal nAChRs in determining the output of neural networks.

4.4.2 Bgtx showed no binding effect on β2 subunit in McCann's (2006) study

With regard to subunit selectivity in $GABA_A$ receptors, McCann (2006) found that Bgtx binds only β3, but has no effect on β2. The discrepancy between their conclusion and the present results on Bgtx selectivity may arise due to the different methodologies adopted in the two studies. McCann assessed the effects of Bgtx on rat $GABA_A$ β1, β2, β3, α2, or γ2 subunits expressed in HEK cells using fluorescence microscopy. One limitation of the experimental approach used in their study was the inability to evaluate β2 receptor assembly. The interpretation that Bgtx does not bind to

the β2 subunit did not take into account that the β2 subunit, unlike β3, can not form homooligomeric channels on its own. In the present study, using electrophysiology method, we observed a selective inhibitory effect of Bgtx in α1β2 $GABA_A$Rs functionally expressed in oocytes. The fact that Bgtx did not bind the β2 subunit in the study of McCann (2006) could reflect a lack of functional expressed recombinant homomeric β2 receptors in their preparation. Overall however, the inhibitory effects of Bgtx appear to be generally similar in two studies in that Bgtx inhibition in α1β2 $GABA_A$Rs likely occurs at β-β subunit interface, consistent with McCann's findings.

4.4.3 $GABA_A$R β2 subunit may contain a previously uncharacterized Bgtx-binding sequence

Surprisingly, $GABA_A$R β2 did not share residues critical for Bgtx binding to nAChRs in high-affinity Bgtx binding domain (Figure 50). In McCann's report, they constructed $GABA_A$R β1 chimera with corresponding β3 subunit sequence to localize the Bgtx-binding site. They found Bgtx bound to chimeric $GABA_A$R subunits in which the amino-terminal extracellular domain of $GABA_A$R β1 was replaced by the corresponding domain of $GABA_A$R β3, whereas no binding was detected to chimeras in which the amino-terminal extracellular domain of $GABA_A$R β3 was replaced by the corresponding domain of $GABA_A$R β1. From these results, they concluded that Bgtx binds to the amino-terminal extracellular domain of $GABA_A$R β3. Whether Bgtx binding site is also located

at N-terminus of $GABA_AR$ β2, similar experiments need to be done to β2 subunits. Nevertheless, the results generated in our lab together with McCann's report should indicate that $GABA_AR$ β2 and β3 may contain a previously uncharacterized BTX-binding sequence. This sequence could add to existing knowledge on the structures underlying BTX-binding peptides and help to elucidate structural similarities between AChRs and $GABA_ARs$.

4.4.4 Low-affinity Bgtx binding sites

Although genetic and pharmacological studies clearly show that most high affinity Bgtx-binding sites in brain correspond to α7 nAChRs, low-affinity Bgtx-binding sites have long been noticed and reported (Meeker, Michels et al. 1986). Studies of ANS and CNS Bgtx binding have focused on high-affinity sites with sensitivity in several nano-molar ranges. A number of studies have shown that occupation of these sites is inadequate to block putative cholinoceptive responses in the mammalian CNS (Lukas 1984). Meanwhile, in radioactive Bgtx binding studies in brains of α7(-/-) knockout mouse, Phil Caffery observed nicotine-resistant ^{125}I-Bgtx binding sites in the brains of both α7(-/-) knockout and wild type animals (Caffery dissertation, 2007). To address this question, an autoradiographic analysis was carried out in the presence of $GABA_AR$ antagonist bicuculline. Treatment with 500 μM bicuculline had little effect on the majority of ^{125}I-Bgtx binding sites in most regions of the brain of wild type mouse. However, there was a significant reduction on signal intensity in the endopririform nucleus and a slight reduction in the thalamic regions. More strikingly, bicuculline had more widespread

effect on ^{125}I-Bgtx binding in α7 knockout brains. Nearly all ^{125}I-Bgtx binding in α7 knockout brains was abolished by bicuculline treatment (Figure 51). Bgtx binding in α7 knockout brains can represent low-affinity Bgtx binding sites because α7 null mice are expected lack endogenous high affinity ^{125}I-Bgtx binding sites (Freedman, Coon et al. 1997). The results raised the possibility that low-affinity Bgtx-binding could represent novel nAChRs or previously unrecognized $GABA_A$Rs, as the $GABA_A$R antagonist bicuculline could block the low-affinity Bgtx-binding.

Due to technical difficulties and limitations of these assays, the precise identity of the source of the low Bgtx-bind sites remains unsolved. In order to identify these bicuculline sensitive low-Bgtx binding sites and to provide conclusive evidence $GABA_A$Rs are attributable to low affinity toxin binding sites, more experiments need to be done in the future. Taken together with the results from recombinant α1β2 $GABA_A$R studies, it opens the door for further examination of the functional relevance of the low affinity Bgtx binding sites. Meanwhile the results may also complicate interpretation of some studies on neuronal nAChRs.

4.4.5 Native αβ receptor isoforms

Generally it is thought that αβ receptors are unlikely to exist in neurons; however, immunocytochemistry (Sieghart and Sperk 2002) and single-channel (Bencsits, Ebert et al. 1999; Mortensen and Smart 2006) studies have provided evidence to the contrary. αβ

$GABA_AR$s are likely to reside at extrasynaptically in relative low abundance. In hippocampal pyramidal neurons, αβ isoforms are estimated to account for up to 10% of all extrasynaptic $GABA_AR$s (Mortensen and Smart 2006). Extrasynaptic receptors are ideally located to sense GABA over-spilled after a synaptic release process from nearby boutons, or to be activated by the ambient levels of GABA present in the extracellular space. Recent studies have shown that extrasynaptic receptors give rise to a tonic form of inhibition that can potently suppress neuronal excitability, suggesting that extrasynaptic receptors and their mechanisms of regulation are expected to be important pharmacological targets (Belelli, Peden et al. 2005; Hanchar, Dodson et al. 2005; Kullmann, Ruiz et al. 2005).

4.4.6 Bgtx, a potentional useful probe for investigating αβ receptors in neurons?

There continues to be some debate regarding the stoichiometry of αβ-expressing receptors (De Koninck and Cooper 1995; Dalziel, Cox et al. 2000; Baumann, Baur et al. 2001; Baumann, Baur et al. 2002; Boileau, Pearce et al. 2005; Gonzales, Bell-Horner et al. 2008) Although not definitive, our studies support the presence of 3β and 2α subunits in these receptors. Altogether, these results indicate that Bgtx subtype-selective antagonism represents a useful approach for studying these receptors. Our report should add valuable structure-function information for future design of novel subtype selective compounds. The expression of such receptor isoforms will also open the way for the

screening of potentially useful substances at defined $GABA_A$ receptor subtypes. The molecular interaction between Bgtx and $GABA_A$Rs, however, remained undisclosed. Nevertheless, our identification of Bgtx inhibition on recombinant $\alpha1\beta2$ $GABA_A$Rs suggests the potential exist for inhibitive modulation of $GABA_A$Rs at a β2-β2 subunit interface. This result also makes Bgtx a potential probe to seek $GABA_A$R subtypes which contain adjacent β2-β2 subunits.

4.4.7 Future directions

Presently, most drug therapies for anxiety, epilepsy and surgical sedation and often for insomnia target $GABA_A$ receptor subtypes non-selectively, but the heterogeneity of these receptors theoretically holds the promise for brain region- or even cell-selective pharmacological intervention, which would increase the specificity of the effects and decrease the incidence of undesirable side effects. However, the development of such therapeutics with improved beneficial effects and fewer side effects has been hampered by a general shortage of data pertaining to subtype selectivity. Meanwhile, the total number of $GABA_A$ receptor subtypes and the function of many of these are currently unknown(Sieghart and Sperk 2002; Whiting 2003). There is potentially an enormous variability in the stoichiometry of $GABA_A$Rs at central nervous system synapses and it remains a major challenge to establish which subunit combinations are expressed at particular synapses and why. Thus, an increased understanding of $GABA_A$

receptors can be utilized in many ways for drug development. Different strategies also exist to minimize undesirable effects: Current research efforts focused on designing subunit-selective or subtype-selective ligands and partial agonists. In general, it seems desirable to have subtype-selective ligands that only act on a certain receptor subtype that is involved in transducing the desired effect and not on other subtypes that are involved in undesired effects. In conclusion, the molecular structures of $\alpha 1\beta 2$ $GABA_AR$ and nAChRs are distinct, yet apparently they both possess a binding site for Bgtx. Unraveling the molecular mechanism of the interactions between Bgtx and $GABA_ARs$ may yield critical insight for understanding this $GABA_AR$ subtype. The site may also prove useful in developing subtype-selective compounds for studying receptor subtype assembly and localization.

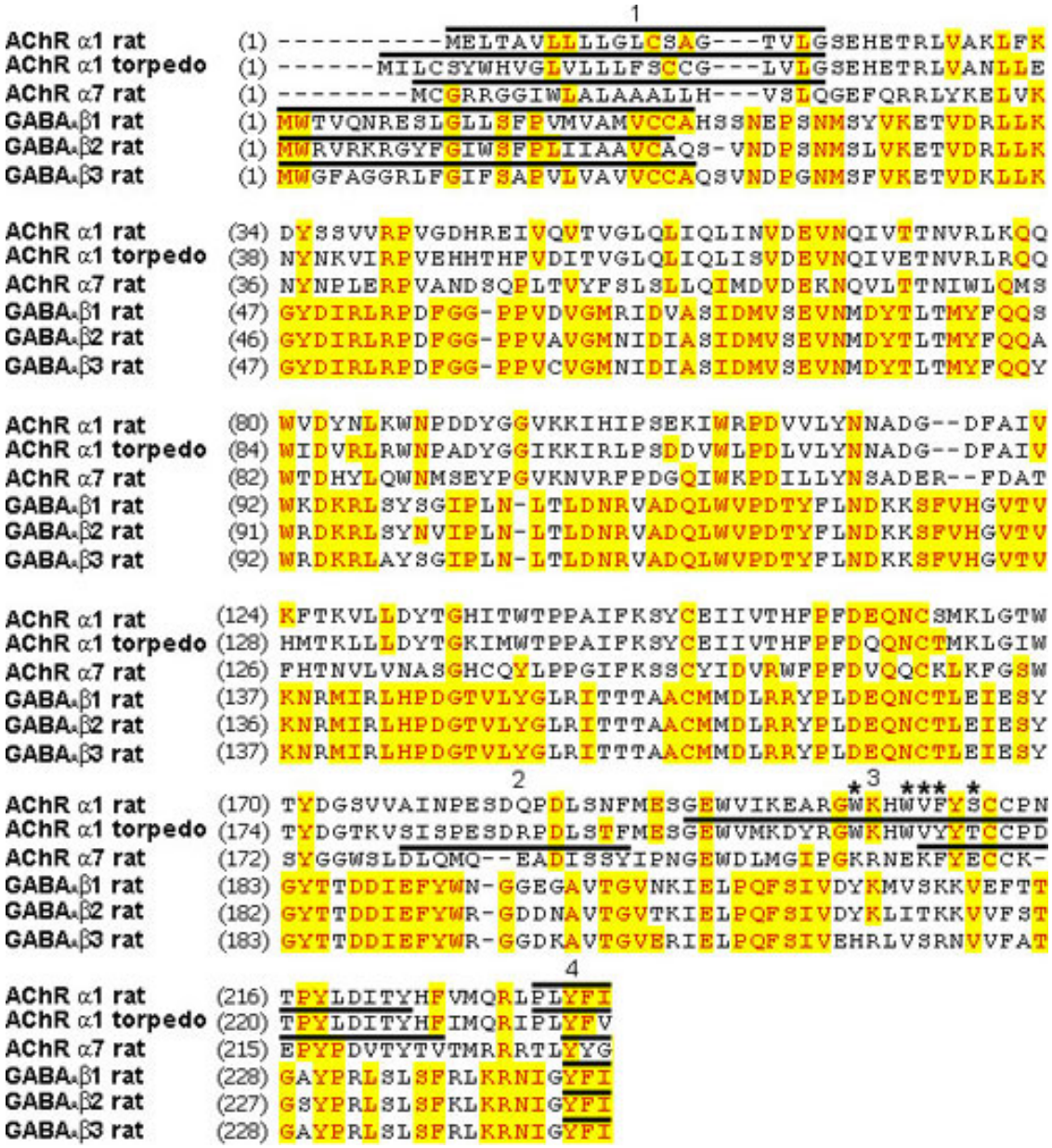
1
AChR α1 rat (1) ----------MELTAVLLLLGLCSAG---TVLGSEHETRLVAKLFK
AChR α1 torpedo (1) ------MILCSYWHVGLVLLLFSCCG---LVLGSEHETRLVANLLE
AChR α7 rat (1) --------MCGRRGGIWLALAAALLH---VSLQGEFQRRLYKELVK
GABAAβ1 rat (1) MWTVQNRESLGLLSFPVMVAMVCCAHSSNEPSNMSYVKETVDRLLK
GABAAβ2 rat (1) MWRVRKRGYFGIWSFPLIIAAVCAQS-VNDPSNMSLVKETVDRLLK
GABAAβ3 rat (1) MWGFAGGRLFGIFSAPVLVAVVCCAQSVNDPGNMSFVKETVDKLLK
AChR α1 rat (34) DYSSVVRPVGDHREIVQVTVGLQLIQLINVDEVNQIVTTNVRLKQQ
AChR α1 torpedo (38) NYNKVIRPVEHHTHFVDITVGLQLIQLISVDEVNQIVETNVRLRQQ
AChR α7 rat (36) NYNPLERPVANDSQPLTVYFSLSLLQIMDVDEKNQVLTTNIWLQMS
GABAAβ1 rat (47) GYDIRLRPDFGG-PPVDVGMRIDVASIDMVSEVNMDYTLTMYFQQS
GABAAβ2 rat (46) GYDIRLRPDFGG-PPVAVGMNIDIASIDMVSEVNMDYTLTMYFQQA
GABAAβ3 rat (47) GYDIRLRPDFGG-PPVCVGMNIDIASIDMVSEVNMDYTLTMYFQQY
AChR α1 rat (80) WVDYNLKWNPDDYGGVKKIHIPSEKIWRPDVVLYNNADG--DFAIV
AChR α1 torpedo (84) WIDVRLRWNPADYGGIKKIRLPSDDVWLPDLVLYNNADG--DFAIV
AChR α7 rat (82) WTDHYLQWNMSEYPGVKNVRFPDGQIWKPDILLYNSADER--FDAT
GABAAβ1 rat (92) WKDKRLSYSGIPLN-LTLDNRVADQLWVPDTYFLNDKKSFVHGVTV
GABAAβ2 rat (91) WRDKRLSYNVIPLN-LTLDNRVADQLWVPDTYFLNDKKSFVHGVTV
GABAAβ3 rat (92) WRDKRLAYSGIPLN-LTLDNRVADQLWVPDTYFLNDKKSFVHGVTV
AChR α1 rat (124) KFTKVLLDYTGHITWTPPAIFKSYCEIIVTHFPFDEQNCSMKLGTW
AChR α1 torpedo (128) HMTKLLLDYTGKIMWTPPAIFKSYCEIIVTHFPFDQQNCTMKLGIW
AChR α7 rat (126) FHTNVLVNASGHCQYLPPGIFKSSCYIDVRWFPFDVQQCKLKFGSW
GABAAβ1 rat (137) KNRMIRLHPDGTVLYGLRITTTAACMMDLRRYPLDEQNCTLEIESY
GABAAβ2 rat (136) KNRMIRLHPDGTVLYGLRITTTAACMMDLRRYPLDEQNCTLEIESY
GABAAβ3 rat (137) KNRMIRLHPDGTVLYGLRITTTAACMMDLRRYPLDEQNCTLEIESY
2
3
AChR α1 rat (170) TYDGSVVAINPESDQPDLSNFMESGEWVIKEARGWKHWVFYSCCPN
AChR α1 torpedo (174) TYDGTKVSISPESDRPDLSTFMESGEWVMKDYRGWKHWVYYTCCPD
AChR α7 rat (172) SYGGWSLDLQMQ--EADISSYIPNGEWDLMGIPGKRNEKFYECCK-
GABAAβ1 rat (183) GYTTDDIEFYWN-GGEGAVTGVNKIELPQFSIVDYKMVSKKVEFTT
GABAAβ2 rat (182) GYTTDDIEFYWR-GDDNAVTGVTKIELPQFSIVDYKLITKKVVFST
GABAAβ3 rat (183) GYTTDDIEFYWR-GGDKAVTGVERIELPQFSIVEHRLVSRNVVFAT
4
AChR α1 rat (216) TPYLDITYHFVMQRLPLYFI
AChR α1 torpedo (220) TPYLDITYHFIMQRIPLYFV
AChR α7 rat (215) EPYPDVTYTVTMRRRTLYYG
GABAAβ1 rat (228) GAYPRLSLSFRLKRNIGYFI
GABAAβ2 rat (227) GSYPRLSLSFKLKRNIGYFI
GABAAβ3 rat (228) GAYPRLSLSFRLKRNIGYFI

Figure 50. Sequence alignment of the amino-terminal extracellular domains of rat nAChR α1 and α7, $GABA_AR$ β1, β2 and β3, and *Torpedo* nAChR α1. Residues boxed in yellow are identical in at least three of the six sequences examined. Underlined regions correspond to the following: 1, predicted signal sequence for each protein; 2, low-affinity Bgtx-binding site on rat nAChR α7 (Marinou and Tzartos 2003); 3, high-affinity Bgtx-binding sites on *Torpedo* nAChR α1 (Levandoski, Lin et al. 1999) and rat nAChR α7 (Marinou and Tzartos 2003); 4, predicted transmembrane domain for each protein. (Adapted from McCann, 2006)

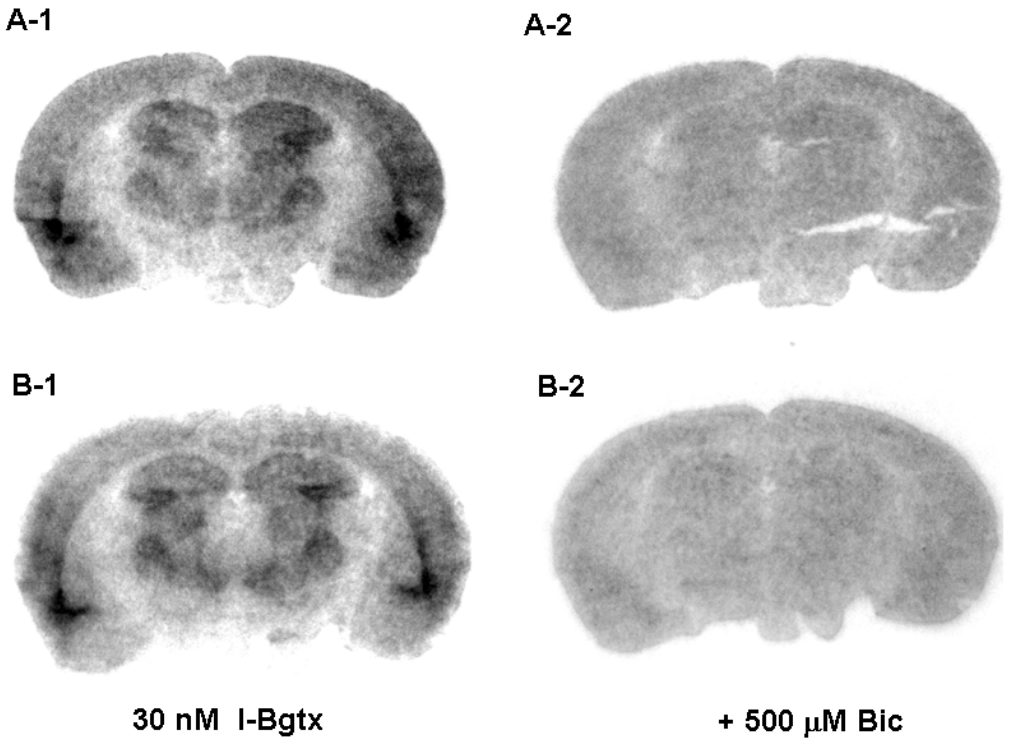

Figure 51. ^{125}I-BTX-binding in α7(-/-) mice is inhibited by 500 μM bicuculline. CNS sections prepared from α7(-/-) mice (both rows) show that total ^{125}I-BTX-binding is significantly reduced in the presence 500 μM bicuculline. (Data collected by Phil Caffery, Brown University)

REFERENCE

Akabas, M. H. (2004). "GABAA receptor structure-function studies: a reexamination in light of new acetylcholine receptor structures." Int Rev Neurobiol **62**: 1-43.

Albuquerque, E. X., E. F. Pereira, et al. (2009). "Mammalian nicotinic acetylcholine receptors: from structure to function." Physiol Rev **89**(1): 73-120.

Allen, N. D., M. L. Norris, et al. (1990). "Epigenetic control of transgene expression and imprinting by genotype-specific modifiers." Cell **61**(5): 853-61.

Anderson, A. D., M. Troyanovskaya, et al. (1997). "Differential expression of alpha2-7, alpha9 and beta2-4 nicotinic acetylcholine receptor subunit mRNA in the vestibular end-organs and Scarpa's ganglia of the rat." Brain Res **778**(2): 409-13.

Anderson, A. E., J. P. Adams, et al. (2000). "Kv4.2 phosphorylation by cyclic AMP-dependent protein kinase." J Biol Chem **275**(8): 5337-46.

Bahring, R., J. Dannenberg, et al. (2001). "Conserved Kv4 N-terminal domain critical for effects of Kv channel-interacting protein 2.2 on channel expression and gating." J Biol Chem **276**(26): 23888-94.

Balass, M., E. Katchalski-Katzir, et al. (1997). "The alpha-bungarotoxin binding site on the nicotinic acetylcholine receptor: analysis using a phage-epitope library." Proc Natl Acad Sci U S A **94**(12): 6054-8.

Basus, V. J., M. Billeter, et al. (1988). "Structural studies of alpha-bungarotoxin. 1. Sequence-specific 1H NMR resonance assignments." Biochemistry **27**(8): 2763-71.

Baumann, S. W., R. Baur, et al. (2001). "Subunit arrangement of gamma-aminobutyric acid type A receptors." J Biol Chem **276**(39): 36275-80.

Baumann, S. W., R. Baur, et al. (2002). "Forced subunit assembly in alpha1beta2gamma2 GABAA receptors. Insight into the absolute arrangement." J Biol Chem **277**(48): 46020-5.

Belelli, D., D. R. Peden, et al. (2005). "Extrasynaptic GABAA receptors of thalamocortical neurons: a molecular target for hypnotics." J Neurosci **25**(50): 11513-20.

Bencsits, E., V. Ebert, et al. (1999). "A significant part of native gamma-aminobutyric AcidA receptors containing alpha4 subunits do not contain gamma or delta subunits." J Biol Chem **274**(28): 19613-6.

Bichet, D., F. A. Haass, et al. (2003). "Merging functional studies with structures of inward-rectifier K(+) channels." Nat Rev Neurosci **4**(12): 957-67.

Birnbaum, S. G., A. W. Varga, et al. (2004). "Structure and function of Kv4-family transient potassium channels." Physiol Rev **84**(3): 803-33.

Bogdanov, Y., G. Michels, et al. (2006). "Synaptic GABAA receptors are directly recruited from their extrasynaptic counterparts." EMBO J **25**(18): 4381-9.

Boileau, A. J., R. Baur, et al. (2002). "The relative amount of cRNA coding for gamma2 subunits affects stimulation by benzodiazepines in GABA(A) receptors expressed in Xenopus oocytes." Neuropharmacology **43**(4): 695-700.

Boileau, A. J., R. A. Pearce, et al. (2005). "Tandem subunits effectively constrain GABAA receptor stoichiometry and recapitulate receptor kinetics but are insensitive to GABAA receptor-associated protein." J Neurosci **25**(49): 11219-30.
Bolivar, V. J., M. N. Cook, et al. (2001). "Mapping of quantitative trait loci with knockout/congenic strains." Genome Res **11**(9): 1549-52.
Brickley, S. G., S. G. Cull-Candy, et al. (1999). "Single-channel properties of synaptic and extrasynaptic GABAA receptors suggest differential targeting of receptor subtypes." J Neurosci **19**(8): 2960-73.
Callsen, B., D. Isbrandt, et al. (2005). "Contribution of N- and C-terminal Kv4.2 channel domains to KChIP interaction [corrected]." J Physiol **568**(Pt 2): 397-412.
Cartier, G. E., D. Yoshikami, et al. (1996). "A new alpha-conotoxin which targets alpha3beta2 nicotinic acetylcholine receptors." J Biol Chem **271**(13): 7522-8.
Champtiaux, N. and J. P. Changeux (2002). "Knock-out and knock-in mice to investigate the role of nicotinic receptors in the central nervous system." Curr Drug Targets CNS Neurol Disord **1**(4): 319-30.
Changeux, J. P., M. Kasai, et al. (1970). "Use of a snake venom toxin to characterize the cholinergic receptor protein." Proc Natl Acad Sci U S A **67**(3): 1241-7.
Chen, D. and J. W. Patrick (1997). "The alpha-bungarotoxin-binding nicotinic acetylcholine receptor from rat brain contains only the alpha7 subunit." J Biol Chem **272**(38): 24024-9.
Cherubini, E., J. L. Gaiarsa, et al. (1991). "GABA: an excitatory transmitter in early postnatal life." Trends Neurosci **14**(12): 515-9.
Chia, R., F. Achilli, et al. (2005). "The origins and uses of mouse outbred stocks." Nat Genet **37**(11): 1181-6.
Chiappinelli, V. A., J. B. Cohen, et al. (1981). "The effects of alpha- and beta-neurotoxins from the venoms of various snakes on transmission in autonomic ganglia." Brain Res **211**(1): 107-26.
Claudio, T., W. N. Green, et al. (1987). "Genetic reconstitution of functional acetylcholine receptor channels in mouse fibroblasts." Science **238**(4834): 1688-94.
Clementi, F., D. Fornasari, et al. (2000). "Neuronal nicotinic receptors, important new players in brain function." Eur J Pharmacol **393**(1-3): 3-10.
Coetzee, W. A., Y. Amarillo, et al. (1999). "Molecular diversity of K+ channels." Ann N Y Acad Sci **868**: 233-85.
Colquhoun, L. M. and J. W. Patrick (1997). "Alpha3, beta2, and beta4 form heterotrimeric neuronal nicotinic acetylcholine receptors in Xenopus oocytes." J Neurochem **69**(6): 2355-62.
Conti-Fine, B. M., D. Navaneetham, et al. (2000). "Neuronal nicotinic receptors in non-neuronal cells: new mediators of tobacco toxicity?" Eur J Pharmacol **393**(1-3): 279-94.
Cooper, S. T. and N. S. Millar (1997). "Host cell-specific folding and assembly of the neuronal nicotinic acetylcholine receptor alpha7 subunit." J Neurochem **68**(5): 2140-51.
Couturier, S., D. Bertrand, et al. (1990). "A neuronal nicotinic acetylcholine receptor subunit (alpha 7) is developmentally regulated and forms a homo-oligomeric channel blocked by alpha-BTX." Neuron **5**(6): 847-56.

Covernton, P. J., H. Kojima, et al. (1994). "Comparison of neuronal nicotinic receptors in rat sympathetic neurones with subunit pairs expressed in Xenopus oocytes." J Physiol **481 (Pt 1)**: 27-34.
Cromer, B. A., C. J. Morton, et al. (2002). "Anxiety over GABA(A) receptor structure relieved by AChBP." Trends Biochem Sci **27**(6): 280-7.
Dalziel, J. E., G. B. Cox, et al. (2000). "Mutating the highly conserved second membrane-spanning region 9' leucine residue in the alpha(1) or beta(1) subunit produces subunit-specific changes in the function of human alpha(1)beta(1) gamma-aminobutyric Acid(A) receptors." Mol Pharmacol **57**(5): 875-82.
De Koninck, P. and E. Cooper (1995). "Differential regulation of neuronal nicotinic ACh receptor subunit genes in cultured neonatal rat sympathetic neurons: specific induction of alpha 7 by membrane depolarization through a Ca2+/calmodulin-dependent kinase pathway." J Neurosci **15**(12): 7966-78.
Dechant, G. (2002). "Chat in the trophic web: NGF activates Ret by inter-RTK signaling." Neuron **33**(2): 156-8.
Dellisanti, C. D., Y. Yao, et al. (2007). "Crystal structure of the extracellular domain of nAChR alpha1 bound to alpha-bungarotoxin at 1.94 A resolution." Nat Neurosci **10**(8): 953-62.
Diochot, S., M. D. Drici, et al. (1999). "Effects of phrixotoxins on the Kv4 family of potassium channels and implications for the role of Ito1 in cardiac electrogenesis." Br J Pharmacol **126**(1): 251-63.
Dixon, J. E., W. Shi, et al. (1996). "Role of the Kv4.3 K+ channel in ventricular muscle. A molecular correlate for the transient outward current." Circ Res **79**(4): 659-68.
Drisdel, R. C. and W. N. Green (2000). "Neuronal alpha-bungarotoxin receptors are alpha7 subunit homomers." J Neurosci **20**(1): 133-9.
Elgoyhen, A. B., D. S. Johnson, et al. (1994). "Alpha 9: an acetylcholine receptor with novel pharmacological properties expressed in rat cochlear hair cells." Cell **79**(4): 705-15.
Endo, T., M. Nakanishi, et al. (1986). "Stopped-flow fluorescence studies on binding kinetics of neurotoxins with acetylcholine receptor." Biochemistry **25**(2): 395-404.
Fambrough, D. M. and H. C. Hartzell (1972). "Acetylcholine receptors: number and distribution at neuromuscular junctions in rat diaphragm." Science **176**(31): 189-91.
Feng, G., R. H. Mellor, et al. (2000). "Imaging neuronal subsets in transgenic mice expressing multiple spectral variants of GFP." Neuron **28**(1): 41-51.
Fertuck, H. C. and M. M. Salpeter (1974). "Localization of acetylcholine receptor by 125I-labeled alpha-bungarotoxin binding at mouse motor endplates." Proc Natl Acad Sci U S A **71**(4): 1376-8.
Festing, M. F. W. (1993). International Index of Laboratory Animals 6th. Newbury, England.
Fiset, C., R. B. Clark, et al. (1997). "Shal-type channels contribute to the Ca2+-independent transient outward K+ current in rat ventricle." J Physiol **500 (Pt 1)**: 51-64.
Freedman, R., H. Coon, et al. (1997). "Linkage of a neurophysiological deficit in schizophrenia to a chromosome 15 locus." Proc Natl Acad Sci U S A **94**(2): 587-92.

Gahring, L. C., E. L. Meyer, et al. (2003). "Nicotine-induced neuroprotection against N-methyl-D-aspartic acid or beta-amyloid peptide occur through independent mechanisms distinguished by pro-inflammatory cytokines." J Neurochem **87**(5): 1125-36.
Gardoni, F., D. Mauceri, et al. (2007). "SAP97 directs the localization of Kv4.2 to spines in hippocampal neurons: regulation by CaMKII." J Biol Chem **282**(39): 28691-9.
Gonzales, E. B., C. L. Bell-Horner, et al. (2008). "Stoichiometric analysis of the TM2 6' phenylalanine mutation on desensitization in alpha1beta2 and alpha1beta2gamma2 GABA A receptors." Neurosci Lett **431**(2): 184-9.
Gotti, C., W. Hanke, et al. (1992). "A functional alpha-bungarotoxin receptor is present in chick cerebellum: purification and characterization." Neuroscience **50**(1): 117-27.
Gotti, C., L. Riganti, et al. (2006). "Brain neuronal nicotinic receptors as new targets for drug discovery." Curr Pharm Des **12**(4): 407-28.
Grady, S., M. J. Marks, et al. (1992). "Characterization of nicotinic receptor-mediated [3H]dopamine release from synaptosomes prepared from mouse striatum." J Neurochem **59**(3): 848-56.
Grigoriadis, D. E., S. R. Hoare, et al. (2009). "Drugability of extracellular targets: discovery of small molecule drugs targeting allosteric, functional, and subunit-selective sites on GPCRs and ion channels." Neuropsychopharmacology **34**(1): 106-25.
Gutman, G. A., K. G. Chandy, et al. (2003). "International Union of Pharmacology. XLI. Compendium of voltage-gated ion channels: potassium channels." Pharmacol Rev **55**(4): 583-6.
Haghighi, A. P. and E. Cooper (1998). "Neuronal nicotinic acetylcholine receptors are blocked by intracellular spermine in a voltage-dependent manner." J Neurosci **18**(11): 4050-62.
Haghighi, A. P. and E. Cooper (2000). "A molecular link between inward rectification and calcium permeability of neuronal nicotinic acetylcholine alpha3beta4 and alpha4beta2 receptors." J Neurosci **20**(2): 529-41.
Hamill, O. P., A. Marty, et al. (1981). "Improved patch-clamp techniques for high-resolution current recording from cells and cell-free membrane patches." Pflugers Arch **391**(2): 85-100.
Hanchar, H. J., P. D. Dodson, et al. (2005). "Alcohol-induced motor impairment caused by increased extrasynaptic GABA(A) receptor activity." Nat Neurosci **8**(3): 339-45.
Harel, M., R. Kasher, et al. (2001). "The binding site of acetylcholine receptor as visualized in the X-Ray structure of a complex between alpha-bungarotoxin and a mimotope peptide." Neuron **32**(2): 265-75.
Hasdemir, B., D. J. Fitzgerald, et al. (2005). "Traffic of Kv4 K+ channels mediated by KChIP1 is via a novel post-ER vesicular pathway." J Cell Biol **171**(3): 459-69.
Herber, D. L., E. G. Severance, et al. (2004). "Biochemical and histochemical evidence of nonspecific binding of alpha7nAChR antibodies to mouse brain tissue." J Histochem Cytochem **52**(10): 1367-76.
Heusser, K. and B. Schwappach (2005). "Trafficking of potassium channels." Curr Opin Neurobiol **15**(3): 364-9.

Hevers, W. and H. Luddens (1998). "The diversity of GABAA receptors. Pharmacological and electrophysiological properties of GABAA channel subtypes." Mol Neurobiol **18**(1): 35-86.
Hoffman, D. A., J. C. Magee, et al. (1997). "K+ channel regulation of signal propagation in dendrites of hippocampal pyramidal neurons." Nature **387**(6636): 869-75.
Holschneider, D. P. and J. C. Shih (2000). "Genotype to phenotype: challenges and opportunities." Int J Dev Neurosci **18**(6): 615-8.
Horn, R. (2000). "A new twist in the saga of charge movement in voltage-dependent ion channels." Neuron **25**(3): 511-4.
Im, W. B., J. F. Pregenzer, et al. (1995). "Chloride channel expression with the tandem construct of alpha 6-beta 2 GABAA receptor subunit requires a monomeric subunit of alpha 6 or gamma 2." J Biol Chem **270**(44): 26063-6.
Jacob, T. C., S. J. Moss, et al. (2008). "GABA(A) receptor trafficking and its role in the dynamic modulation of neuronal inhibition." Nat Rev Neurosci **9**(5): 331-43.
James G. Fox, S. W. B., Muriel T. Davisson, Christian E. Newcomer (2007). The Mouse in biomedical research, Academic Press.
Jan, L. Y. and Y. N. Jan (1997). "Cloned potassium channels from eukaryotes and prokaryotes." Annu Rev Neurosci **20**: 91-123.
Jones, S., S. Sudweeks, et al. (1999). "Nicotinic receptors in the brain: correlating physiology with function." Trends Neurosci **22**(12): 555-61.
Kaab, S., J. Dixon, et al. (1998). "Molecular basis of transient outward potassium current downregulation in human heart failure: a decrease in Kv4.3 mRNA correlates with a reduction in current density." Circulation **98**(14): 1383-93.
Karlin, A. (2002). "Emerging structure of the nicotinic acetylcholine receptors." Nat Rev Neurosci **3**(2): 102-14.
Katz, B. and R. Miledi (1973). "The effect of alpha-bungarotoxin on acetylcholine receptors." Br J Pharmacol **49**(1): 138-9.
Korpi, E. R. and H. Luddens (1997). "Furosemide interactions with brain GABAA receptors." Br J Pharmacol **120**(5): 741-8.
Korpi, E. R., M. J. Mattila, et al. (1997). "GABA(A)-receptor subtypes: clinical efficacy and selectivity of benzodiazepine site ligands." Ann Med **29**(4): 275-82.
Korpi, E. R. and S. T. Sinkkonen (2006). "GABA(A) receptor subtypes as targets for neuropsychiatric drug development." Pharmacol Ther **109**(1-2): 12-32.
Korpi, E. R., G. Wong, et al. (1995). "Subtype specificity of gamma-aminobutyric acid type A receptor antagonism by clozapine." Naunyn Schmiedebergs Arch Pharmacol **352**(4): 365-73.
Kosen, P. A., J. Finer-Moore, et al. (1988). "Structural studies of alpha-bungarotoxin. 3. Corrections in the primary sequence and X-ray structure and characterization of an isotoxic alpha-bungarotoxin." Biochemistry **27**(8): 2775-81.
Krishek, B. J., S. J. Moss, et al. (1996). "Homomeric beta 1 gamma-aminobutyric acid A receptor-ion channels: evaluation of pharmacological and physiological properties." Mol Pharmacol **49**(3): 494-504.
Kullmann, D. M., A. Ruiz, et al. (2005). "Presynaptic, extrasynaptic and axonal GABAA receptors in the CNS: where and why?" Prog Biophys Mol Biol **87**(1): 33-46.
Kunjilwar, K., C. Strang, et al. (2004). "KChIP3 rescues the functional expression of Shal channel tetramerization mutants." J Biol Chem **279**(52): 54542-51.

Lansdell, S. J., B. Schmitt, et al. (1997). "Temperature-sensitive expression of Drosophila neuronal nicotinic acetylcholine receptors." J Neurochem **68**(5): 1812-9.
Lee, C. Y., L. F. Tseng, et al. (1967). "Influence of denervation on localization of neurotoxins from clapid venoms in rat diaphragm." Nature **215**(5106): 1177-8.
Levandoski, M. M., Y. Lin, et al. (1999). "Chimeric analysis of a neuronal nicotinic acetylcholine receptor reveals amino acids conferring sensitivity to alpha-bungarotoxin." J Biol Chem **274**(37): 26113-9.
Lindstrom, J., R. Anand, et al. (1995). "Neuronal nicotinic receptor subtypes." Ann N Y Acad Sci **757**: 100-16.
Long, S. B., X. Tao, et al. (2007). "Atomic structure of a voltage-dependent K+ channel in a lipid membrane-like environment." Nature **450**(7168): 376-82.
Loring, R. H., D. W. Sah, et al. (1988). "The ultrastructural distribution of putative nicotinic receptors on cultured neurons from the rat superior cervical ganglion." Neuroscience **24**(3): 1071-80.
Love, R. A. and R. M. Stroud (1986). "The crystal structure of alpha-bungarotoxin at 2.5 A resolution: relation to solution structure and binding to acetylcholine receptor." Protein Eng **1**(1): 37-46.
Lukas, R. J. (1984). "Detection of low-affinity alpha-bungarotoxin binding sites in the rat central nervous system." Biochemistry **23**(6): 1160-4.
Ma, D. and L. Y. Jan (2002). "ER transport signals and trafficking of potassium channels and receptors." Curr Opin Neurobiol **12**(3): 287-92.
Macdonald, R. L. and R. W. Olsen (1994). "GABAA receptor channels." Annu Rev Neurosci **17**: 569-602.
MacKinnon, R. (2003). "Potassium channels." FEBS Lett **555**(1): 62-5.
Mandelzys, A., B. Pie, et al. (1994). "The developmental increase in ACh current densities on rat sympathetic neurons correlates with changes in nicotinic ACh receptor alpha-subunit gene expression and occurs independent of innervation." J Neurosci **14**(4): 2357-64.
Marinou, M. and S. J. Tzartos (2003). "Identification of regions involved in the binding of alpha-bungarotoxin to the human alpha7 neuronal nicotinic acetylcholine receptor using synthetic peptides." Biochem J **372**(Pt 2): 543-54.
Mathie, A., D. Colquhoun, et al. (1990). "Rectification of currents activated by nicotinic acetylcholine receptors in rat sympathetic ganglion neurones." J Physiol **427**: 625-55.
McCann, C. M., J. Bracamontes, et al. (2006). "The cholinergic antagonist alpha-bungarotoxin also binds and blocks a subset of GABA receptors." Proc Natl Acad Sci U S A **103**(13): 5149-54.
McIntosh, J. M., L. Azam, et al. (2004). "Analogs of alpha-conotoxin MII are selective for alpha6-containing nicotinic acetylcholine receptors." Mol Pharmacol **65**(4): 944-52.
Meeker, R. B., K. M. Michels, et al. (1986). "Characteristics and distribution of high- and low-affinity alpha bungarotoxin binding sites in the rat hypothalamus." J Neurosci **6**(7): 1866-75.
Moise, L., A. Piserchio, et al. (2002). "NMR structural analysis of alpha-bungarotoxin and its complex with the principal alpha-neurotoxin-binding sequence on the

alpha 7 subunit of a neuronal nicotinic acetylcholine receptor." J Biol Chem **277**(14): 12406-17.
Mortensen, M. and T. G. Smart (2006). "Extrasynaptic alphabeta subunit GABAA receptors on rat hippocampal pyramidal neurons." J Physiol **577**(Pt 3): 841-56.
Moser, N., N. Mechawar, et al. (2007). "Evaluating the suitability of nicotinic acetylcholine receptor antibodies for standard immunodetection procedures." J Neurochem **102**(2): 479-92.
Mulle, C., C. Vidal, et al. (1991). "Existence of different subtypes of nicotinic acetylcholine receptors in the rat habenulo-interpeduncular system." J Neurosci **11**(8): 2588-97.
Navarro, H. A., H. Xu, et al. (2002). "In vitro and in vivo characterization of [125I]iodomethyllycaconitine in the rat." Synapse **44**(3): 117-23.
Nelson, R. J. and K. A. Young (1998). "Behavior in mice with targeted disruption of single genes." Neurosci Biobehav Rev **22**(3): 453-62.
Nusser, Z., W. Sieghart, et al. (1998). "Segregation of different GABAA receptors to synaptic and extrasynaptic membranes of cerebellar granule cells." J Neurosci **18**(5): 1693-703.
Okada, H., N. Matsushita, et al. (2004). "Identification of GABAA receptor subunit variants in midbrain dopaminergic neurons." J Neurochem **89**(1): 7-14.
Orr-Urtreger, A., F. M. Goldner, et al. (1997). "Mice deficient in the alpha7 neuronal nicotinic acetylcholine receptor lack alpha-bungarotoxin binding sites and hippocampal fast nicotinic currents." J Neurosci **17**(23): 9165-71.
Orser, B. A. (2006). "Extrasynaptic GABAA receptors are critical targets for sedative-hypnotic drugs." J Clin Sleep Med **2**(2): S12-8.
Ortells, M. O. and G. G. Lunt (1995). "Evolutionary history of the ligand-gated ion-channel superfamily of receptors." Trends Neurosci **18**(3): 121-7.
Owens, J. C., S. A. Balogh, et al. (2003). "Alpha 4 beta 2* nicotinic acetylcholine receptors modulate the effects of ethanol and nicotine on the acoustic startle response." Alcohol Clin Exp Res **27**(12): 1867-75.
Palma, E., L. Maggi, et al. (1999). "Nicotinic acetylcholine receptors assembled from the alpha7 and beta3 subunits." J Biol Chem **274**(26): 18335-40.
Papazian, D. M., T. L. Schwarz, et al. (1987). "Cloning of genomic and complementary DNA from Shaker, a putative potassium channel gene from Drosophila." Science **237**(4816): 749-53.
Patel, S. P. and D. L. Campbell (2005). "Transient outward potassium current, 'Ito', phenotypes in the mammalian left ventricle: underlying molecular, cellular and biophysical mechanisms." J Physiol **569**(Pt 1): 7-39.
Petrecca, K., D. M. Miller, et al. (2000). "Localization and enhanced current density of the Kv4.2 potassium channel by interaction with the actin-binding protein filamin." J Neurosci **20**(23): 8736-44.
Pidoplichko, V. I., M. DeBiasi, et al. (1997). "Nicotine activates and desensitizes midbrain dopamine neurons." Nature **390**(6658): 401-4.
Pirker, S., C. Schwarzer, et al. (2000). "GABA(A) receptors: immunocytochemical distribution of 13 subunits in the adult rat brain." Neuroscience **101**(4): 815-50.
Plummer, H. K., 3rd, M. Dhar, et al. (2005). "Expression of the alpha7 nicotinic acetylcholine receptor in human lung cells." Respir Res **6**: 29.

Pontieri, F. E., G. Tanda, et al. (1996). "Effects of nicotine on the nucleus accumbens and similarity to those of addictive drugs." Nature **382**(6588): 255-7.
Pourrier, M., D. Herrera, et al. (2004). "The Kv4.2 N-terminal restores fast inactivation and confers KChlP2 modulatory effects on N-terminal-deleted Kv1.4 channels." Pflugers Arch **449**(3): 235-47.
Pritchett, D. B., H. Sontheimer, et al. (1989). "Importance of a novel GABAA receptor subunit for benzodiazepine pharmacology." Nature **338**(6216): 582-5.
Purves, D. and J. W. Lichtman (1978). "Formation and maintenance of synaptic connections in autonomic ganglia." Physiol Rev **58**(4): 821-62.
Rhodes, K. J., K. I. Carroll, et al. (2004). "KChIPs and Kv4 alpha subunits as integral components of A-type potassium channels in mammalian brain." J Neurosci **24**(36): 7903-15.
Rhodes, K. J. and J. S. Trimmer (2006). "Antibodies as valuable neuroscience research tools versus reagents of mass distraction." J Neurosci **26**(31): 8017-20.
Rivera, C., J. Voipio, et al. (1999). "The K+/Cl- co-transporter KCC2 renders GABA hyperpolarizing during neuronal maturation." Nature **397**(6716): 251-5.
Rivera, J. F., S. Ahmad, et al. (2003). "An evolutionarily conserved dileucine motif in Shal K+ channels mediates dendritic targeting." Nat Neurosci **6**(3): 243-50.
Rosenthal, J. A., M. M. Levandoski, et al. (1999). "The functional role of positively charged amino acid side chains in alpha-bungarotoxin revealed by site-directed mutagenesis of a His-tagged recombinant alpha-bungarotoxin." Biochemistry **38**(24): 7847-55.
Rudolph, U. and H. Mohler (2006). "GABA-based therapeutic approaches: GABAA receptor subtype functions." Curr Opin Pharmacol **6**(1): 18-23.
Saarelainen, K. S., M. Ranna, et al. (2008). "Enhanced behavioral sensitivity to the competitive GABA agonist, gaboxadol, in transgenic mice over-expressing hippocampal extrasynaptic alpha6beta GABA(A) receptors." J Neurochem **105**(2): 338-50.
Sanders, T. and E. Hawrot (2004). "A novel pharmatope tag inserted into the beta4 subunit confers allosteric modulation to neuronal nicotinic receptors." J Biol Chem **279**(49): 51460-5.
Sands, S. B. and M. E. Barish (1992). "Neuronal nicotinic acetylcholine receptor currents in phaeochromocytoma (PC12) cells: dual mechanisms of rectification." J Physiol **447**: 467-87.
Sanguinetti, M. C., J. H. Johnson, et al. (1997). "Heteropodatoxins: peptides isolated from spider venom that block Kv4.2 potassium channels." Mol Pharmacol **51**(3): 491-8.
Sansom, M. S., I. H. Shrivastava, et al. (2002). "Potassium channels: structures, models, simulations." Biochim Biophys Acta **1565**(2): 294-307.
Schoppa, N. E. and G. L. Westbrook (1999). "Regulation of synaptic timing in the olfactory bulb by an A-type potassium current." Nat Neurosci **2**(12): 1106-13.
Seeburg, P. H., W. Wisden, et al. (1990). "The GABAA receptor family: molecular and functional diversity." Cold Spring Harb Symp Quant Biol **55**: 29-40.
Sekine-Aizawa, Y. and R. L. Huganir (2004). "Imaging of receptor trafficking by using alpha-bungarotoxin-binding-site-tagged receptors." Proc Natl Acad Sci U S A **101**(49): 17114-9.

Serodio, P., C. Kentros, et al. (1994). "Identification of molecular components of A-type channels activating at subthreshold potentials." J Neurophysiol **72**(4): 1516-29.
Shelukhina, I. V., E. V. Kryukova, et al. (2006). "Analysis of specificity of antibodies against synthetic fragments of different neuronal nicotinic acetylcholine receptor subunits." Biochemistry (Mosc) **71**(7): 749-58.
Shibata, R., H. Misonou, et al. (2003). "A fundamental role for KChIPs in determining the molecular properties and trafficking of Kv4.2 potassium channels." J Biol Chem **278**(38): 36445-54.
Sieghart, W. (1995). "Structure and pharmacology of gamma-aminobutyric acidA receptor subtypes." Pharmacol Rev **47**(2): 181-234.
Sieghart, W. and G. Sperk (2002). "Subunit composition, distribution and function of GABA(A) receptor subtypes." Curr Top Med Chem **2**(8): 795-816.
Skok, V. I. (2002). "Nicotinic acetylcholine receptors in autonomic ganglia." Auton Neurosci **97**(1): 1-11.
Song, W. J., T. Tkatch, et al. (1998). "Somatodendritic depolarization-activated potassium currents in rat neostriatal cholinergic interneurons are predominantly of the A type and attributable to coexpression of Kv4.2 and Kv4.1 subunits." J Neurosci **18**(9): 3124-37.
Stitzel, J. A. (2008). "Naturally occurring genetic variability in the nicotinic acetylcholine receptor alpha4 and alpha7 subunit genes and phenotypic diversity in humans and mice." Front Biosci **13**: 477-91.
Takeuchi, S., Y. Takagishi, et al. (2000). "Voltage-gated K(+)Channel, Kv4.2, localizes predominantly to the transverse-axial tubular system of the rat myocyte." J Mol Cell Cardiol **32**(7): 1361-9.
Tang, S. H., F. J. Silva, et al. (2002). "A Cre/loxP-deleter transgenic line in mouse strain 129S1/SvImJ." Genesis **32**(3): 199-202.
Taylor, P. M., P. Thomas, et al. (1999). "Identification of amino acid residues within GABA(A) receptor beta subunits that mediate both homomeric and heteromeric receptor expression." J Neurosci **19**(15): 6360-71.
Temburni, M. K., R. C. Blitzblau, et al. (2000). "Receptor targeting and heterogeneity at interneuronal nicotinic cholinergic synapses in vivo." J Physiol **525 Pt 1**: 21-9.
Trimmer, J. S. and K. J. Rhodes (2004). "Localization of voltage-gated ion channels in mammalian brain." Annu Rev Physiol **66**: 477-519.
Tritto, T., J. A. Stitzel, et al. (2002). "Variability in response to nicotine in the LSxSS RI strains: potential role of polymorphisms in alpha4 and alpha6 nicotinic receptor genes." Pharmacogenetics **12**(3): 197-208.
Trudell, J. (2002). "Unique assignment of inter-subunit association in GABA(A) alpha 1 beta 3 gamma 2 receptors determined by molecular modeling." Biochim Biophys Acta **1565**(1): 91-6.
Wang, N., A. Orr-Urtreger, et al. (2002). "The role of neuronal nicotinic acetylcholine receptor subunits in autonomic ganglia: lessons from knockout mice." Prog Neurobiol **68**(5): 341-60.
Ward, J. M., V. B. Cockcroft, et al. (1990). "Methyllycaconitine: a selective probe for neuronal alpha-bungarotoxin binding sites." FEBS Lett **270**(1-2): 45-8.
Weiland, S., D. Bertrand, et al. (2000). "Neuronal nicotinic acetylcholine receptors: from the gene to the disease." Behav Brain Res **113**(1-2): 43-56.

Wessler, I. and C. J. Kirkpatrick (2008). "Acetylcholine beyond neurons: the non-neuronal cholinergic system in humans." Br J Pharmacol **154**(8): 1558-71.
Whiting, P. J. (2003). "GABA-A receptor subtypes in the brain: a paradigm for CNS drug discovery?" Drug Discov Today **8**(10): 445-50.
Wilkins, M. E., X. Li, et al. (2008). "Tracking cell surface GABAB receptors using an alpha -bungarotoxin-tag." J Biol Chem.
Wong, W., E. W. Newell, et al. (2002). "Cell surface targeting and clustering interactions between heterologously expressed PSD-95 and the Shal voltage-gated potassium channel, Kv4.2." J Biol Chem **277**(23): 20423-30.
Xu, W., S. Gelber, et al. (1999). "Megacystis, mydriasis, and ion channel defect in mice lacking the alpha3 neuronal nicotinic acetylcholine receptor." Proc Natl Acad Sci U S A **96**(10): 5746-51.
Yeola, S. W. and D. J. Snyders (1997). "Electrophysiological and pharmacological correspondence between Kv4.2 current and rat cardiac transient outward current." Cardiovasc Res **33**(3): 540-7.
Zeng, H., L. Moise, et al. (2001). "The solution structure of the complex formed between alpha-bungarotoxin and an 18-mer cognate peptide derived from the alpha 1 subunit of the nicotinic acetylcholine receptor from Torpedo californica." J Biol Chem **276**(25): 22930-40.
Zhou, Y., E. Deneris, et al. (1998). "Differential regulation of levels of nicotinic receptor subunit transcripts in adult sympathetic neurons after axotomy." J Neurobiol **34**(2): 164-78.